FERRIMAGNETIC OXIDE-COMPOSITE MATERIALS FOR SUPERCAPACITORS

MAGNETICALLY ORDERED BIMETTALIC OXIDE-COMPOSITE PSEUDOCAPACITIVE MATERIALS FOR SUPERCAPACITORS APPLICATIONS

By Michael John MacDonald, B.Eng.

A Thesis Submitted to the School of Graduate Studies in Partial Fulfillment of the Requirements for the Degree Master of Applied Science

McMaster University MASTER OF APPLIED SCIENCE (2024) Hamilton, Ontario (Materials Science & Engineering)

TITLE: Magnetically Ordered Bimetallic Oxide-Composite Pseudocapacitive Materials for Supercapacitor Applications

AUTHOR: Michael John MacDonald, B.Eng. (McMaster University)

SUPERVISOR: Dr. Igor Zhitomirsky

NUMBER OF PAGES: CXX, 123

Lay Abstract

The global power demand has been increasing rapidly since the advent of the industrial era, unfortunately human civilization has mostly relied upon fossil fuels to provide the necessary energy for the function of society resulting in vast quantities of greenhouse gases being released into the atmosphere, having a global warming effect on the planet. Recently renewable energy production technologies have been developed but many are intermittent in nature and require efficient energy storage devices to properly hold that energy. Additionally, with countless industries requiring varying quantities of energy or power, the solution for adequate energy storage is a complex multifaceted one that cannot be solved by one energy storage technology alone. For this reason, additional energy storage technology must be developed. The main goal of this work is to develop electrochemical capacitor (ECs) technology, an energy storage solution with greater capacitance retention, cycle stability and cycle lifetime attributes at high charge-discharge rates relative to current battery technology, meaning that ECs can outperform batteries in high power demand applications such as; regenerative breaking, hand-held power tools, heavy construction equipment and even the large energy fluctuations associated with grid level energy storage. Materials with novel magnetic properties were explored to be developed for high active mass loaded electrodes using advanced nano-materials preparation techniques to enhance capacitance. Doing so increased the performance of these energy storage devices drastically, overcoming the poor intercalation attributes associated with high active mass loaded electrodes, making them viable for practical energy storage applications.

Abstract

The enhanced cycle stability, cycle lifetime, capacitance retention, and power densities of electrochemical capacitors make them an increasingly attractive option for modern energy storage needs, including grid level energy storage systems, mobile electronics, heavy construction equipment, military communication devices, power tools, public transportation, electric vehicles and capacitive water deionization systems to name a few. Recently, materials that displayed magnetoelectric coupling phenomena leading to enhanced magneto-capacitive properties are of particular interest, specifically ferrimagnetic spinels and hexagonal ferrites. This thesis is aimed at improving the capacitive performance of $NiFe_2O_4$ (NFO) and $SrFe_{12}O_{19}$ (SFO) based magnetically ordered pseudocapacitor electrodes by elucidating the effects of various nanomaterials preparation techniques on capacitance. The nanomaterials preparation techniques explored in this body of work include the addition of biomimetic dispersing agents, application of high energy ball milling, and forming composites using n-doped conducting pseudocapacitive polypyrrole polymers. Project 1 explored how the addition of gallocyanine dye (GCD) dispersing agent affects the capacitance of NFO. Additionally, the effects of the high energy ball milling (HEBM) process on capacitance were explored and these results were combined with the optimized gallocyanine dye results. Lastly NFO composites with Tiron-doped PPy were prepared at varying mass ratios and combined with optimized HEBM results to achieve the best capacitance results. Project 2 utilized the optimized GCD mass ratios with HEBM to enhance the capacitance of SFO. Tiron doped PPy was used with HEBM SFO at varying mass ratios to achieve the best performing composite electrode. Lastly, the best electrode composition from project 2 was used as anode in an aqueous

asymmetric cell using MnO_2 as the cathode, proving to be a viable anode chemistry in practical electrochemical capacitor applications.

Acknowledgements

I would like to take this opportunity to reflect on the last 2 years of my academic career and on those who helped me succeed throughout my master's degree. Throughout the past 2 years I have faced many challenges; long lab hours, broken electrodes and beakers, along with waiting in anticipation for hours for the experiment that I conducted to either work or fail. None of the progress I have made in advancing my research skills, knowledge in the field and confidence in my abilities would have been possible without the diligent guidance of my supervisor Dr. Igor Zhitomirsky. Dr. Zhitomirsky's deep knowledge of electrochemistry, nanomaterials fabrication techniques, and materials science in general, has helped cultivate my own knowledge of the field through extensive conversations and instruction. Over the past two years I have asked Dr. Zhitomirsky countless questions, made mistakes in presenting and interpreting data, along with many more blunders that were only met with patience, understanding and guidance. Thank you Dr. Zhitomirsky for the amazing support you have provided me these past 2 years. I am truly grateful to have been your student. I would also like to thank all of my lab colleagues, who over the past two years have indulged in my ideas of lab creations, shared their expert knowledge on the countless electrochemical and materials science questions I have had, as well as provide honest feedback on my work. Finally, I would like to thank the many technicians and staff at the CCEM, MAX, and Biointerfaces institute whose technical skills have shed light on the characteristics of the materials that I have studied over the past two years.

Table of Contents

Table of Figures

Table of abbreviations and Symbols

[ox]	Concentration of oxidized species
[red]	Concentration of reduced species
mA, A	Milliamperes, Amperes
mL	Milliliter
mV, V	Millivolt, Volt
μF, F	Microfarad, Farad
μg, mg, g	Microgram, milligram, gram
nm, μm, cm, m	nanometer, micrometer, centimeter, meter
C	Coulomb
J	Joule
K	Kelvin
s	Second
Ohm	Ohm
A	Electrode Area

AC	Activated Carbon
APS	Ammonium persulfate
ARNFO	As-received $NiFe_2O_4$
ARSFO	As-Received $SrFe_{12}O_{19}$
C	Capacitance
C’	Real component of capacitance from EIS data
C”	Imaginary component of capacitance from EIS data
$C_{Diffuse}$	Capacitance of diffuse double layer
C_{double}	Capacitance of the electrical double layer
$C_{helmholtz}$	Capacitance of compact Helmholtz double layer
C_{pseudo}	Capacitance associated with pseudocapacitance
CP, CD	Chrono potentiometry, charge discharge measurement
CV	Cyclic Voltammetry
d	Separation distance (distance between electrodes)
4,5-Dihydroxy-1,3-benzenedisulfonic acid disodium salt monohydrate	Tiron dopant molecule
DI	Deionized
E	Electrode potential

e^-	Electron
E^0	Standard electrode potential
ECs	Electrochemical capacitors
EDLC	Electrical Double layer capacitor
EIS	Electrochemical impedance spectroscopy
F	Faraday's constant
FTIR	Fourier transform infrared spectroscopy
GCD/GD	Gallocyanine Dye
HEBM	High energy ball milled
HEBM NFO	High energy ball milled nickel iron oxide ($NiFe_2O_4$)
HEBM SFO	High energy ball milled strontium iron oxide ($SrFe_{12}O_{19}$)
$i>$, $<i$	Forward and reverse current of redox reactions
IR_{drop}	Voltage drop associated with the internal resistance of a capacitor
K	Proportionality constant
K_f, k_r	Forward and reverse reaction constants for redox reactions
MWCNT	Multiwalled carbon nanotubes
NFO	Nickel Iron Oxide ($NiFe_2O_4$)
Py	Pyrrole

PPy	polypyrrole
PVB	Polyvinyl butyral
Q	Charge
R	Resistance
$R_{internal}$	Internal Resistance
SCE	Saturated calomel electrode
SEM	Scanning electron microscopy
t	Time
T	Temperature
TEM	Transmission electron microscopy
V	Voltage
XRD	X-ray diffraction spectroscopy
Z’	Real component of the impedance measured by EIS
Z”	Imaginary component of the impedance measured by EIS
ε_o	Permittivity of free space
ε_r	Dielectric permittivity of material

Declaration of Academic Achievements

This thesis is written to fulfill the requirements of the M.A.Sc. degree in the department of Materials Science and Engineering at McMaster University. The work contained in this thesis was carried out between September 2022 and August 2024. Below is a list of papers and publications that I contributed to throughout my master's degree. Under the supervision and collaboration with Dr. Igor Zhitomirsky, the experiments described in this dissertation were carried out by the author. The content in this thesis is covered by two papers 1 of which is published in a peer review journal, while the second is currently under peer review:

1. **M. MacDonald** and I. Zhitomirsky, "Capacitive Properties of Ferrimagnetic $NiFe_2O_4$-Conductive Polypyrrole Nanocomposites," *Journal of Composites Science*, vol. 8, no. 2, p. 51, 2024, doi: 10.3390/jcs8020051.
2. **M. MacDonald** and I. Zhitomirsky, "Pseudocapacitive and Magnetic Properties of $SrFe_{12}O_{19}$-Polypyrrole Composites," *Journal of Composites Science*, vol. 8, no. x, 2024, doi: 10.3390/xxxxx.

I have also contributed to an additional paper published in a peer-reviewed journal that is not covered in this thesis.

1. Imani SM, Osman E, Bakhshandeh F, Qian S, Sakib S, **MacDonald M**, Gaskin M, Zhitomirsky I, Yamamura D, Li Y, Didar TF, Soleymani L. Liquid NanoBiosensors Enable One-Pot Electrochemical Detection of Bacteria in Complex Matrices. Adv Sci (Weinh). 2023 Jul;10(19):e2207223. doi: 10.1002/advs.202207223. Epub 2023 Apr 23. PMID: 37088731; PMCID: PMC103

1. Introduction

Since the advent of the industrial era, humanity has incessantly produced vast quantities of greenhouse gas emissions. Recently the global reliance on fossil fuels has resulted in over 30 billion tons of CO_2 emissions per year among other gases with high warming potential [1]. The short wavelength high energy photons from the sun warm the earth's surface, and the earth dissipates this heat as long wavelength infrared photons. CO_2 acts as an insulating gas as it has a different refractive index for infrared photons than other gases in the atmosphere. This causes the infrared light being reflected from earth to become trapped in the atmosphere refracting for longer than it would with other gases. Heat that can't escape slowly increases the global average temperatures causing a butterfly effect that exacerbates the greenhouse gas effect and will eventually wreak havoc on our ecosystems [2]. Realizing this, there has been a worldwide shift to renewable or carbon neutral energy sources many of which have intermittent energy production properties such as wind, solar and tidal.

The intermittent nature of these energy sources makes it difficult to integrate into the energy grid, meaning that there needs to be an intermediate energy storage step so that the energy can be released in predictable, controllable time frames. To achieve this, research and development into new innovative energy storage technology must be developed so that these renewable energy sources can be connected to energy storage systems such as large-scale battery and electrochemical capacitor systems. Currently the largest capacity of energy is stored using pumped hydro making up around 96% of the world's total energy storage at 1310 GW [3], however global battery storage will eventually overtake pumped hydro due to their superior energy storage efficiency. Modern batteries are great at storing large amounts of energy due to high energy densities; however, they

are not well equipped to handle high power fluctuations over long cycle times that would be associated with intermittent energy storage systems. The high-power input may stress the batteries leading to a reduction in health and cycle life.

Electrochemical capacitors are energy storage devices of interest to complement battery technology, as can be seen in Figure 1.1, electrochemical capacitors can be used to bridge the gap between conventional high power density capacitor technology and high energy density battery technology, allowing for a wide range of applications. Electrochemical capacitors have long cycle lifetimes being able to last for 10^5-10^6 cycles for EDLCs and on the scale of 10^3 to 10^4 for pseudocapacitors, much higher scales than modern day lithium-ion batteries 10^3-$3{\cdot}10^3$ [4, 5]. ECs also display increased capacitance retention at higher charge and discharge rates, giving them a greater ability to handle high power applications. By using them in tandem with battery systems ECs can protect them by handling the high-power fluctuations and releasing the energy to batteries at the optimal charge rate to effectively store grid level energy. ECs can also be used as mobile energy storage devices for a plethora of technology such as flashlights, construction equipment, public transportation systems, electric vehicles and as water filters in capacitive water deionization systems.

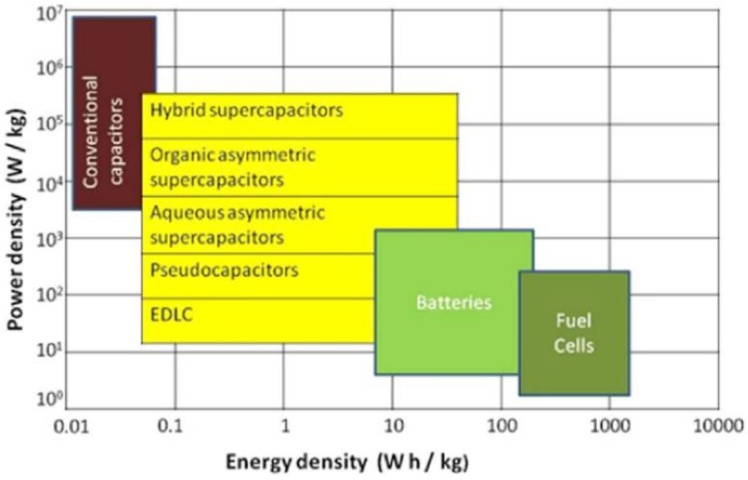

Figure 1.1 Ragone plot displaying energy density vs power density of various energy storage technologies [6]. Reproduced (adapted) with permission from A. Muzaffar, M.B. Ahamed, K. Deshmukh, J. Thirumalai, A review on recent advances in hybrid supercapacitors: Design, fabrication and applications, Renewable and Sustainable Energy Reviews 101 (2019) 123-145.

ECs are generally fabricated with parallel electrodes separated by an electrolyte to enable the storage of energy. The electrodes consist of active materials which facilitate the storage of charge and current collectors that transfer electrons through the external circuit. There exists an electrolyte between the two electrodes to allow for the transfer of charges from anode to cathode during discharging and vice versa during charging. A crucial component of EC construction is the semipermeable membrane within the electrolyte which possesses high electronic resistivity and high ionic conductivity to facilitate the motion of ions between the electrodes during discharging, while blocking the transfer of electrons between electrodes, protecting the cell against a short circuit during operation. Electrochemical capacitors can be divided into 3 main categories: electrical double layer capacitors, pseudo capacitors, and a combination of the two called hybrid capacitors [7].

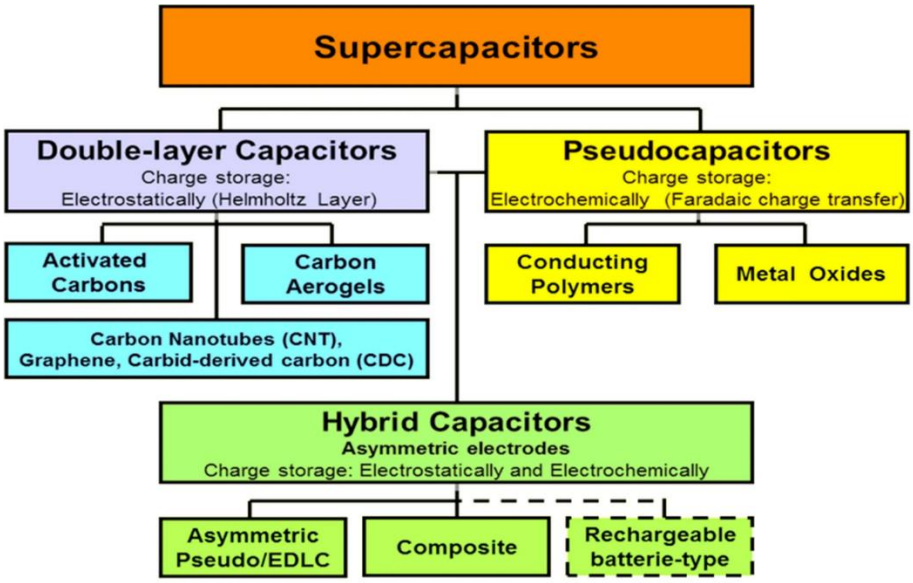

Figure 1.2 Electrochemical capacitor category chart [7]. Reproduced (adapted) with permission from K.O. Oyedotun, J.O. Ighalo, J.F. Amaku, C. Olisah, A.O. Adeola, K.O. Iwuozor, K.G. Akpomie, J. Conradie, K.A. Adegoke, Advances in Supercapacitor Development: Materials, Processes, and Applications, Journal of Electronic Materials 52(1) (2022) 96-129.

Electrical double layer capacitors (EDLCs) store charge electrostatically on the surface of electrodes in the Helmholtz double layer, their enhanced surface area properties allow for increased charge storage properties resulting in larger energy densities than that of the traditional parallel plate capacitor. Pseudocapacitors store energy faradaically in fast redox reactions throughout the bulk of active material such that it mimics the thermodynamic charge storage behaviour of EDLCs hence the name “pseudo”capacitance.

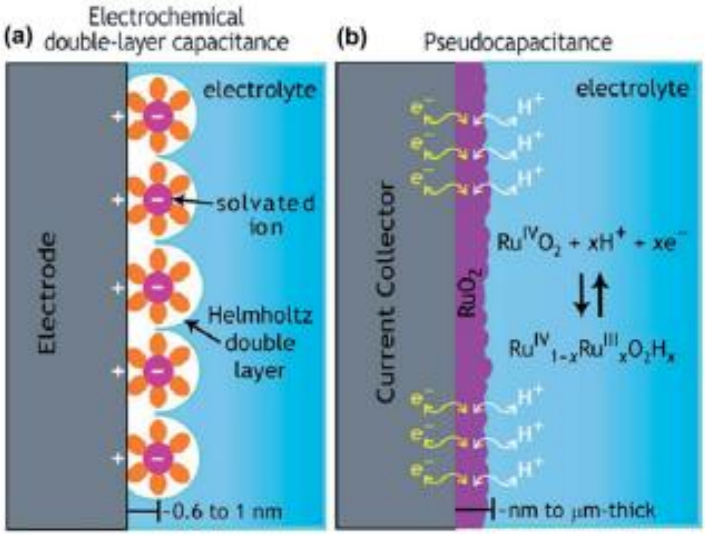

Figure 1.3 Energy storage mechanisms of EDLCs and PCs [8]. Reproduced (adapted) with permission from M. Huang, F. Li, F. Dong, Y.X. Zhang, L.L. Zhang, MnO2-based nanostructures for high-performance supercapacitors, Journal of Materials Chemistry A 3(43) (2015) 21380-21423.

The goal of this thesis is to improve the capacitive properties of magnetically ordered pseudocapacitor electrodes through the investigation of novel nanomaterials preparation techniques, specifically; the addition of advanced biomimetic catecholate dispersing agents, conductive additives, HEBM of nanomaterials, and the fabrication of composite electrodes with conducting pseudocapacitive polymers. These techniques were successfully used for $SrFe_{12}O_{19}$ and $NiFe_2O_4$ nanoparticles to fabricate high active mass loaded electrodes with enhanced capacitance retention (at a mass loading of 40 mg cm^{-2}), cycle stability, lower resistivity, and greater overall capacitance. The capacitance of $NiFe_2O_4$ was increased from 0.1 F cm^{-2} to 4.01 F cm^{-2} at a scan rate of 2 mV s^{-1} for a HEBMNFO-PPy composite electrode with mass ratios of 4 HEBM NFO: 4 PPy: 2 MWCNT (composite=4:4:2), the capacitance of $SrFe_{12}O_{19}$ was increased from 0.05 F cm^{-2} to 3.7 F cm^{-2} at 2 mV s^{-1} for a HEBMSFO-PPy composite electrode with mass

ratios of 4 HEBM SFO: 4 PPy: 2 MWCNT. However, the best performance for $SrFe_{12}0_{19}$ was with the HEBMSFO-PPy composite electrode with mass ratios of 6 HEBMSFO: 2 PPy: 2 MWCNT resulting in a capacitance of 2.7 F cm^{-2} and enhanced capacitance retention at high scan rates over the 4:4:2 electrode. Furthermore, the 6 HEBMSFO: 2 PPy: 2 MWCNT electrode was successfully utilized as an anode in a 2-electrode aqueous asymmetric cell with MnO_2 acting as the cathode, displaying promising anode chemistry for practical energy storage device applications.

1.1 Introduction References

[1] W.J. Sarjeant, Capacitor fundamentals, Proceedings of the 19th Electrical Electronics Insulation Conference, 1989.
[2] D. Kweku, O. Bismark, A. Maxwell, K. Desmond, K. Danso, E. Oti-Mensah, A. Quachie, B. Adormaa, Greenhouse Effect: Greenhouse Gases and Their Impact on Global Warming, Journal of Scientific Research and Reports 17(6) (2018) 1-9.
[3] A. Blakers, M. Stocks, B. Lu, C. Cheng, A review of pumped hydro energy storage, Progress in Energy 3(2) (2021).
[4] A.F. Burke, J. Zhao, Past, present and future of electrochemical capacitors: Technologies, performance and applications, Journal of Energy Storage 35 (2021).
[5] P.E. Lokhande, U.S. Chavan, A. Pandey, Materials and Fabrication Methods for Electrochemical Supercapacitors: Overview, Electrochemical Energy Reviews 3(1) (2019) 155-186.
[6] A. Muzaffar, M.B. Ahamed, K. Deshmukh, J. Thirumalai, A review on recent advances in hybrid supercapacitors: Design, fabrication and applications, Renewable and Sustainable Energy Reviews 101 (2019) 123-145.
[7] K.O. Oyedotun, J.O. Ighalo, J.F. Amaku, C. Olisah, A.O. Adeola, K.O. Iwuozor, K.G. Akpomie, J. Conradie, K.A. Adegoke, Advances in Supercapacitor Development: Materials, Processes, and Applications, Journal of Electronic Materials 52(1) (2022) 96-129.
[8] M. Huang, F. Li, F. Dong, Y.X. Zhang, L.L. Zhang, MnO2-based nanostructures for high-performance supercapacitors, Journal of Materials Chemistry A 3(43) (2015) 21380-21423.

2. Literature Review

2.1 Introduction to Capacitor Technology

Capacitor technology has historically been used for niche high power applications due to their ability to store and release charge in ultra short periods of time. Unlike batteries which store energy via reversible red-ox reactions through intercalation of electrolyte ions into the bulk of active electrode, generally resulting in a phase change in the active material, traditional capacitor technology stores charge electrostatically. It does so by connecting two conducting plates that are separated by a dielectric material externally, to provide a path for electrons to move during charge-discharge cycles. During the charging process a voltage is applied to the plates creating a potential difference between the two electrodes, now there exists a net positive charge on the cathode and a net negative charge on the anode, as a consequence of this the dielectric material is polarized in the electric field generated by the potential difference between the two plates. During discharging electrons will travel quickly through the external circuit from the anode plate down the potential difference gradient towards the positively charged plate where they will recombine with holes and sit happily at in a lower energy state. These electrons can be passed through an electrical load while they travel through the external circuit to perform work[1].

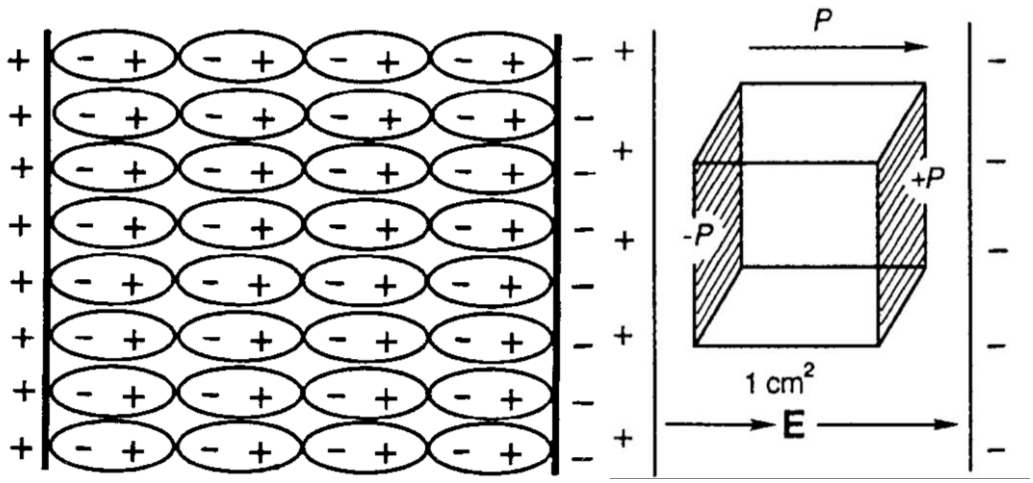

Figure 2.1 Polarization of dielectric material in an electric field [2]. Reproduced (adapted) with permission from B. E. Conway, Behavior of Dielectrics in Capacitors and Theories of Dielectric Polarization, Springer Science+Business Media, LLC Kluwer Academic / Plenum Publishers.

The net charge stored electrostatically at the surface of the electrodes by the polarization of the dielectric material can be accumulated and discharged over extremely short time periods from the surfaces of the conducting plates. It is this mechanism that makes capacitors incredible for frequent high power loads that batteries would find strenuous. Capacitors store charge on the surface of their electrodes electrostatically meaning that there is very little physical stress on the electrode material from charging mechanics resulting in very long cycle lifetime from hundreds of thousands to millions of charge-discharge cycles. Although capacitors can store and release energy on the scale of seconds and possess high power density potentially in the millions of watts per kilogram, they lack the ability to store a large quantity of energy which severely limits their applications resulting in energy density on the scale of tenths to 1 Wh per kg [2]. Capacitors work with two metal plates separated by a dielectric material; these metal plates don't have an incredibly high surface area, so the charges stored on the surfaces are limited. To combat the low energy

density of traditional capacitors a material must be developed which possesses a vastly greater active surface area than two simple conducting plates.

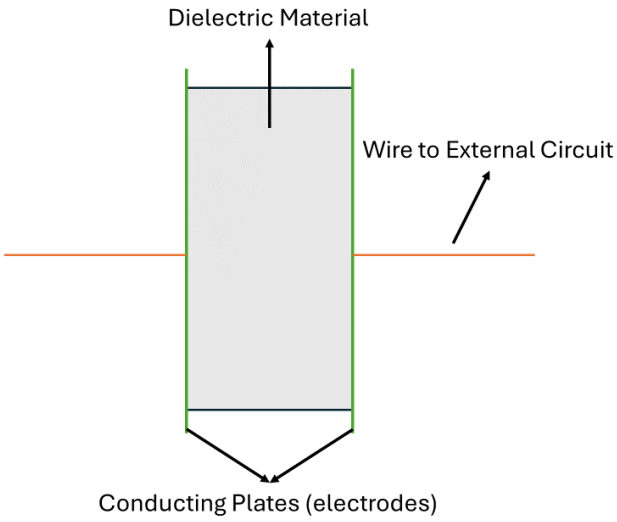

Figure 2.2 Parallel plate capacitor construction.

.

The capacitance of a parallel plate capacitor is described by the equation:

$$C = \frac{Q}{V} \qquad \text{Eq. (2.1)}$$

Which states that capacitance C, is the charge built up on the plates Q, divided by the total applied voltage V. This equation can then be written as:

$$C = \varepsilon_r \varepsilon_0 \frac{A}{d} \qquad \text{Eq. (2.2)}$$

Where ε_r is the dielectric permittivity of the material separating the conducting plates, ε_0 is the dielectric permittivity of free space (or vacuum) A is the area of the conducting plates and d

is the distance between them. Therefore, the capacitance is maximized when ε and A are maximized and the distance between the plates is minimized.

The total energy of a capacitor is described by the equation.

$$E_{cap} = \int_0^{V_{max}} V dQ \qquad \text{Eq. (2.3)}$$

The sum of charge built up on the plates over a voltage range.

Where:

$$Q = C \cdot V \qquad \text{Eq. (2.4)}$$

Therefore:

$$dQ = CdV \qquad \text{Eq. (2.5)}$$

Equation 2.5 can then be substituted into equation 2.3 to obtain:

$$E_{cap} = C \int_0^{V_{max}} V dV \qquad \text{Eq. (2.6)}$$

And finally:

$$E_{cap} = \frac{1}{2} CV^2 \qquad \text{Eq. (2.7)}$$

Where the energy stored is heavily influenced by the applied voltage to the system, as it increases by the square of the voltage. The power of the capacitor can be described as

$$P = VI \qquad \text{Eq. (2.8)}$$

Where maximum voltage can be described as the maximum allowable voltage that can be applied across the capacitor accounting for the internal resistance of the capacitor:

$$V = V_{max} - IR_{internal} \quad \text{Eq. (2.9)}$$

Equation 2.9 can be substituted into equation 2.8 to obtain:

$$P = IV_{max} - I^2R_{internal} \quad \text{Eq. (2.10)}$$

The derivative of the above equation can be taken to describe the voltage, current and internal resistance of the capacitor at maximum power, given that the change in power with respect to the change in current is 0 at maximum power.

Therefore:

$$\frac{dP}{dI} \; at \; P_{max} = 0 \quad \text{Eq. (2.11)}$$

and equation x can now be written as:

$$0 = V_{max} - 2I_{maxpower}R_{internal} \quad \text{Eq. (2.12)}$$

$$I_{max} = \frac{V_{max}}{2R_{internal}} \quad \text{Eq. (2.13)}$$

Equations 2.13 and 2.12 can then be substituted into equation 2.9 to obtain the potential at maximum power:

$$V_{max\,power} = V_{max} - I_{max\,power}R_{internal} = V_{max} - \frac{V_{max}}{2} = \frac{V_{max}}{2} \quad \text{Eq. (2.14)}$$

Meaning that the maximum power of a capacitor is obtained when the potential applied on the system is half of the maximum allowable applied potential and leads to the equation:

$$P_{max} = V_{max\,power}I_{max\,power} \quad \text{Eq. (2.15)}$$

$$P_{max} = \frac{V_{max}}{2} \cdot \frac{V_{max}}{2R_{internal}} \quad \text{Eq. (2.16)}$$

$$P_{max} = \frac{V_{max}^2}{4R_{internal}} \quad \text{Eq. (2.17)}$$

Similarly to the total energy in a capacitor the maximum power is very heavily influenced by the potential as any change in potential will result in a power change in accordance with the square of that potential value. Of course, it is also beneficial to minimize the internal resistance of the circuit as much as possible for optimal capacitor function [2].

2.2 Electrochemical Capacitors - Electrical Double Layer Capacitors

The charge storage mechanisms for EDLCs are like that of the traditional capacitor but the dielectric material is replaced with more complex electrolytes which offer greater ionic conductivity and capacitance. Activated carbons possess high electronic conductivity and great structural properties to allow for enhanced interaction with ions in solution and are the primary materials used in making EDLC's. In the context of the traditional capacitor where a dielectric material is used to oppose the electric field and stop the flow of electrons through the internal circuit, a separator material is used in the case of an electrochemical capacitor. Although electrolytes are selected to maximize ionic conductivity and minimize electronic conductivity a separator needs to be employed as a short circuit would be catastrophic for an electrochemical energy storage device. The separator material allows ions to flow through so that the circuit can still be completed with the mobile ions in the electrolyte material while blocking the direct exchange of electrons from anode to cathode. For the sake of simplicity, aqueous electrolytes will

be used to describe the functions of an EDLC as they are the best for visualizing the transport of ions to the surfaces of electrodes [3].

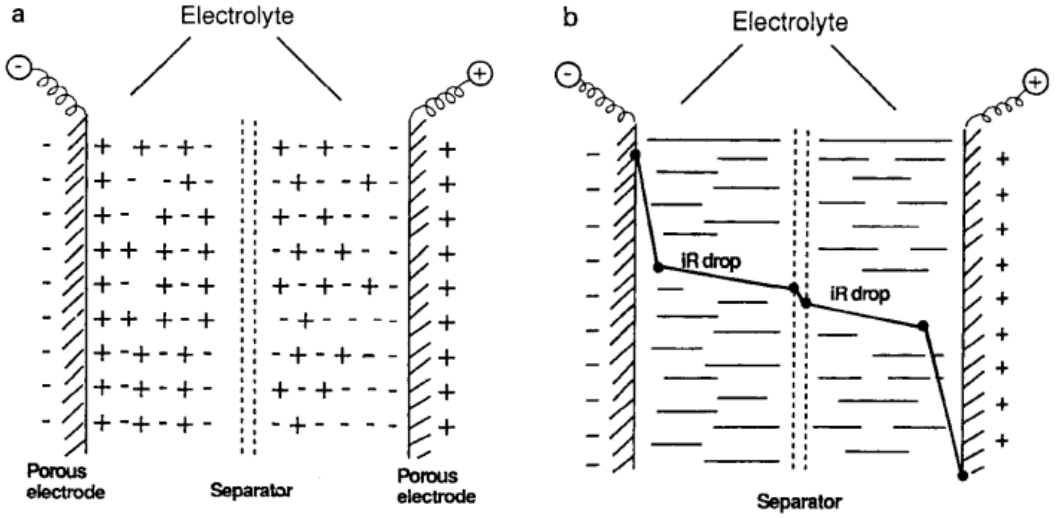

Figure 2.3 Electrolyte behaviour in an EDLC under an applied potential (a) and potential across two electrodes of an EDLC during discharging (b) [2]. Reproduced (adapted) with permission from B. E. Conway, Behavior of Dielectrics in Capacitors and Theories of Dielectric Polarization, Springer Science+Business Media, LLC Kluwer Academic / Plenum Publishers.

The charge stored in an EDLC is heavily dependent on the structure of the double layer, ionic mobility of solvated species, electronic conductivity of the electrodes, and the operating voltage window that the device is stable in. For this reason, the structure of the double layer will be first analyzed with ionic mobility in mind. The double layer size is dependent on the size of the solvation sheath size of ions interacting with the active material along with concentration of active and inert ionic species within the electrolyte [2]. The solvation of an ion in electrolyte is dependent on the size of the charge, atomic radius, and solvent molecule polarity. In the case of aqueous electrolytes, the polar water molecule is responsible for dissolving ions, the high polarity of the water molecule is what makes it the universal solvent. When a charged species is dissolved in

water the charged poles of the water molecules align opposite to the charge of the ion. In the case of a positive ion like Li the negatively charged oxygen side will align, conversely for a negative ion like fluorine the positively charged hydrogen atoms will align. This alignment of water molecules in the immediate vicinity of the ion is called the primary solvation sheath, there are secondary and tertiary sheaths with more disordered alignment and no alignment in the bulk of the electrolyte respectively. The size of the sheath is heavily dependent on the strength of the charge on the ion as well as the size of the atom itself [4].

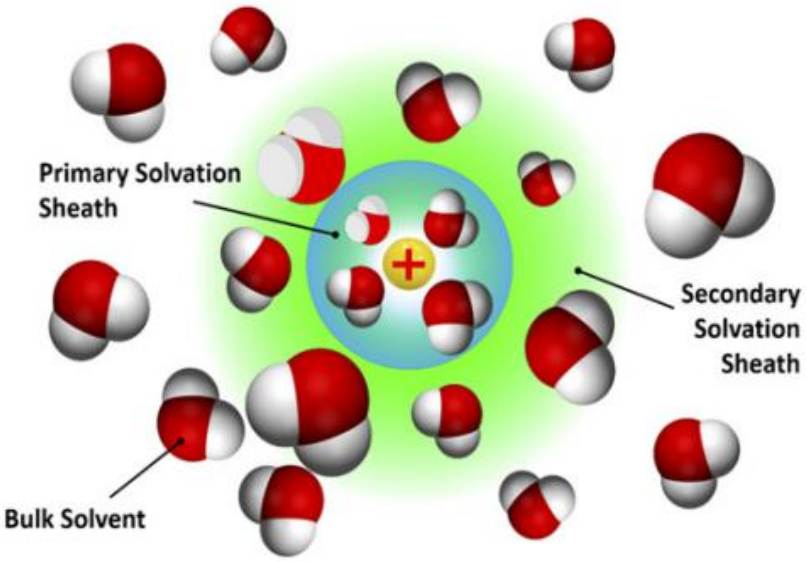

Figure 2.4 Solvation sheath formation in water [4]. Reproduced (adapted) with permission from K. Xu, Electrolytes, Interfaces and Interphases, Fundamentals and Applications in Batteries, Royal Society of Chemistry, 2023.

These sheaths heavily influence the transport of ionic species as well as the double layer thickness itself, in general cationic species have smaller ionic radius which results in greater solvation sheath retention properties relative to their anionic counter parts. Anions with larger ionic

radius will not hold on to their solvation sheaths as strongly, thus the distance of closest approach for anions will be smaller than that of the cation allowing for superior EDLC charging mechanics. When an electric field is present due to a potential difference between two electrodes the polar water molecules will align opposite to the gradient of the electric field and the cations in the electrolyte will travel towards the negatively charged electrode [2]. As they travel the local water molecules will align as previously described until the ion reaches the surface of the electrode, where near the surface exists the electrical double layer and the diffuse layer closer to the bulk of the electrolyte [2].

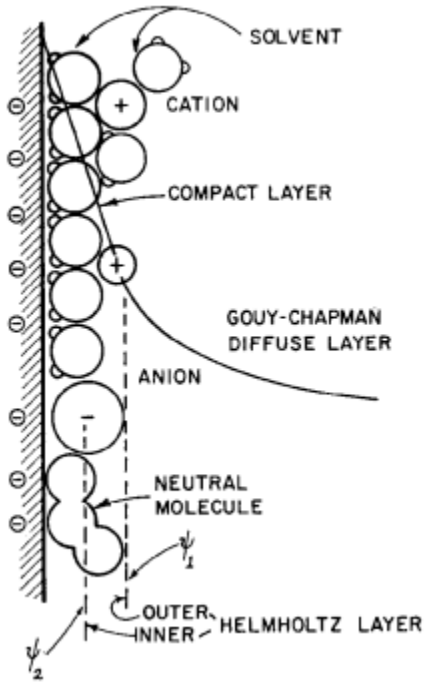

Figure 2.5 Schematic comparing the distance of closest approach for cations and anions [2]. Reproduced (adapted) with permission from B. E. Conway, Behavior of Dielectrics in Capacitors and Theories of Dielectric Polarization, Springer Science+Business Media, LLC Kluwer Academic / Plenum Publishers.

At the electrode interface the properties of closest approach become more relevant to ionic interactions with the active materials. Near the surface of the electrode the electrolyte ions interact with the electrode material via delocalized conduction band electrons so that the ions are electrostatically stored on the surface of the electrode.

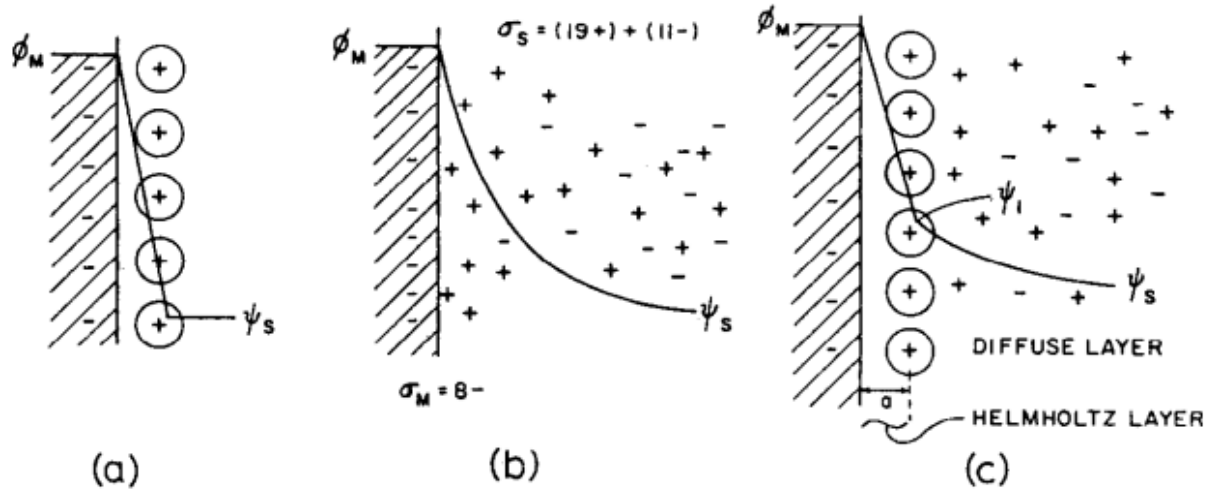

Figure 2.6 Varying models of the electrical double layer at the electrode surface, a) Helmholtz, b) Gouy-Chapman, c) Stern Models [2]. Reproduced (adapted) with permission from B. E. Conway, Behavior of Dielectrics in Capacitors and Theories of Dielectric Polarization, Springer Science+Business Media, LLC Kluwer Academic / Plenum Publishers.

The most accurate description of the structure of the electrical double layer near the surface of the electrode is proposed by the Stern model, combining the compact layer of charged particles from the Helmholtz model and the electrically and thermally influenced point charges from the Gouy-Chapman model. The stern model describes 2 major regions of the electrical double layer, the compact layer: charged particles stored electrostatically within 0.1 nm of the surface of the electrode, and the diffuse layer: charged particles in the bulk of the electrolyte that are more loosely oriented towards the electrode due to the charge screening from the compact layer. Both layers

contribute to the capacitance of an EDLC with the compact layer being responsible for most of the charge storage associated with the electrode[2]. However, the Helmholtz and diffuse layer form a capacitor in series system as seen in Figure 2.7.

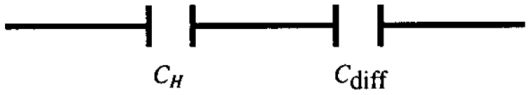

Figure 2.7 series circuit diagram of two capacitors in series [2]. Reproduced (adapted) with permission from B. E. Conway, Behavior of Dielectrics in Capacitors and Theories of Dielectric Polarization, Springer Science+Business Media, LLC Kluwer Academic / Plenum Publishers.

Where:

$$\frac{1}{C_{Total}} = \frac{1}{C_{dl}} = \frac{1}{C_{Helm}} + \frac{1}{C_{diff}} \qquad \text{Eq. (2.18)}$$

It is important to note that majority of the charge stored is from the compact Helmholtz layer, however the lower capacitance from the diffuse layer will result in a larger value compared to the compact layer due to the reciprocal nature of this equation, meaning that the total capacitance is controlled by the region with the lower capacitance value, and is especially true for electrolytes with sufficiently low concentrations. This effect can be reduced by increasing the concentration of electrolyte ions, improving mass transport kinetics in the solution and inducing a large potential window in the EDLC system [2].

The current generated by a potential difference between two electrodes of an EDLC can be described by the following equation:

$$I = \frac{dQ}{dt} = C_{dl}\frac{dV}{dt} \qquad \text{Eq. (2.19)}$$

Where I is the current generated, $\frac{dQ}{dt}$ is the change in charge over change in time, C_{dl} is the capacitance of the electrical double layer, and $\frac{dV}{dt}$ is the change in potential over change in time. This equation indicates how an ideal EDLC should possess constant capacitance behaviour under constant rate of potential change and constant current values and can be depicted by rectangular shaped cyclic voltammetry and triangular charge-discharge characteristics. This topic will be discussed in greater detail in the next section when relating the behaviour of an ideal pseudocapacitor to that of an ideal EDLC.

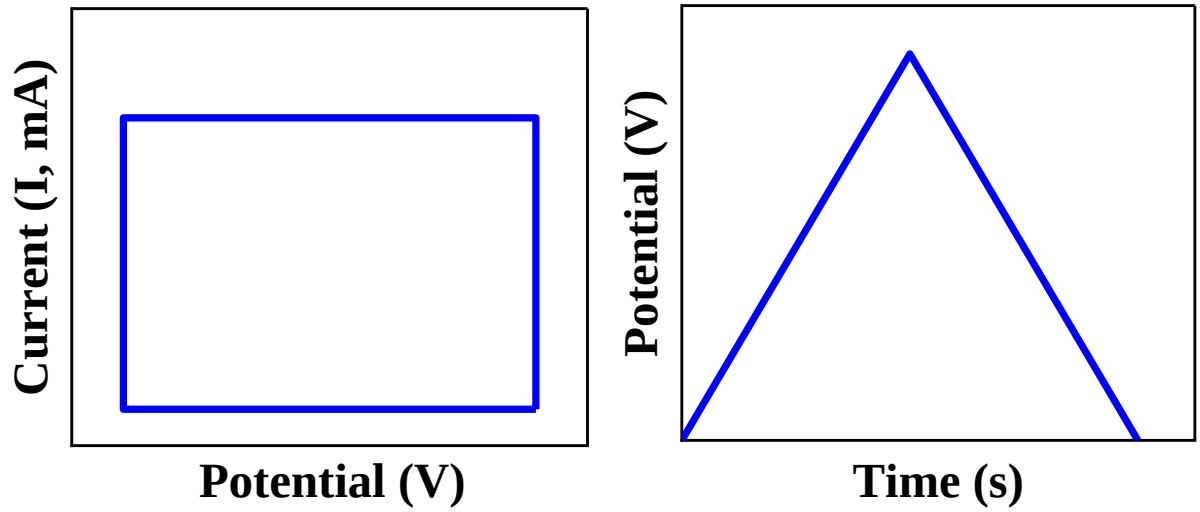

Figure 2.8 Shows the ideal CV and CP behaviour of an EDLC [5].

By combining complex electrolytes with activated carbon materials with practical surface areas of 1000-2000 $m^2\ g^{-1}$ most commonly used in EDLC industry one can increase the capacitance by several orders of magnitude over the traditional plate capacitor [6]. Activated carbons can be created by a wide variety of organic precursors such as chitosan from crab shells, cellulose from

plants, or from hydrocarbon precursors to be used in various fabrication routes like plasma vapor deposition, and calcination. Making EDLC's a viable technology to bridge the gap between traditional capacitors and batteries [7].

2.3 Pseudocapacitance

Pseudocapacitors are a class of electrochemical capacitors that store energy through fast reversible faradic reactions in the bulk of the electrode. Much like a battery, reduction occurs at the cathode and oxidation occurs at the anode during discharge. Unlike EDLCs which store charge electrostatically, solvated ions are intercalating into the material and partaking in electron exchange reactions with the active electrode materials. When the PC is being charged a potential difference is induced onto the device which forces electrons into the anode where they will interact with solvated cations, reducing them. At the cathode a net positive charge is assigned due to the removal of electrons. During the discharge phase the electrons will travel back to the cathode from the anode, oxidizing the cations, who will then travel from the anode through the electrolyte and recombine with the electrons and reduce on the surface of the cathode [8]. Pseudocapacitance energy storage relies on adsorption and desorption of solvated ionic species in the electrolyte to work. Contrary to a battery there is no permanent phase change in pseudocapacitors even though faradaic processes are still occurring. This drastically increases the cyclic stability of a pseudocapacitor over conventional batteries. Pseudocapacitance occurs when the extent of a faradaic reaction has a relationship with potential difference that is analogous to EDLC energy storage thermodynamics. Therefore, the change in charge relative to the change in potential throughout a red/ox reaction will be identical to that of an EDLC. This definition can be described as the logarithmic relationship between y, a variable used to describe the extent of the reaction, or a portion of the charge passed (amount of electrolyte ions reacting Faradaically at the electrode)

relative to the total amount of available charge carries, and the change in potential induced in the system [2].

Such that:

$$\frac{y}{1-y} = Kexp(\frac{VF}{RT}) \qquad \text{Eq. (2.20)}$$

Where K is a constant, V is electrode potential, F is Faraday's constant, R is Rydberg's constant, and T is the absolute temperature during the reaction. The derivative of equation 2.20 can be taken to describe the change in y (extent of red/ox reaction, fractional absorption of ions by active electrode material or fractional coverage of an electrode surface area by ionic species (charge carriers)) relative to the change of electrode potential.

$$\frac{dy}{dV} = \frac{F}{RT} \cdot \frac{Kexp\left(\frac{VF}{RT}\right)}{[1+Kexp\left(\frac{VF}{RT}\right)]^2} \qquad \text{Eq. (2.21)}$$

The resulting units from this equation are in C/J meaning that if we multiply both sides by the charge associated with the extent of the faradaic reactions dictated by the term y, then a capacitance can be defined for the reaction.

$$Q\frac{dy}{dV} = Q(\frac{F}{RT} \cdot \frac{Kexp\left(\frac{VF}{RT}\right)}{\left[1+Kexp\left(\frac{VF}{RT}\right)\right]^2}) = C\frac{C}{J} = C \cdot \frac{1}{V} = \frac{C}{V} = F \qquad \text{Eq. (2.22)}$$

The red/ox reactions in the faradaic processes described by the above equations can be simply written.

$$AOx_a + Ze = BRed_b \qquad \text{Eq. (2.23)}$$

Where Ox is the species in the reaction being reduced to obtain Red in the forward reaction by the addition of Z number of electrons while in the reverse reaction it is being oxidized via removal of Z number of electrons from Red. A and B are positive integers indicating the number of moles of the oxidized or reduced species respectively, a and b are subscripts denoting the number of atoms in a chemical.

An example of such a reaction is that of MnO_2:

$$Mn^{4+}O_2 + C^+ + e^- = Mn^{3+}O_2C^+ \qquad \text{Eq. (2.24)}$$

Here the oxidation state of MnO_2 is changing to allow for the storage of a cation such as Na^+, K^+ or H^+ when electrons are supplied, on the left side of the reaction as in equation (2.23) an electron is interacting with Mn^{4+} and the cation to reduce the oxidation state to Mn^{3+} on the right side of the reaction [9]. The thermodynamics of the pseudocapacitive red/ox reaction can be elegantly described by a simplified derivation of the Nernst equation.

The Gibbs free energy of reaction can be written as the relationship between charge and change in cell potential.

$$\Delta G = -Q\Delta E \qquad \text{Eq. (2.25)}$$

Where ΔG is the change in Gibbs free energy and depends on the charge accumulated in the reaction Q and change in potential ΔE. Q is the charge in coulombs based on the moles of electrons (n) involved in the reaction and the amount of charge a mole of electrons contains (F) also known as Faraday's constant, replacing Q with these terms eq. (2.25) can be written as:

$$\Delta G = -nFE \qquad \text{Eq. (2.26)}$$

For standard reaction conditions the change in Gibbs free energy can be related to the standard potential values of the electrode as such:

$$\Delta G^{\circ} = -nFE^{\circ} \quad \text{Eq. (2.27)}$$

Where ΔG° is the standard Gibbs free energy of the reaction and E° is the standard electrode potential (the electrode half cell reaction at 298K and 1 atm of pressure) [2, 10]. Therefore, the Gibbs free energy of an electrode reaction at non-standard conditions is:

$$\Delta G = \Delta G^{\circ} + RTlnQ \quad \text{Eq. (2.28)}$$

$$-nFE = -nFE^{\circ} + RTlnQ \quad \text{Eq. (2.29)}$$

$$E_{cell} = E^{\circ}_{cell} - \frac{RT}{NF} lnQ \quad \text{Eq. (2.30)}$$

Here it can be observed that the rightmost term is responsible for the deviation of the cell potential from the standard cell potential where Q is a reaction quotient that relates the activity of the products in the reaction to the reactants and can be simplified to depend on the concentrations of reactants and products in aqueous systems when a reducing or oxidizing potential is applied. In the case of a reducing potential or the forward direction of eq. (2.24) the following Nernst equation can be derived [10].

$$E_{cell} = E^{\circ}_{cell} - \frac{RT}{NF} \ln \left(\frac{B[Red]^b}{A[Ox]^a}\right) \quad \text{Eq. (2.31)}$$

For oxidizing potentials:

$$E_{cell} = E^{\circ}_{cell} + \frac{RT}{NF} \ln \left(\frac{A[Ox]^a}{B[Red]^b}\right) \quad \text{Eq. (2.32)}$$

Therefore, the Nernst equation can be used to accurately describe the reversible potential of electrode reactions under various conditions, which is essential for the optimal operation of pseudocapacitive systems, especially over longer cycle lifetimes. In doing so the stable potential window for pseudocapacitive systems such as MnO_2 can be determined to encourage ideal capacitive behaviour. Awad and Zhitomirsky conducted tests of MnO_2 based PC electrodes displaying ideal capacitive behaviour in a potential window of +0.9 V vs SCE in aqueous sodium sulfate as displayed in Figure (2.9) [11].

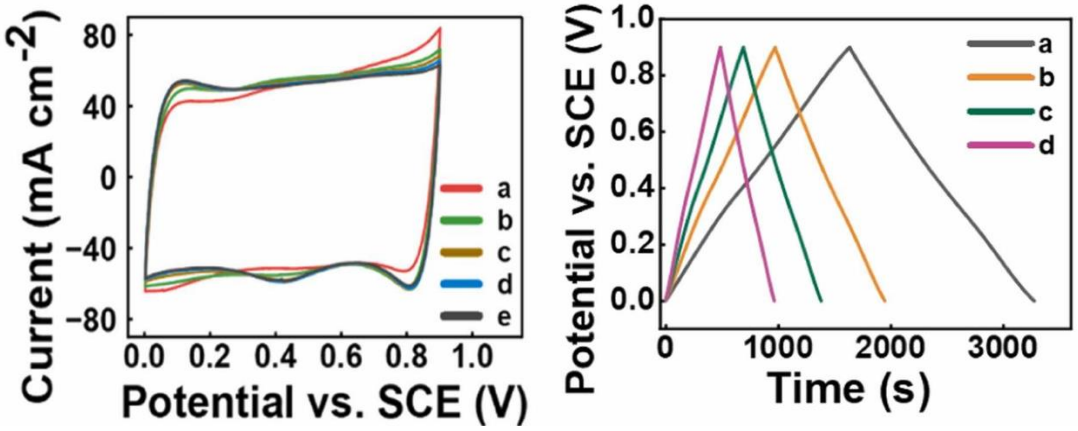

Figure 2.9 Ideal CV and CD behaviour of an MnO_2 pseudo-capacitor electrode [11]. Reproduced (adapted) with permission from M. Awad, I. Zhitomirsky, Boosting the activation rate and capacitance retention of MnOx electrodes prepared using capping agents, Colloids and Surfaces A: Physicochemical and Engineering Aspects, Elsevier, 676 (2023).

We can see that the ideal behaving pseudocapacitor electrodes display box-like shape for the cyclic voltammetry curve, and triangular chronopotentiometry (charge-discharge) behaviour. This is because the pseudocapacitor in this case is displaying electrochemical characteristics similar to an ideal capacitor whose capacitance is independent of the change in potential when the rate of change in potential is constant. For this reason, a relatively symmetrical current response can be observed in the CV of Figure (2.9) as the current response should remain constant

throughout the potential range. The same can be said for the charge discharge curve, the rate of change of potential should not change over time when a constant current is applied, this is why the symmetrical triangular shape is present, because the slope of the line should remain constant throughout the time is takes the electrode to be charged up to 0.9 V and discharged back down to 0 V.

Recently pseudocapacitive electrode systems have been developed using bimetallic transition metal oxide materials because single metal oxides (such as those listed above) suffer from poor conductivity which lowers the faradaic efficiency of the cell due to increased resistance at the electrodes. Examples of materials used to increase conductivity in pseudocapacitive systems are Ni, Cu, Co, Fe and Mn for certain systems like, $NiFe_2O_4$, $CuFe_2O_4$, and $MnFe_2O_4$. However, transition metal oxide based electrochemical capacitors suffer from poor ionic transport in the bulk of the electrode especially at higher mass loadings and scan rates, which are crucial for practical applications that require higher energy densities [12].

2.4 High active mass loading issues with Pseudo Capacitor technology

High active mass loading greater than 10 mg cm^{-2} is critical for practical high energy density applications of PC devices as the amount of redox active sites increases with increasing mass of active materials. The main challenge with high active mass is that the ions in electrolyte have trouble reaching and interacting with those redox active sites. This can be for several reasons such as: structure, morphology, size of ion, and scan rate (or adsorption and desorption rates).

The challenge with ion intercalation in high active mass loaded electrochemical capacitors can be represented by Figure 2.10. It shows that the ions can intercalate with relative ease for thin film (or low mass loading capacitors) but has more trouble fully intercalating with high active mass loading, creating a 2-capacitors in series effect. When 2 capacitors are placed in series the total capacitance is $\frac{1}{C_{total}} = \frac{1}{C_1} + \frac{1}{C_2}$ (a version of this is shown in Eq. 2.18) and is further reduced at higher scan rates where the intercalation of ions is scarce closer to the current collector creating regions of high charge density and low charge density. The areas with high charge density possess larger capacitance values than those without ions meaning that C2 > C1, when added in series the total capacitance is dominated by the region with a lower capacitance value and drastically reduces the total capacitance at high scan rates causing significant loss in capacitance retention. For this reason, it is critical to ensure an even distribution of ions throughout the active material for the best performance [13].

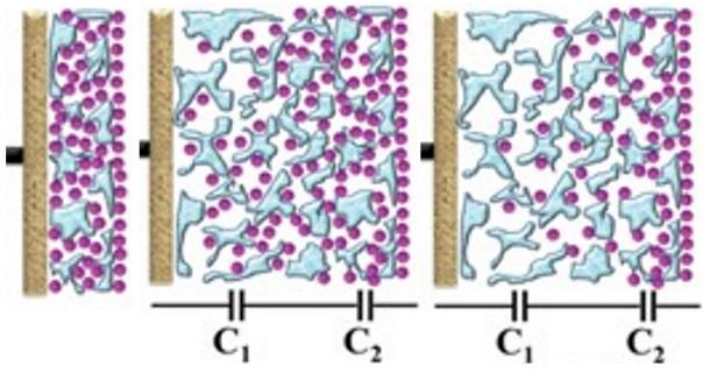

Figure 2.10 intercalation in electrodes at low mass loading and low scan rate, high mass loading and low scan rate, and high mass loading and high scan rate [13]. Reproduced (adapted) with permission from R. Chen, M. Yu, R.P. Sahu, I.K. Puri, I. Zhitomirsky, The Development of Pseudocapacitor Electrodes and Devices with High Active Mass Loading, Advanced Energy Materials, John Wiley and Sons 10(20) (2020).

A variety of techniques can be utilized to enhance ionic intercalation including nanomaterials preparation techniques, use of dispersing and capping agents, template methods, hetero-coagulation methods, surface modification and novel synthesis techniques. Nanomaterials have enhanced electrochemical characteristics due to their small particle size which increases the surface area to volume ratio for individual particles can be increased allowing for enhanced interaction with ions in electrolyte. By creating active materials using nanoparticle synthesis techniques like hydrothermal synthesis and electrosynthesis one can tune the shape, size and crystal structure of the active materials to further enhance the electrochemical properties. This is why the same material will store energy differently depending on the phase of material. An example of this is the study conducted by S. Devaraj and N. Munichandraiah [14]. showing that varying phases of MnO_2 have an impact on electrochemical properties when used as a pseudocapacitor electrode. MnO_2 has 5 different phases: α, β, γ, δ and λ each with their own unique arrangement of the crystal structure.

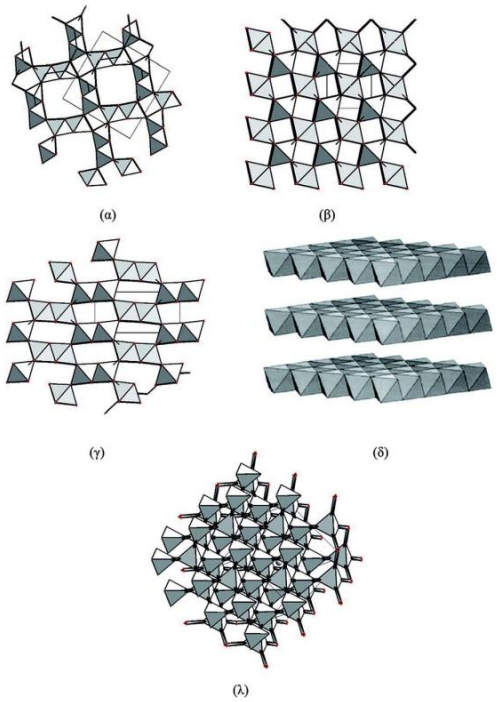

Figure 2.11 Varying phases of MnO_2 (α) (β) (γ) (δ) (λ) [14]. Reproduced (adapted) with permission from N.M. S. Devaraj, Effect of Crystallographic Structure of MnO_2 on Its Electrochemical Capacitance Properties, J. Phys. Chem. C 11 (2008) 4406-4417. Copyright 2008 American Chemical Society.

The study found that the electrochemical properties of MnO_2 were heavily impacted by the size of the spaces (or tunnels) in each crystal phase. These tunnels function as passageways for the ions in the electrolyte to intercalate and interact with electrochemically active sites of the material. The MnO_2 phases that possess large tunnels and interlayer separation were reported to possess higher specific capacitance owing to easy and fast ion intercalation kinetics. Additionally, each phase contains unique specific surface area quantities where the larger surface areas display better capacitive performance as there is more electrochemically active sites that can be accessed by ions when the ratio of surface area to volume is high. By selecting for specific phases in various

materials (with considerations for ionic and electronic conductivity) one can maximize the intercalation aspects of a material which is crucial for high active mass loaded electrodes.

2.5 High Energy Ball Milling

After synthesis, nanoparticles can still suffer from agglomeration effects on the macroscale, diminishing the benefits provided by the nanocrystal structure synthesized. Popular techniques to reduce agglomeration are mechanical deformation techniques like HEBM. This technique utilizes hardened spheres of varying size and mass to either crush or grind the sample materials, where the density, mass, radius of grinding media and speed at which the high energy ball milling are important factors contributing to grinding or crushing outcome.

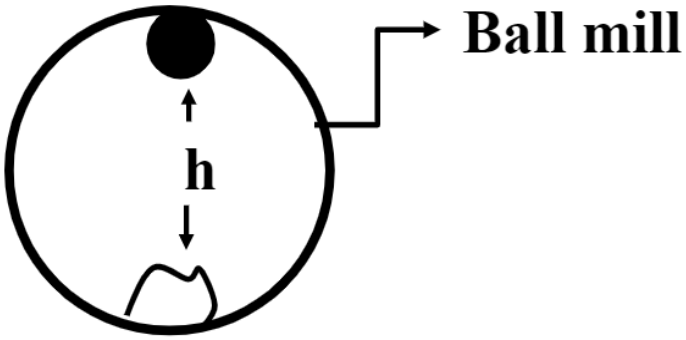

Figure 2.12 Schematic of HEBM procedure showing grinding media and sample material [15].

The grinding media has crushing and grinding effects depending on the size of the balling milling media and sample materials. Usually, the larger and heavier balls are used for crushing particles and drastically reduce the size of particles and presence of agglomerates. A smaller diameter of ball milling media will have more of a grinding effect which changes the surface morphology characteristics of particles. The use of the nanomaterials preparation techniques has

been shown to enhance electrochemical performance of active materials. Additionally, the use of dispersing agents, conductive additives and forming composite electrodes can drastically improve the performance of high active mass loaded electrodes and will be discussed in further detail in the next 3 individual sections [15].

2.6 Multiwalled Carbon Nanotubes

To compensate for the large resistivity of high active mass loaded electrodes, conductive additives can be used. As in the research contained in this thesis around 80% of the mass of the electrode is comprised of the active material and 20% is the conductive additive (ignoring the 3% PVB binder). One of the most effective conductive additives to use are carbon nanotubes. Graphene sheets are carbon atoms bonded covalently in a hexagonal pattern via sp^2 hybridized bonds. The sp^2 bonds are responsible for superb mechanical, chemical and electrical properties of graphene allowing for high tensile strength, chemical stability and high conductivity. Delocalized pi electrons can move freely throughout the graphene structure allowing for incredibly high electronic conductivity on the order of S/m, several orders of magnitude higher than single and bimetallic oxides. Carbon nanotubes are thin sheets of single layer graphene rolled concentrically around a common axis as seen in Figure 2.13 [16].

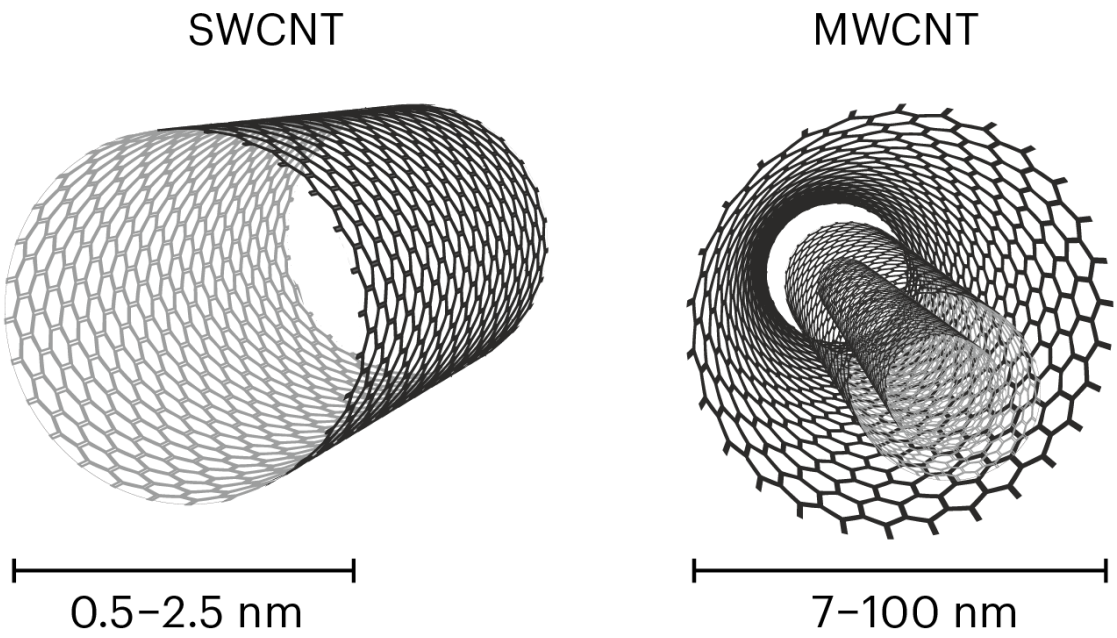

Figure 2.13 Single walled carbon nanotubes and multiwalled carbon nanotubes [17].

They possess great chemical stability and mechanical strength in a wide range of media owing to their strong covalent bonds. Additionally, they have great electronic conductivity on the scale of graphene. Carbon nanotubes can be manufactured in several ways including arc vapor deposition, and pulse laser vapor deposition. The nanotubes can be grown in single tube structure or multi walled structures. Single layer carbon nanotubes are more difficult to grow than multi walled carbon nanotubes and require expensive substrates along with lengthy selective growth processes making them uneconomical for large scale manufacturing of high active mass loaded electrochemical capacitors. For this reason, the focus for this section will be multi walled carbon nanotubes (MWCNTs).

MWCNTs consist of 2 or more concentrically rolled graphene layers with varying radii. When successfully mixed with electrochemically active material such as MnO_2 they can drastically reduce the impedance of the electrode. Metal oxides have high resistance due to the oxygen atoms which are poor conductors of electrons compared to pure metals but are more electrochemically active than their pure counterparts. When carbon nanotubes are present, they can transfer electrons to and from the external circuit more effectively allowing for superior charge transfer efficiency of the device [12]. There needs to be appropriate compensation made with carbon nanotubes as it is replacing a percentage of the active material so that the increase in electronic conductivity matches the decrease in electrochemical activity.

For this to be an effective improvement strategy the MWCNTs must be evenly distributed throughout the electrode structure. Difficulties arise in this area due to MWCNTs affinity for forming bundles due to π-π stacking interactions. The delocalized π electrons in MWCNTs will interact with each other and begin to agglomerate, this can be mitigated via ultrasonication in organic solvents like ethanol. The frequency of the ultrasonication machine will agitate the bundles of MWCNTs causing them to unravel [18]. This is a temporary solution as they will begin to form bundles again overtime in solution. Specialized molecules called dispersing agents can be used to prevent the agglomeration of carbon nanotubes after ultrasonication, promoting stable suspensions for greater time scales. Furthermore, certain molecules can effectively disperse both organic and inorganic particles promoting an even mixture of MWCNT conductive additives and electrochemically active inorganic particles. These molecules come in many forms and can mimic the adsorption qualities of living organisms and biological systems, referred to as bio-mimetic catecholate dispersing agents and will be discussed in greater detail in the next section.

2.7 Biomimetic Catechol Based Dispersing Agents

In nature many organisms use binding molecules to adhere to surfaces in their environment. One such example is the mussel which uses ligand molecules with catechol groups that attach to rocks to prevent being swept away by strong currents. Generally, ligands are molecules containing functional groups that absorb metal atoms. In this case mussels employ ligands that possess hydroxyl (OH) functional groups which facilitate adsorption on common inorganic elements found in rocks like iron, calcium and magnesium [19].

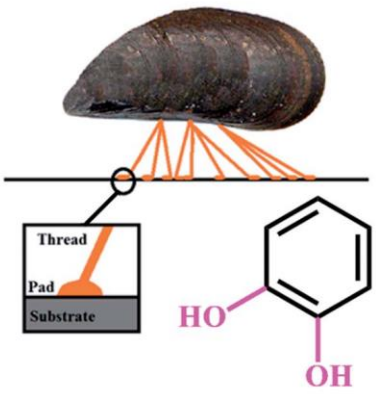

Figure 2.14 adsorption mechanism of mussels on to inorganic substrates in nature using catechol molecules[19]. Reproduced **(**adapted) with permission from M.S. Ata, Y. Liu, I. Zhitomirsky, A review of new methods of surface chemical modification, dispersion and electrophoretic deposition of metal oxide particles, RSC Advances 4(43) (2014).

The benzene ring with adjacent hydroxyl groups is called the catechol molecule. The catechol adsorption mechanism is paramount for proper dispersion of metal oxide particles. Once adsorption occurs the aromatic rings will keep other inorganic particles away from each other

either sterically (using long carbon tails) or electro statically with charged functional groups. Organic particles will also be dispersed via interaction with the π electrons of the aromatic rings which will keep carbon nanotubes from forming bundles via π stacking interactions. Carbon nanotube dispersion can be promoted via sonication, covalent dispersion mechanisms and non-covalent dispersion mechanisms. Covalent dispersion mechanisms rely on the functionalization of carbon nanotubes via popular functionalization routes such as acidic oxidation that add oxygen rich functional groups such as carboxylic, carbonyl and nitric acid groups to the CNT structure that promote the repulsion between carbon nanotubes. However, the functionalization of carbon nanotubes diminishes the number of sp^2 bonds in the carbon nanotube structure, impeding the free motion of π electrons thus hindering the electronic conductivity and mechanical properties of the CNTs [20, 21]. Non-covalent dispersion takes advantage of the hydrophobicity of carbon nanotubes by using polymers with both hydrophobic and hydrophilic tails to perform adsorption and dispersion functions respectively. The main drawback of this approach is the wrapping of the polymer chain around the carbon nanotube structure which will not only facilitate dispersion but also form an insulating barrier, reducing the effectiveness of CNTs as conductive additives[22].

Improving the stability and dispersion qualities of active material suspensions is essential to the development of high active mass loaded electrode because dispersing agents facilitate an even distribution of active mass and conductive additives. Dispersing agents also reduce the formation of agglomerates within the active material, counteracting the thermodynamic effects of surface energy minimization, which drives materials towards forming larger agglomerated particles. As a result of this, the active surface area of the material can be maximized. There is a myriad of catechol based dispersing agents being investigated for their dispersion qualities as seen in Figure 2.15.

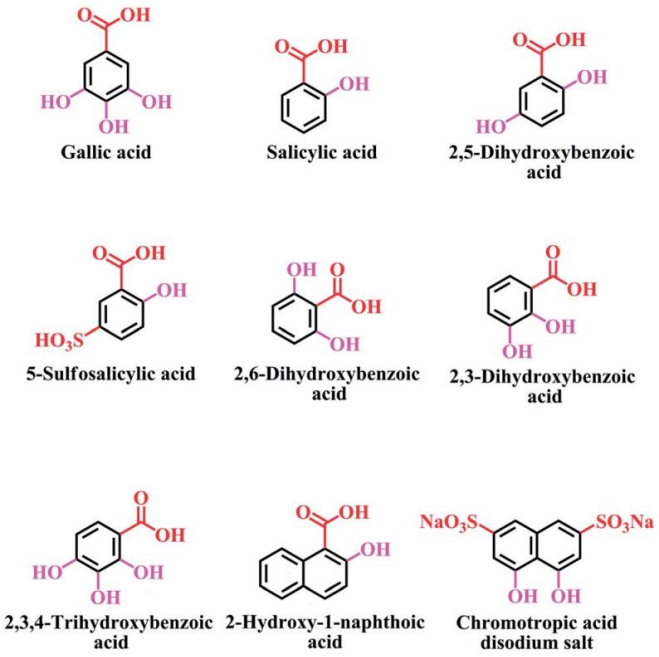

Figure 2.15 Shows the structure of various catechol dispersing agents [19]. Reproduced (adapted) with permission from M.S. Ata, Y. Liu, I. Zhitomirsky, A review of new methods of surface chemical modification, dispersion and electrophoretic deposition of metal oxide particles, RSC Advances 4(43) (2014).

2.7.1. DLVO Theory

Dispersing agents take advantage of DLVO theory which describes the forces governing charged particles in colloidal suspensions. This theory simply states that sufficiently small particles in suspension that possess too low of a mass to be significantly impacted by gravitational forces, instead are impacted largely by electrostatic forces; the Van der Waals attraction forces and surface charge repulsion forces[23]. This can be summed up by one simple equation which states that the total energy of the interaction between two particles with identical charge is:

$$V_T = V_A + V_R \qquad \text{Eq. (2.33)}$$

Where V_T is the total energy, V_A is the energy associated with the Van der Waals attraction force and V_R is the energy associated with the repulsive force produced by identical surface charges.

Each chemical element has a unique surface charge associated with the formation of a suspension in solvent media, this surface charge is heavily dependent on the pH of the solution and can switch between positive and negative according to the pH of the solution. Switching sign of charge assumes that there is a point where the pH of the solution will result in a neutral charge on the particles in suspension, this is called the isoelectric point and is unique to each material [24].

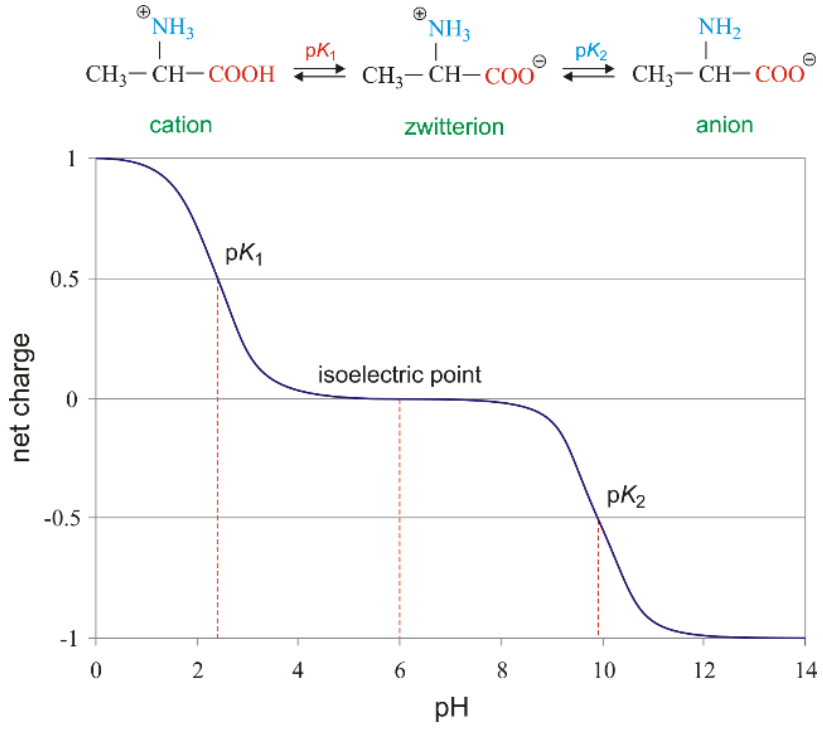

Figure 2.16 The state of charge of alanine as a function of pH [25].

Surface charge arises initially in particles placed into solvent media due to many factors such as dissociation of charged species, substitution of charged species, and the adsorption/desorption of ions present in the solvent. For polar aqueous media such as water, the charge of the solute

particle will induce an attraction force on the surrounding polar molecules, forming a solvation sheath. The solvation sheath can be schematically represented as a cloud of point charges surrounding a particle with opposite charge such that the charge density is symmetrical in three dimensions forming a spherical distribution of charged particles as seen in Figure 2.17 [4].

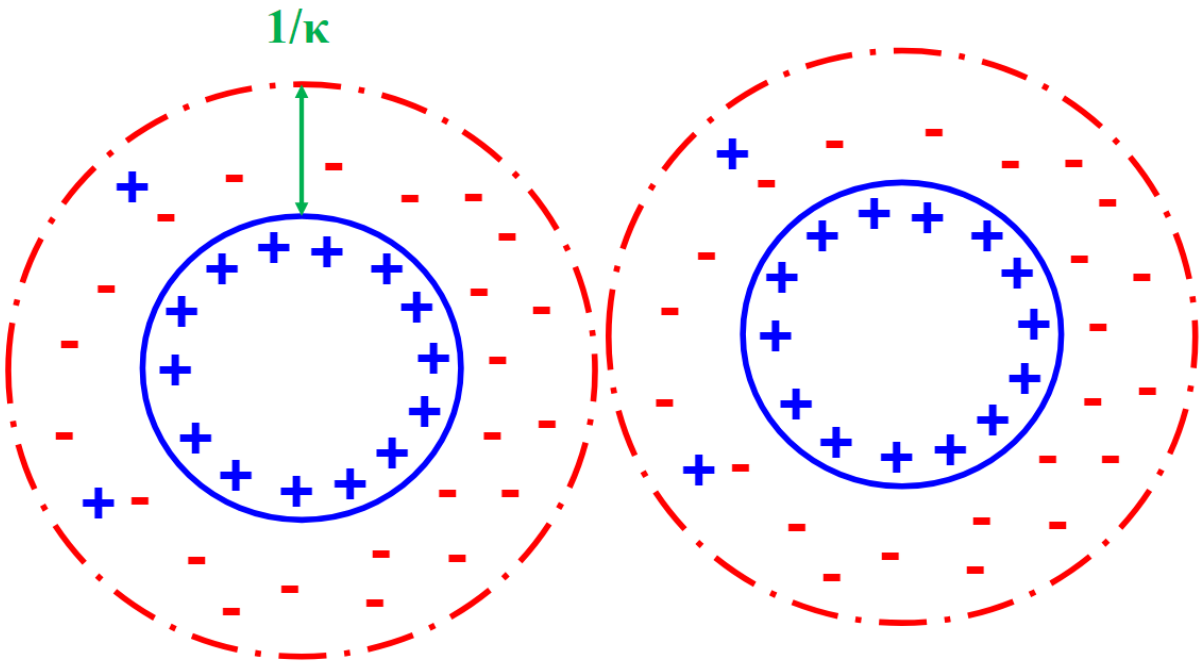

Figure 2.17 2 dimensional representation of solvation shells forming double layers of opposite sign for two particles with identical charge suspended in aqueous media [26].

Notice the term 1/k in Figure 2.17 this term represents the Debye length of a charged particle in solution, the Debye length expresses the extent of effective charge screening from the solvation sheath or double layer originating from the cloud of point charges surrounding a charged particle of opposite sign. The effective distance at which screening occurs is dependent on the electrostatic potential generated by the charged cloud such that the Debye length occurs at a distance $X =$

$\frac{1}{k}$ where the local electric flux (ϕ) is reduced to $\frac{1}{e}$ of its initial value at the surface of the charged solute particle [4, 26].

$$\phi = \psi e^{-kx} \qquad \text{Eq. (2.34)}$$

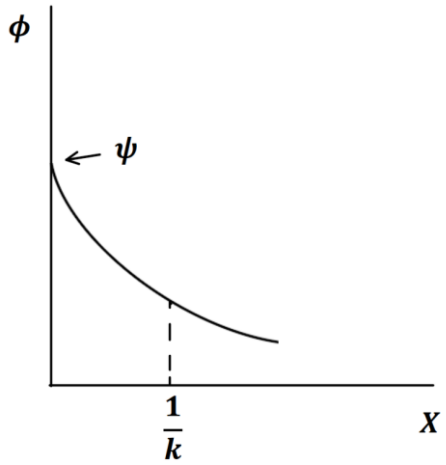

Figure 2.18 Flux vs distance diagram of a charged particle [26].

The Debye length can be defined mathematically as:

$$\frac{1}{k}\ where\ k = \frac{(e_o^2 \sum n_i z_i^2)^{\frac{1}{2}}}{\varepsilon \varepsilon_o KT} \qquad \text{Eq. (2.34)}$$

Here we can see that the value of k is the square root of the sum of charges n_i (concentration of ions or number of ions) and z_i^2 (valence state of the ions) multiplied by the charge of an electron e_o^2, and divided by the dielectric permittivity of the charged cloud $\varepsilon\varepsilon_o$, and Boltzmann constant K at a temperature T of the solution. The Debye length is important because it describes the distance that charged particles will begin to form soft and eventually hard flocculates (or agglomerates) due to Van der Waals attraction forces. It can be observed from Eq.

(2.34) that the Debye length decreases with increasing electrolyte concentration and more drastically with increasing valence state [26].

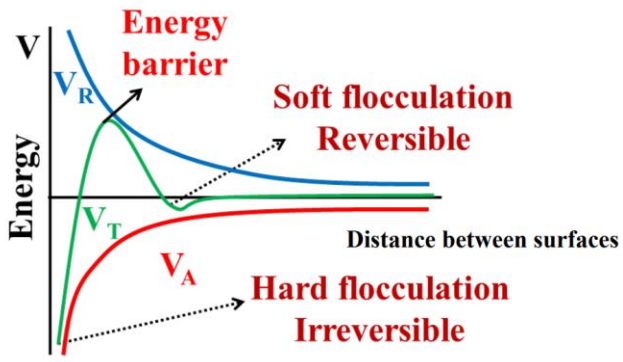

Figure 2.19 Hard flocculation (agglomeration) and soft flocculation in relation to the attractive and repulsive energies as a function of the distance between two spherical point charges [26].

Biomimetic dispersing agents take advantage of colloidal suspension principles by forming various bonds with the surfaces of charged particles such as chelating, and bridging bond types which essentially increases the energy barrier between soft and hard flocculation regions. The better the dispersing agent is at forming bonds with metal cations the larger the repulsive energy barrier is, thus making it difficult for particles to form agglomerates [19].

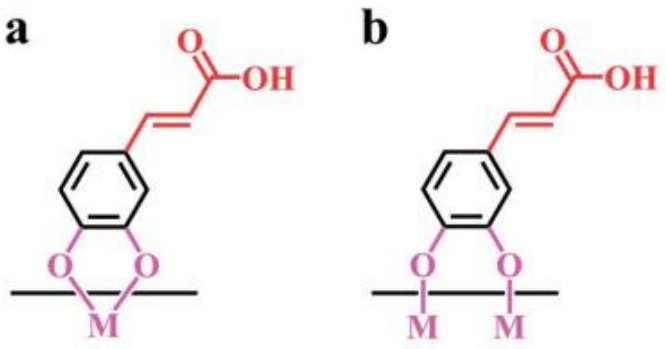

Figure 2.20 shows an example of a) chelating and b) bridging mechanisms for catechol bonding [19]. Reproduced (adapted) with permission from M.S. Ata, Y. Liu, I. Zhitomirsky, A review of new methods of surface chemical modification, dispersion and electrophoretic deposition of metal oxide particles, RSC Advances 4(43) (2014).

It is important to note that certain kinds of dispersing agents possess charged functional groups that repel other particles in suspension that possess like charges from the dispersing agent adsorption. One such molecule is called gallocyanine dye which possesses a secondary amine group located opposite to that of the catechol group. In solution the nitrogen carries a positive charge and will repel other gallocyanine molecules. Additionally, functional groups present in dispersing agents and that of gallocyanine specifically, are hypothesized to be responsible for charge transfer mediation in redox reactions as seen in Figure (2.21).

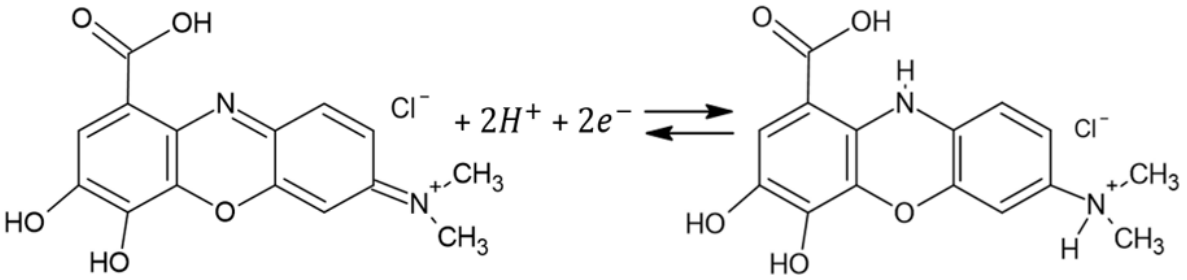

Figure 2.21 Redox reaction of gallocyanine.

2.8 Pseudocapacitive Conducting Polymers

Pseudocapacitors utilizing conducting polymers provide several advantages over other pseudocapacitive materials, including low cost, high specific energy and power, superior conductivity, lightweight design, and improved flexibility. Among all conductive polymers that can be applied for electrochemical energy storage application, polypyrrole, polyaniline, polythiophene and poly(3,4-ethylenedioxythiophene) have garnered lots of attention recently. The structure of these polymers is shown in Figure 2.22 below. These conjugated materials are ideal candidates for energy storage due to their accessible redox sites, controllable mechanical properties, and facile chemical synthesis avenues. Compared with other pseudocapacitive conducting polymers, these materials do not require a very high surface area[27].

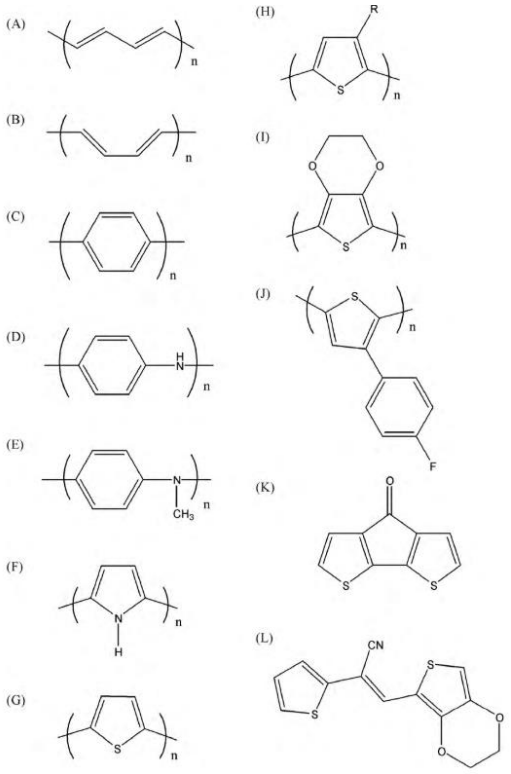

Figure 2.22 Structures of pseudocapacitive polymers (A) Trans-poly(acetylene)(B) cis-poly(acetylene) (C) poly(p-phenylene) (D) polyaniline (PAni) (E) poly(n-methyl aniline) (PNMA) (F) polypyrrole (PPy) (G) polythiophene (PTh) (PEDOT), (H) 3-substituted polythiophene (I) poly(3,4-ethylenedioxythiophene) (J) poly(3- (4-fluorophenyl)thiophene) (PFPT) (K) poly(cyclopenta [2,1-b;3,4-b-dithiophen-4-one]) (PcDT) (L) 1-cyano-2-(2-[3,4-ethylenedioxylthienyl])-1-(2-thienyl)vinylene (PThCNVEDT) [27]. Reproduced (adapted**)** with permission from G.A. Snook, P. Kao, A.S. Best, Conducting-polymer-based supercapacitor devices and electrodes, Journal of Power Sources 196(1) (2011) 1-12.

Conducting polymers store and release charge via fast reversable redox processes similar to other pseudocapacitive materials like MnO_2. Unlike activated carbons, where charge and discharge phenomena predominantly occur on the surface in the electrical double layer, conducting polymer films can facilitate these processes throughout their bulk volume at electrochemically active sites. This characteristic presents an opportunity to achieve high specific capacitance levels. Electron insertion into the conduction band through n-doping (reduction) and removal of an electron from the valence band via p-doping (oxidation) increases the charge carrier concentration

in these polymers. Equation 2.35 illustrates a typical n-doping reaction, while Equation 2.36 demonstrates p-doping using an undoped conducting polymer chain (CP), an oxidant (Ox), a reductant (Red), a counter anion (A^-), and a counter cation (C^+).

$$CP + nRed - (C^+)_n CP^{n-} + nRed^+ \qquad \text{Eq. (2.35)}$$

$$CP + nOx - (A^-)_n CP^{n+} + nOx^- \qquad \text{Eq. (2.36)}$$

In addition, the charging mechanism of conducting polymers can be illustrated by Figure 2.23. The external circuit will provide electrons to be transported onto the polymer backbone and the cations from solution will be inserted in the polymer to maintain charge neutrality[28].

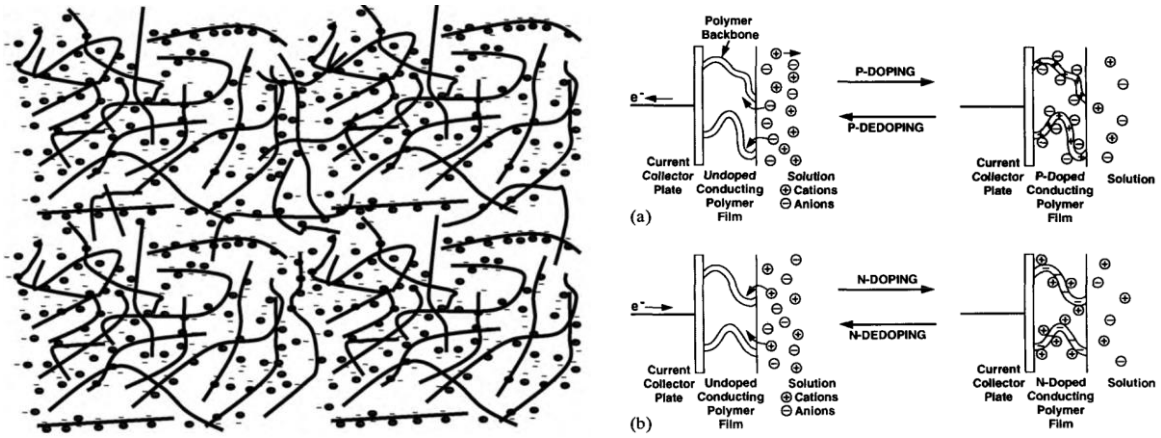

Figure 2.23 intercalation of cations in the porous structure of a pseudocapacitive polymer via p and n doping mechanism [27, 28]. Reproduced **(**adapted) with permission from G.A. Snook, P. Kao, A.S. Best, Conducting-polymer-based supercapacitor devices and electrodes, Journal of Power Sources 196(1) (2011) 1-12 and J.D. Andy Rudge, Ian Raistrick and Shimshon Gottesfeld, John P. Ferraris Conducting polymers as active materials in electrochemical capacitors, Journal of Power Sources 47(1-2) (1994) 89-107, respectively.

Conductive polymers operate within a defined potential window for effective charge transfer. Exceeding this range can lead to degradation at higher positive potentials, while excessively negative potentials can cause the polymer to transition to an insulating state (undoped

state). In an aqueous, pH-neutral electrolyte with an inert electrode, water splits into oxygen at approximately 1 V vs Ag/AgCl and hydrogen at around -0.3 V vs Ag/AgCl. To mitigate this, the safe operational range for a symmetric aqueous device is typically confined to 0.6 to 0.8 V to maximize device longevity. Certain electrode materials can suppress hydrogen or oxygen evolution depending on their specific interactions at the material surface. For instance, PANi tends to be positively polarized, while PEDOT is negatively polarized relative to the Ag/AgCl reference electrode.

Polypyrrole (PPy) provides significant advantages in electrochemical processing, primarily due to its flexibility and high density, resulting in a high capacitance per unit volume (400–500 F cm^{-3}). The synthesis of PPy can be achieved through chemical or electrochemical methods. Electrochemical synthesis relies on electrode reactions as the driving force, whereas the chemical method utilizes oxidants to initiate polymerization.

The polymerization of pyrrole is catalyzed by acids, which protonate the pyrrole ring at the α, β, or N positions. This protonation disrupts the aromaticity of the ring and facilitates oxidation to form a radical cation. The radical cation then undergoes a chain-growth mechanism by reacting with additional pyrrole monomer molecules. As the concentration of monomers decreases over time, polymerization slows down and eventually stops when two radical cations in solution combine to terminate the process. This stepwise mechanism allows for controlled growth of the polypyrrole chain during its synthesis [29].

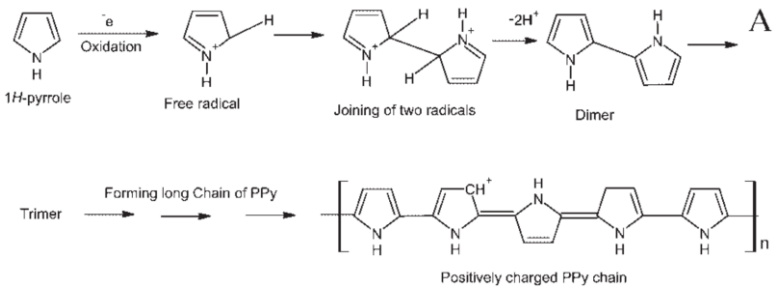

Figure 2.24 oxidation of the pyrrole monomer using an acid to achieve polymerization of polypyrrole [29]. Reproduced (adapted) with permission from S. Goel, N.A. Mazumdar, A. Gupta, Synthesis and characterization of polypyrrole nanofibers with different dopants, Polymers for Advanced Technologies 21(3) (2009) 205-210.

Anions like Cl^- and SO_4^{2-} that associate with polypyrrole (PPy) chains are classified as dopants. Understanding the polarization mechanism of PPy remains a contentious issue, along with this, due to its rapid polymerization and non-crystalline structure, determining the reaction stages through structural characterization and analysis of physical properties presents significant challenges[27].

Achieving high specific capacitance in conducting polymers can be facilitated by increasing the doping level. Numerous studies have concentrated on advancing anionic dopants specifically for polypyrrole (PPy). Research indicates that varying the dopant anion can lead to significant differences in PPy conductivity, sometimes varying by up to three orders of magnitude [27]. This variability underscores the importance of selecting appropriate dopants to optimize the electrical properties of PPy for various applications in energy storage and beyond. In addition to influencing conductivity, dopants can enhance several other properties of polypyrrole (PPy), including thermal stability, surface morphology, and mechanical strength. Studies on aromatic dopants containing sulfonic anionic groups have demonstrated that the conductivity of PPy films rises with an increase in the charge-to-mass ratio of the dopant molecules. Given these findings,

there is significant interest in developing advanced dopants to achieve high electrochemical activity in PPy for energy storage applications. These efforts aim to optimize PPy's performance across various parameters critical to its application in electrochemical energy storage. However, the primary drawback of conducting polymer electrodes is their lack of long-term stability, which is compromised by swelling and shrinking during the intercalation and deintercalation processes during charging and discharging cycles. During charging and discharging cycles ions are forced into the pores of the electrode, this intercalation imposes a stress on the active material and causes the structure to expand and contract throughout intercalation and deintercalation respectively. The stress imposed on the electrode is exacerbated at high charge-discharge rates as the ion intercalation and deintercalation occurs more rapidly, resulting in swelling that can cause permanent structural changes in the electrode active material leading to significant loss of capacitance. Pseudocapacitive polymers are especially vulnerable to this form of failure and previous research indicates that electrodes based on conducting polymers can degrade significantly in fewer than a thousand cycles [27].

However, studies have shown that the cycle stability of polypyrrole (PPy) can be enhanced through structural modifications, improvements in morphologies of PPy films, and the development of composite materials, especially with magnetic materials. Tang et al., developed PPy composite electrode with ferrimagnetic materials and enhanced electrode stability by spontaneous magnetic field [30]. These strategies aim to mitigate the mechanical stresses and volume changes that occur during charge-discharge cycles, thereby improving the overall durability and lifespan of PPy-based electrodes in EC applications.

2.9 Electrochemical Capacitor Electrolytes

The electrolyte is a crucial component of electrochemical capacitors as it facilitates the transportation of charged ionic species to the surfaces of electrodes so that both faradaic and non-faradaic reactions can occur. For the electrolyte to be effective it must have high ionic conductivity and mobility so that the reactions kinetics will not be impeded by slow mass transport. Additionally, it should possess low electronic conductivity to prevent a short circuit between the cathode and anode of the cell (which is aided by the separator). Electrolytes need to be chemically stable in a wide potential range as the capacitance of a device is directly correlated to the operating voltage. If the electrolyte is only stable in a limited window of potential ranges, then it will break down or "dry up" by reacting irreversibly with the electrodes when safe operating range is exceeded [31].

Along with this the electrolyte must be stable in its given voltage window over the cycle life of the electrochemical capacitor which for certain EC technology can be on the scale of $> 10^6$ cycles. Furthermore, electrolytes need to be scalable as energy storage systems come in a wide range of sizes and are meant for mass production. Part of the scalability is the cost associated with manufacturing the electrolyte and placing it into these EC systems. Factors that impact cost are supply chain of required chemicals, the environmental friendliness and especially the toxicity of the electrolyte as the more dangerous (i.e. caustic and flammable) an electrolyte is, the more research efforts need to be invested to prevent any leak of the electrolyte by adding extra protection. Electrolytes can be categorized into aqueous, acidic, alkaline, neutral, organic, polymer and ionic liquids[4, 32]. Each electrolyte possesses varying magnitudes of dielectric constant and viscosity which play vital roles in dissolution and mass transport of charged species. The dielectric

constant is a materials property which describes the degree to which a specific material is polarized in the presence of an electric field relative to free space and is very heavily corelated to the performance of electrolytes.

2.9.1. Aqueous Electrolytes

Aqueous electrolytes are commonly water-based electrolytes with varying concentrations of dissolved ionic species in them. Aqueous electrolytes can be categorized as neutral, acidic and basic electrolytes. Water is a good solvent for electrolyte molecules due to its permanent dipole structure which forms solvation shells around the dissolved species. The strength of water's permanent dipole (and dielectric constant) along with its environmental friendliness makes it a great candidate for energy storage devices. Aqueous electrolytes possess high ionic mobility which increases the mass transport kinetics of solvated ions and will increase the interactions between active materials of the electrodes with charges species. Despite being a widely available resource, easily manufacturable and regarded as the universal solvent, water is not stable in a wide potential range due to a breakdown voltage of 1.23 V. When a voltage of 1.23 V is applied across the electrodes in an electrochemical cell containing an aqueous electrolyte, water will be electrolyzed causing it to breakdown into H_2 and O_2 on the surfaces of the cathode and anode respectively. This will not only dry up the electrolyte over time, but the gaseous bubbles formed on the surface of the electrodes impede the mass transfer of solvated ions, destroying the performance of the electrode. Due to this limited voltage window the energy density associated with aqueous electrolytes is lower than other available electrolytes. Additionally, aqueous electrolytes have limited temperature ranges as the ionic mobility is severely hindered at lower temperatures due to freezing effects. Conversely, they cannot be operated at higher temperatures to avoid evaporation

of water. Despite their low toxicity, aqueous electrolyte-based energy storage devices have limited applications due to low energy density. Aqueous electrolytes can be further divided into acidic, neutral and basic type electrolytes [32].

$$Na^{+}_{solid}Cl^{-}_{solid} = Na^{+}_{aq.} + Cl^{-}_{aq.} \qquad \text{Eq. (2.37)}$$

Equation 2.9.1-1 shows a simple aqueous sodium chloride electrolyte being dissolved in water [4].

2.9.2. Aqueous Electrolytes – Acidic Electrolytes

Acidic electrolytes are those which contain a surplus of protons such as sulfuric acid (H_2SO_4) which possesses high ionic conductivity, but strong acids required for strong ionic conductivity are corrosive and dangerous to work with[33]. There is also the possibility of acid leaking out when the device has become damaged which can have significant environmental and safety impacts. To combat the corrosivity of H_2SO_4, it can be blended with higher concentration of inorganic salts like potassium nitrate (KNO_3) which reduce the corrosive effects of the electrolyte[32].

2.9.3. Aqueous Electrolytes – Alkaline Electrolytes

Alkaline electrolytes have more proton acceptor molecules than donors, making them basic solutions with high ionic conductivity. KOH is widely used as an alkaline electrolyte for EDLC supercapacitor electrodes for the small ionic size of K^+ and its high ionic conductivity [33]. Similarly to their acidic counterpart, alkaline electrolytes also possess harmful corrosion and toxicity properties that can lead to difficulty in handling and manufacturing[32].

2.9.4. Aqueous Electrolytes – Neutral Electrolytes

Neutral electrolytes are composed of equally balanced proton donator and acceptor species, a popular example of this is Na_2SO_4 which dissolves into Na^+ and SO_4^- in water [33]. Neutral electrolytes have the lowest conductivity of the three (acidic, alkaline and neutral) which results in lower capacitance but higher energy density due to increased stability in a wider potential window, additionally, due to its neutral pH it possesses the lowest corrosion properties as well, making it a safer more environmentally friendly option than acidic and alkaline electrolytes [32].

2.9.5. Organic Electrolytes

Organic electrolytes are a popular alternative to aqueous as they are more stable in a much wider potential range up to 4 V (larger than the 1.23 – 1.5V of aqueous kind). Due to this large potential window organic electrolytes have much higher energy densities than aqueous electrolytes. Organic electrolytes possess high concentration of solvated ions but suffer from low dielectric constant and ionic mobility properties limiting effectiveness for use in pseudocapacitive energy storage devices. Contributing to this is the large size of ions for OEs, slowing their motion in an electric field as well as making it difficult for them to properly interact with the active material through intercalation phenomena. To combat this, pore optimization processes where the structure of the active material is changed through novel nanomaterials synthesis techniques can be employed. Another way to combat this is to use dissolved salts with much smaller sized ions such as lithium-based salts (LiPF, and LCO). Electrolyte aging is a key drawback of organic electrolytes causing the electrolyte to oxidize the surface of the electrode material forming a permanent oxide film which lowers the faradaic efficiency significantly over many cycles if it is not stabilized [4, 32].

2.9.6. Polymer Electrolytes

Polymer electrolytes come in two main forms quasi solid or gel and solid based electrolytes. Polymer gel electrolytes have a jelly-like consistency and is why cylindrical energy storage devices are called jelly rolls. It is a popular form of electrolyte widely used in batteries and supercapacitors alike. The quasi-solid state and solid state of the polymer electrolyte allow for greater physical stability properties than the previously mentioned electrolytes as there is a lower risk of the polymer spilling out if damaged in the jelly state and it becomes a flexible electrolyte in its solid state. In addition to benefits from flexibility, polymer electrolytes are operable in the widest potential windows giving them higher energy density characteristics. However, they have the lowest ionic mobility of electrolytes due to their quasi and solid physical states which impede the motion of ions in the electrolyte. A tradeoff for this drawback is that the GPE and SPE can be used as both the electrolyte and separator for electrochemical capacitors as in the case for PVDF based polymer electrolytes. SPEs and GPEs alike have greater operating temperature ranges than other forms of electrolytes as there is little risk of evaporation with quasi and fully solid-state materials. Because of this there is less impact on ionic mobility at low temperatures too [32].

2.9.6 Ionic Liquid Electrolytes

Ionic liquid electrolytes referred to as water in salt as well as molten salt electrolytes take advantage of extremely high concentrations of very soluble ionic salts to facilitate charge transfer in faradaic processes. They require salts with low melting points below 100 C and high solubility so that high concentrations in water can be achieved. This form of electrolyte can be described as containing an organic cation and inorganic/organic anion pairs dissolved in water. Popular

examples of this are: 1-Ethyl-3-methylimidazolium tetrafluoroborate, 1-butyl-3-methylimidazolium tetrafluoroborate and 1-butyl-1-methylpyrrolidinium dicyanamide. They are stable in a wide potential range due to the low amount of water and the strong bonds formed between ionic constituents and the solvent giving them great energy density characteristics. ILs possess low volatility and are non-flammable making them easy to manufacture and great potential candidates for mobile electronics. Most importantly they are great ionic conductors on the scale of 10^{-3} to 10^{-2} S/cm which can counteract the low ionic mobility due to high viscosity. One of the main difficulties of applicability is the melting temperature of the electrolyte as they can become solid at temperatures above 0°C greatly decreasing the ionic mobility to the point where the conductivity would no longer be able to compensate [32].

$$Na^{+}_{solid}Cl^{-}_{solid} = Na^{+}_{liquid.} + Cl^{-}_{liquid} \qquad \text{Eq. (2.37)}$$

Eq. 2.37 shows a simple example of a molten sodium chloride salt, ionic liquid electrolyte [4].

2.10 Magnetically Ordered Pseudocapacitive Materials

The magnetoelectric (ME) effect is the term used to describe the coupling of electrical and magnetic properties of certain materials, allowing the manipulation of magnetic properties through variations in the electric field, thereby controlling device functions. The discovery of magnetically ordered ferroelectrics or multiferroics has spurred significant research interest in the ME effect. Multiferroics exhibit both ferroelectric and either ferromagnetic or ferrimagnetic ordering. Abnormal phenomena, such as magnetization reversal in an electric field and polarization reversal in a magnetic field, have been observed in these materials near their ferroelectric/magnetic phase transition temperatures (Curie temperatures). However, few multiferroics exhibit both strong

magnetic and ferroelectric properties at room temperature due to their chemical composition and crystal structure, resulting in weak magnetic and ferroelectric properties.

Recent discoveries of pseudocapacitive properties in advanced spinel ferrimagnetic materials, ferrimagnetic hexagonal ferrites, and ferromagnetic perovskites have opened new research avenues in magnetically ordered pseudocapacitive materials and ME interactions. The key to advancing MOPC (magnetically ordered pseudocapacitors) devices lies in combining pseudocapacitive properties with magnetization at room temperature, thus addressing the limitations of multiferroic applications. Spinel structured ferrimagnetic materials are particularly notable for their high magnetization, modifiable: magnetization, curie temperature and conductivity via solid solutions processes.

2.10.1. Pseudocapacitive Magnetic Materials - Spinel Ferrimagnetic Materials

Spinel ferrimagnetic materials, such as Fe_3O_4, γ-Fe_2O_3, $CuFe_2O_4$, $NiFe_2O_4$, $CoFe_2O_4$, and $MnFe_2O_4$, exhibit high spontaneous magnetization at room temperature along with high pseudocapacitance. The paramagnetic cations (Cu^{2+}, Fe^{2+}, Fe^{3+}, Ni^{2+}, Co^{2+}, Mn^{2+}, Mn^{3+}) in these materials enable capacitive redox reactions and super-exchange ferrimagnetic spin ordering, offering high gravimetric specific capacitance due to their relatively low atomic mass. $MnFe_2O_4$ (MFO), for instance, demonstrates capacitive properties in both positive and negative potential ranges, with Mn^{2+} oxidizing to Mn^{3+} in the negative range and Fe^{3+} reducing to Fe^{2+} in the positive range. Similarly, the pseudocapacitive properties of $NiFe_2O_4$ (NFO) have been studied in various potential ranges. Ferrimagnetic super exchange is the phenomenon resulting from the interaction between the magnetic ordering of materials like iron and the bonds they form with oxygen. Oxygen

has 6 electrons in its valence shell, 2 of which are unpaired. According to the Pauli exclusion principle, only 2 electrons can occupy the same orbital and electrons in the same orbital must have opposing spins, either spin up or spin down. Therefore, the electrons in the two half-filled orbitals in oxygen possess antiparallel spin orientation meaning that two metal cations that form bonds with the oxygen anion will have antiparallel electron spin orientation. A crucial component of the super-exchange interaction is that the bond angle formed between two metal cations and an oxygen anion is 180 degrees, resulting in antiparallel alignment of magnetic domains, and facilitating ferrimagnetic spin ordering.

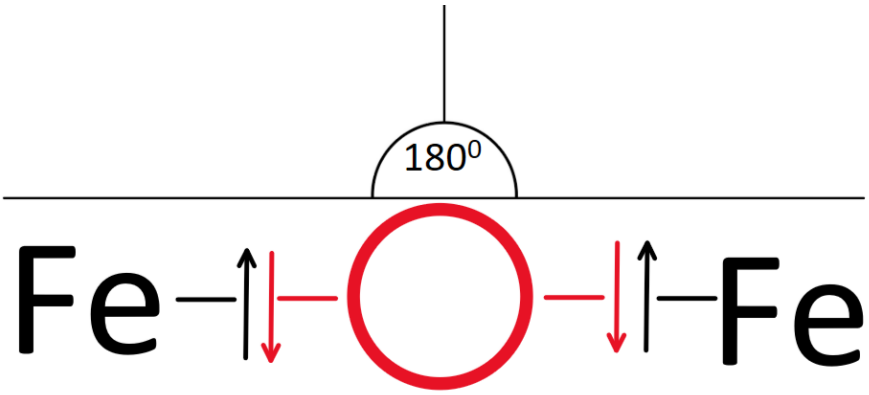

Figure 2.25 Super-exchange interaction schematic of ferrimagnetic oxide materials.

2.10.2. Hexagonal Ferrite Materials

$BaFe_{12}O_{19}$ and $SrFe_{12}O_{19}$ are key hexagonal ferrite materials for MOPC electrodes. $BaFe_{12}O_{19}$ forms oxygen defects near the Ba sites and $Fe^{2+/3+/4+}$ centers, which act as redox centers for pseudocapacitive charging, primarily in the positive range. However, high impedance due to high resistivity can be mitigated by adding conductive additives like carbon nanotubes to enhance charge transfer during redox reactions. $SrFe_{12}O_{19}$ (SFO) exhibits capacitive properties in the

negative potential range due to Fe^{3+}/Fe^{2+} redox reactions. The addition of graphene has been shown to reduce the high resistance of SFO by acting as a charge transfer mediator with high conductivity.

2.10.3. Ferromagnetic Perovskites

$La_{1-x}A_xMnO_3$ (A = Sr, Ca) perovskites hold significant potential for MOPC applications. The double exchange interaction mechanism of Mn ions in various oxidation states promotes ferromagnetic properties. Studies have shown that $La_{1-x}A_xMnO_3$ exhibits electrical conductivity of approximately 44.9 $S \cdot cm^{-1}$ at room temperature, significantly higher than other pseudocapacitive materials. This high conductivity aids in charge transfer during pseudocapacitive redox reactions. The formation of oxygen vacancies and Mn atoms in different oxidation states further enhances both ferromagnetic properties and conductivity.

2.10.4. Magneto-Hydrodynamic Phenomena

Magnetoelectric phenomena enable the control of electrochemical processes using a magnetic field. An external magnetic field can influence electrolyte flow, local pH, and electrochemical reaction rates. Two critical factors affecting electrochemical reaction kinetics are electromigration and diffusion. The Nernst diffusion layer, impacted by the diffusion process, can alter the local pH at the electrode surface, thereby affecting product formation and reaction rates. The Lorentz force describes the impact of an external magnetic field on ion transportation:

$$\vec{F} = \vec{V} \times \vec{B} \qquad \text{Eq. (2.38)}$$

Where V is the velocity of the ions in the magnetic field, B is the magnetic field and F is the force exerted on the ions by the magnetic field given their velocity. Noting the cross-product

nature of the equation, the Lorentz force is zero when V and B vectors are parallel and at a maximum when they are orthogonal.

The Lorentz force can affect the flux of reactants and products, and at high magnetic fields, the induced convection can enhance the electrolyte ion interactions with the active material. This phenomenon is explained by magnetohydrodynamic theory, and its effect on electrolyte diffusion can be described by a modified Fick's law:

$$J = -\frac{D\,\partial \mathrm{C}}{\partial \mathrm{x}} - \frac{nF}{RT} DCvB \qquad \text{Eq (2.39)}$$

Where J is the net flux of electrolyte ions, C is electrolyte concentration, D is the diffusion coefficient, B is the magnetic field strength, v is the velocity of charged species in the electrolyte solution due to the magnetic field, n is the number of moles of electrons passing through the electrode during the reaction, F is the Faraday constant, and RT represents thermal energy where R is the Rydberg's constant and T is the temperature.

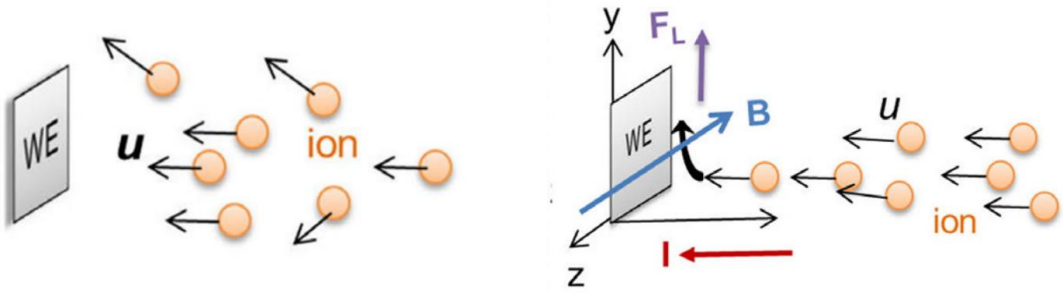

Figure 2.26 The behaviour of charged particles in an electrolyte without (left) and with (right) the influence of an externally applied magnetic field [34]. Reproduced (adapted) with permission from R. Sikkema, I. Zhitomirsky, Magnetic supercapacitors: Charge storage mechanisms, magnetocapacitance, and magnetoelectric phenomena, Applied Physics Reviews 10(2) (2023).

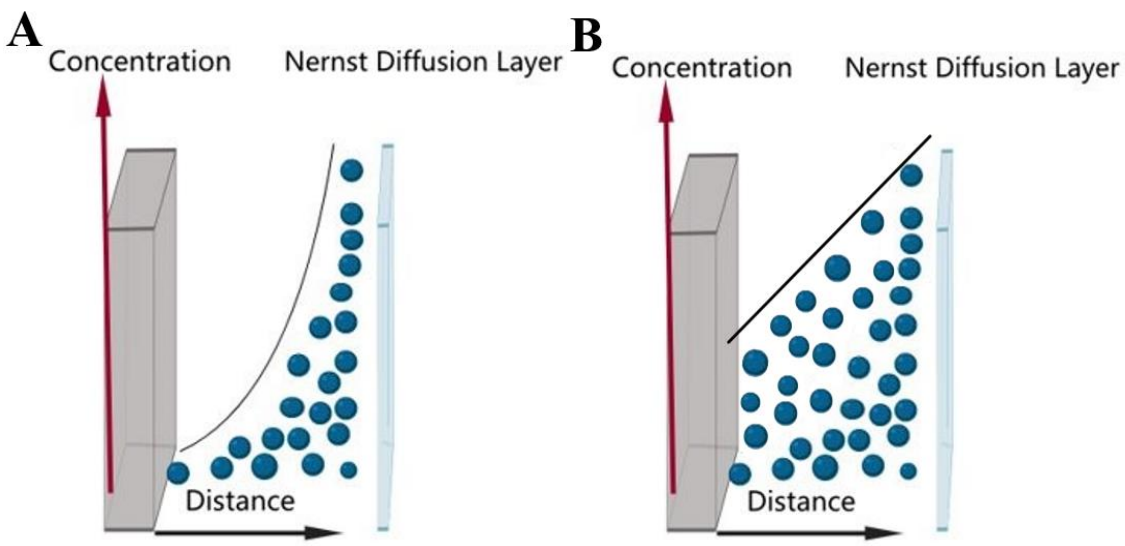

Figure 2.27 Nernst diffusion layer at the surface of the electrode in the absence of a magnetic field (A) and in the presence of a magnetic field (B). Reproduced (adapted) with permission from R. Sikkema, I. Zhitomirsky, Magnetic supercapacitors: Charge storage mechanisms, magnetocapacitance, and magnetoelectric phenomena, Applied Physics Reviews 10(2) (2023).

The Heisenberg Hamiltonian is used to study magnetocapacitive phenomena, and is used to describe the interaction of electron spins between two atoms:

$$\widehat{H} = -2J\hat{S}1 \times \hat{S}2 \qquad \text{Eq (2.40)}$$

Where $\hat{S}1$ and $\hat{S}2$ are spin operators, and J is the exchange integral. J>0 indicates a ferromagnetic interaction (parallel spins), while J<0 indicates a ferrimagnetic interaction (antiparallel spins). For practical applications, it is essential that MOPC exhibits ferromagnetic or ferrimagnetic properties at room temperature. During redox reactions, magnetic moments and interaction energy can change, providing a platform for ME coupling and magnetocapacitive behavior [34].

2.11 Literature Review References

[1] W.J. Sarjeant, Capacitor fundamentals, Proceedings of the 19th Electrical Electronics Insulation Conference, 1989.
[2] B.E. Conway, electrochemical-supercapacitors-scientific-fundamentals-and-technological-application_compress, Springer Science+Business Media, LLC Kluwer Academic / Plenum Publishers.
[3] P. Sharma, T.S. Bhatti, A review on electrochemical double-layer capacitors, Energy Conversion and Management 51(12) (2010) 2901-2912.
[4] K. Xu, Electrolytes, Interfaces and Interphases, Fundamentals and Applications in Batteries, Royal Society of Chemistry, 2023.
[5] Y. Jiang, J. Liu, Definitions of Pseudocapacitive Materials: A Brief Review, Energy & Environmental Materials 2(1) (2019) 30-37.
[6] <Nanostructured Carbons Double-Layer Capacitance and More.pdf>.
[7] L. Miao, Z. Song, D. Zhu, L. Li, L. Gan, M. Liu, Recent advances in carbon-based supercapacitors, Materials Advances 1(5) (2020) 945-966.
[8] <The difference between Faradaic.pdf>.
[9] X. Zhao, Y. Hou, Y. Wang, L. Yang, L. Zhu, R. Cao, Z. Sha, Prepared MnO2 with different crystal forms as electrode materials for supercapacitors: experimental research from hydrothermal crystallization process to electrochemical performances, RSC Advances 7(64) (2017) 40286-40294.
[10] <Brett Ch., Brett A. Electrochemistry.. principles, methods, and applications (Oxford, 1994)(T)(444s) (1).pdf>.
[11] M. Awad, I. Zhitomirsky, Boosting the activation rate and capacitance retention of MnOx electrodes prepared using capping agents, Colloids and Surfaces A: Physicochemical and Engineering Aspects 676 (2023).
[12] C. An, Y. Zhang, H. Guo, Y. Wang, Metal oxide-based supercapacitors: progress and prospectives, Nanoscale Adv 1(12) (2019) 4644-4658.
[13] R. Chen, M. Yu, R.P. Sahu, I.K. Puri, I. Zhitomirsky, The Development of Pseudocapacitor Electrodes and Devices with High Active Mass Loading, Advanced Energy Materials 10(20) (2020).
[14] N.M. S. Devaraj, Effect of Crystallographic Structure of MnO2 on Its Electrochemical Capacitance Properties, J. Phys. Chem. C 11 (2008) 4406-4417.
[15] I. Zhitomirsky, Solid State Synthesis and Sintering, 2023. https://avenue.cllmcmaster.ca/d2l/le/content/524429/viewContent/4036533/View..
[16] V. Popov, Carbon nanotubes: properties and application, Materials Science and Engineering: R: Reports 43(3) (2004) 61-102.
[17] M. Filchakova, What are multi walled carbon nanotubes? MWCNT production, properties, and applications, 2021. https://tuball.com/articles/multi-walled-carbon-nanotubes.
[18] H. Rennhofer, B. Zanghellini, Dispersion State and Damage of Carbon Nanotubes and Carbon Nanofibers by Ultrasonic Dispersion: A Review, Nanomaterials (Basel) 11(6) (2021).
[19] M.S. Ata, Y. Liu, I. Zhitomirsky, A review of new methods of surface chemical modification, dispersion and electrophoretic deposition of metal oxide particles, RSC Advances 4(43) (2014).

[20] F. Avilés, J.V. Cauich-Rodríguez, L. Moo-Tah, A. May-Pat, R. Vargas-Coronado, Evaluation of mild acid oxidation treatments for MWCNT functionalization, Carbon 47(13) (2009) 2970-2975.
[21] J.U. Lee, J. Huh, K.H. Kim, C. Park, W.H. Jo, Aqueous suspension of carbon nanotubes via non-covalent functionalization with oligothiophene-terminated poly(ethylene glycol), Carbon 45(5) (2007) 1051-1057.
[22] S.W. Kim, T. Kim, Y.S. Kim, H.S. Choi, H.J. Lim, S.J. Yang, C.R. Park, Surface modifications for the effective dispersion of carbon nanotubes in solvents and polymers, Carbon 50(1) (2012) 3-33.
[23] M.P.H. Zita Zachariah, and Rosa M. Espinosa-Marzal, Colloidal Interactions—DLVO Theory and Beyond, ACS Publications ACS Symposium Series Vol. 1457(One Hundred Years of Colloid Symposia: Looking Back and Looking Forward
Chapter 2pp 31-47) (2023).
[24] D.I. Zhitomirsky, Chemical Precipitation Methods, 2023. https://avenue.cllmcmaster.ca/d2l/le/content/524429/viewContent/4036534/View..
[25] KTF-Split, Isoelectric point 29 June 2022. https://glossary.periodni.com/glossary.php?en=isoelectric+point.
[26] D.I. Zhitomirsky, Colloidal Methods in Materials Manufacturing, 2023. https://avenue.cllmcmaster.ca/d2l/le/content/524429/viewContent/4036538/View.
[27] G.A. Snook, P. Kao, A.S. Best, Conducting-polymer-based supercapacitor devices and electrodes, Journal of Power Sources 196(1) (2011) 1-12.
[28] J.D. Andy Rudge, Ian Raistrick and Shimshon Gottesfeld, John P. Ferraris Conducting polymers as active materials in
electrochemical capacitors, Journal of Power Sources 47(1-2) (1994) 89-107.
[29] S. Goel, N.A. Mazumdar, A. Gupta, Synthesis and characterization of polypyrrole nanofibers with different dopants, Polymers for Advanced Technologies 21(3) (2009) 205-210.
[30] D. Tang, I. Zhitomirsky, Pseudocapacitive properties of polypyrrole – ferrimagnetic CoFe2O4 composites, Electrochimica Acta 475 (2024).
[31] T.S. Bhat, P.S. Patil, R.B. Rakhi, Recent trends in electrolytes for supercapacitors, Journal of Energy Storage 50 (2022).
[32] A. Mendhe, H.S. Panda, A review on electrolytes for supercapacitor device, Discover Materials 3(1) (2023).
[33] H.K. Jeong*, O. Ibukun, Effects of Aqueous Electrolytes in Supercapacitors, New Physics: Sae Mulli 69(2) (2019) 154-158.
[34] R. Sikkema, I. Zhitomirsky, Magnetic supercapacitors: Charge storage mechanisms, magnetocapacitance, and magnetoelectric phenomena, Applied Physics Reviews 10(2) (2023).

3. Problem Statement and Project Objectives

The goal of this investigation was the development of MOPC materials and composites for application in supercapacitors. It involved the investigation of capacitive properties and magnetic properties of advanced soft ferrimagnetic $NiFe_2O_4$ and hard ferrimagnetic $SrFe_{12}O_{19}$ materials. It involved the investigation of HEBM effect on particle morphology and capacitance. This investigation targeted the fabrication of electrode materials and devices with high active mass loading and application of new concepts based on the use of charge-transfer mediator-dispersants for the fabrication of electrodes with enhanced performance. The analysis of influence of the chemical structure of the charge transfer mediator-dispersants on electrode performance was in the focus of this study as well. Another avenue was focused on the fabrication and testing of composite electrodes and devices, based on composites of $NiFe_2O_4$ –PPy and $SrFe_{12}O_{19}$-PPy, analysis of influence of composite phase content on capacitive properties, impedance, capacitance retention, cyclic stability and magnetic properties. Electrochemical capacitors require a large ratio of active materials to inert components (casings, separators current collectors etc) to be considered a practical energy storage solution. The main problem with fabricating high active mass loaded electrodes is the reduced ion access to electrochemically active sites due to agglomeration and poor ionic conductivity, resulting in reduced capacitance relative to electrodes with low mass loading, exacerbated at high scan rates. Agglomeration occurs due to Van der Waals and magnetic attraction forces between ferrimagnetic particles when making slurries. Additionally, NFO and SFO possess relatively low conductivities resulting in high ohmic losses during red/ox reactions in EC systems. The specific objectives required to achieve the main goal of this thesis are:

1. Utilizing gallocyanine dye as a co-dispersing agent and performing mass ratio optimization steps to mitigate the effects of agglomeration on NFO, SFO and multiwalled carbon nanotube conductive additives in ethanol, in order to promote proper dispersion and suspension qualities of the active material slurries. Additionally, using the charge transfer mediation effects of gallocyanine dye in the negative potential range to enhance capacitive performance of SFO and NFO electrodes.
2. Utilizing the HEBM technique to break apart large agglomerates and increase the surface area to volume ratio of ferrimagnetic SFO and NFO particles in order to improve suspension stability, dispersion qualities and capacitance.
3. Forming composites of varying mass ratios with pseudocapacitive polypyrrole doped with anionic tiron molecule to improve capacitance of SFO and NFO based supercapacitor electrodes.

The effects that each objective had on the capacitance of the SFO and NFO based electrodes were carefully measured via CV, CP and EIS tests to select for the best combination of dispersing agent mass ratio, high energy ball milled product, and conductive polymer mass ratio, in order to develop high active mass loaded supercapacitor electrodes with practical capacitance values.

4. Capacitive Properties of Ferrimagnetic $NiFe_2O_4$-Conductive Polypyrrole Nanocomposites

M. MacDonald and I. Zhitomirsky, "Capacitive Properties of Ferrimagnetic $NiFe_2O_4$-Conductive Polypyrrole Nanocomposites," *Journal of Composites Science*, vol. 8, no. 2, p. 51, 2024, doi: 10.3390/jcs8020051.

Abstract

This investigation addresses increasing interest in advanced composite materials, combining capacitive properties and spontaneous magnetization for energy storage applications in supercapacitors. The capacitive properties of ferrimagnetic $NiFe_2O_4$ (NFO) spinel nanoparticles with magnetization of 30 emu g^{-1} were enhanced using high-energy ball-milling and the use of advanced dispersant, which facilitated charge transfer. NFO electrodes with an active mass of 40 mg cm^{-2} showed a capacitance of 1.46 F cm^{-2} in 0.5 M Na_2SO_4 electrolyte in a negative potential range. The charging mechanism in the negative potential range in Na_2SO_4 electrolyte was proposed. NFO was combined with conductive polypyrrole polymer for the fabrication of composites. The analysis of the capacitive behavior of the composites using cyclic voltammetry, chronopotentiometry and impedance spectroscopy at different electrode potentials revealed synergy of contributions of NFO and PPy. The highest capacitance of 6.64 F cm^{-2} was obtained from cyclic voltammetry data. The capacitance, impedance, and magnetic properties can be varied by variation of electrode composition. Composite electrodes are promising for application in

anodes of asymmetric magnetic supercapacitors for energy storage and magnetically enhanced capacitive water purification devices.

4.1 Introduction

Conductive polymers have generated significant interest for the fabrication of composites, combining various functional properties of individual components. Polyaniline (PANI)- and polypyrrole (PPy)-based composites containing magnetic particles have been developed [1,2,3]. These composite materials have shown interesting properties, which result from the interfacial interactions of magnetic particles and conductive polymers. PANI-coated ferromagnetic particles showed enhanced magnetoresistance [4] due to the spin-polarized tunneling of electrons between grains of the ferromagnetic material, which was facilitated by the conducting electrons of the polymer [4]. Surface modification of a ferromagnetic material with PPy resulted in significant magnetization increase [3]. In such composites, the measured magnetic moment of Mn ions was higher than theoretically expected. The magnetization increase resulted from spin and charge transfer from the conductive polymer to the magnetic material. It was suggested [3] that the π electrons of PPy are polarized in exchange interactions with 3D electrons of Mn ions, resulting in an increase in the total magnetic moment.

There is currently a surge of interest in composites containing conductive polymers [5,6,7,8,9] for application in supercapacitors. It has been reported that the capacitance of PPy composites containing ferromagnetic lanthanum strontium manganate nanoparticles is higher than the capacitance of pure PPy electrodes [10]. Composite materials containing polypyrrole and magnetic particles are scientifically and technologically fascinating. Such composites are promising for energy storage and capacitive deionization of water applications.

$NiFe_2O_4$ (NFO) is a promising ferrimagnetic spinel material for the development of magnetic supercapacitor composites with PPy. Many investigations [11,12,13,14,15] tested capacitive properties of NFO and composites in positive potential windows in KOH electrolyte. Good capacitive properties in KOH electrolyte were reported in a relatively small potential window of ~0.4–0.5 V [16,17,18,19,20]. The tested electrodes had a relatively low active mass, typically below 5 mg cm^{-2}. Significantly higher active mass loadings are required for practical applications. It should be noted that PPy shows poor electrochemical performance and degradation of properties in KOH electrolyte. NFO and composites were also tested in KNO3 [21], LiCl [22], LiClO4 [23], and other electrolytes [24]. NFO-PPy core shell composite materials were tested in H2SO4 electrolyte [25]. However, the use of acidic H2SO4 electrolyte can result in NFO degradation. It is hypothesized that neutral Na2SO4 electrolyte is beneficial for the charge storage of both PPy and NFO.

The objective of this investigation was the fabrication of NFO-PPy composites with high active mass for operation in a Na_2SO_4 electrolyte. The electric charge storage properties of NFO were enhanced using high-energy ball-milling (HEBM) and application of a dispersant-charge transfer mediator. As a result, the capacitance of NFO electrodes was higher than reported in previous investigations. The combination of NFO and PPy offers the advantages of the synergy of contributions of individual components at different electrode potentials. In contrast with previous studies, high capacitance was achieved in a negative potential range. Composite electrodes showed promising electrochemical performance and combined charge storage and ferrimagnetic properties.

4.2 Materials and Methods

Gallocyanine dye (GCD), Na_2SO_4, ammonium persulfate (APS), $NiFe_2O_4$ (NFO, nanoparticles, <50 nm size), pyrrole, 4,5-Dihydroxy-1,3-benzenedisulfonic acid disodium salt monohydrate (Tiron), ethanol, and poly(vinyl butyral) (PVB, 200–300 kDa) were purchased from MilliporeSigma, Burlington, ON, Canada). Carbon nanotubes (CNT, multiwalled, 13 nm diameter, 1–2 μm length, Bayer, Leverkusen, Germany) and commercial Ni foam current collectors (95% porosity, 1.6 mm thickness, Vale, Mississauga, ON, Canada) were used. PPy polymerization was performed using aqueous 0.1 M pyrrole solutions containing 0.01 M Tiron; this was achieved by adding 0.1 M APS at 0 °C.

High-energy ball-milling (HEBM) of NFO was conducted using a Mixer Mill MM 500 Nano (Retsch GmbH, Haan, Germany). HEBM consisted of milling steps at a frequency of 15 Hz during 5 min with 90 s intervals between the steps. The milling duration was 2 h. After HEBM, the NFO material was washed with ethanol and dried.

NFO and CNT were co-dispersed in ethanol using GCD as a dispersant. The mass ratio of NFO–CNT was 8:2. The mass ratio (RD) of GCD dispersant to the total mass of NFO and CNT was RD = 0.02–0.1. The mixtures underwent ultrasonication, washing, and drying and re-dispersion in ethanol containing dissolved PVB binder. The obtained slurries were then utilized for electrode fabrication by impregnating current collectors. PPy-CNT and PPy–NFO–CNT composite powders were also dispersed in PVB solution in ethanol. The mass ratio of PPy–NFO was 1:1 (Composite 1) and 1:3 (Composite 2). All the electrodes contained 20% CNT as conductive additives. In each electrode, the mass ratio of PVB to the total mass of NFO, PPy and

CNT was 0.03. The final mass of the impregnated material, after drying, was 40 mg cm^{-2}. The impregnated Ni foams were pressed to 25% of their initial thickness.

A SQUID magnetometer (Quantum Design, San Diego, CA, USA) was used for investigation of magnetic properties. XRD testing was conducted with a diffractometer Bruker D8 Advance with Cr-Kα radiation. The microstructure investigations involved the use of transmission electron microscopy (TEM, Talos 200 microscope, Thermo Scientific, Waltham, MA, USA). Electrochemical characterization was carried out in aqueous 0.5 M Na_2SO_4 electrolyte using a Biologic potentiostat (VMP 300, BioLogic, Seyssinet-Pariset, France) with a three-electrode system, using a saturated calomel electrode reference (SCE), an NFO-based working electrode, and a Pt mesh counter electrode. Cyclic voltammetry (CV), electrochemical impedance spectroscopy (EIS), and chronopotentiometry (CP) methods were used for electrode characterization. The capacitance was calculated from the CV, EIS and CP data as described in Ref. [26]. Areal (CS) and gravimetric (Cm) capacitances were derived from the CV data using the following equation:

$$C = \Delta Q \Delta U = \frac{\left|\int_0^{t(U_{max})} I dt\right| + \left|\int_{t(U_{max})}^0 I dt\right|}{2U_{max}} \qquad \text{Eq. (4.1)}$$

where ΔQ is charge, I is current, t is time, ΔU is potential range, and from the CP data,

$$C = \frac{I\Delta t}{\Delta U} \qquad \text{Eq. (4.2)}$$

The complex capacitance $C^*(\omega) = C'(\omega) - iC''(\omega)$ was derived at different frequencies (ω) from the complex impedance $Z^*(\omega) = Z'(\omega) + i\,Z''(\omega)$:

$$C'(\omega) = -\frac{Z''(\omega)}{\omega Z(\omega)^2} \qquad \text{Eq. (4.3)}$$

$$C''(\omega) = \frac{Z'(\omega)}{\omega Z(\omega)^2} \qquad \text{Eq. (4.4)}$$

4.3 Results

NFO showed soft ferrimagnetic properties with spontaneous magnetization of 30 emu g^{-1} and a small coercive field (Figure 4.1). The obtained magnetization value is in agreement with data from the literature [27]. However, the magnetization of NFO is dependent on particle size, temperature, distribution of Ni^{2+} and Fe^{3+} ions in the tetrahedral and octahedral positions of the spinel crystalline structure and other factors [28,29,30].

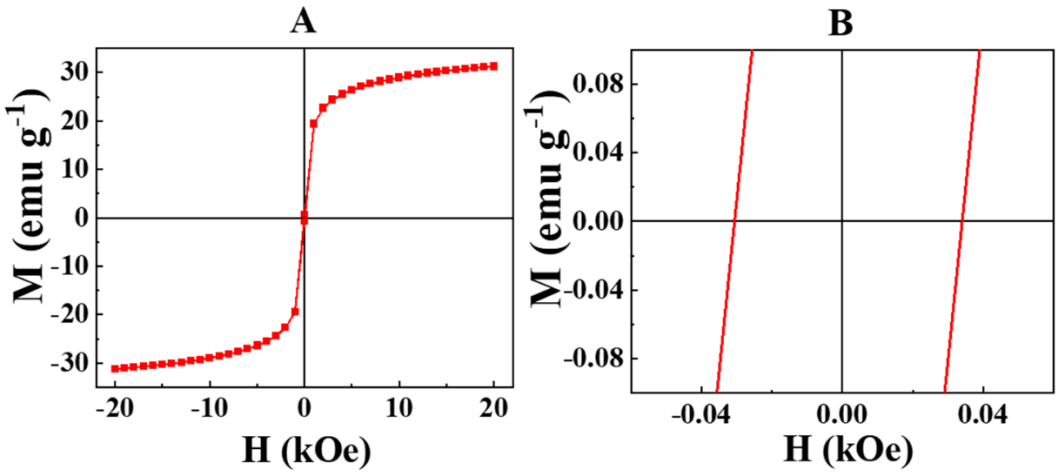

Figure 4.1 (A) Magnetization (M) versus magnetic field (H) and (B) M versus H in the low H range.

The size of the NFO particles was analyzed using TEM. The as-received NFO particles (Figure 4.2A, Supplementary Information, Figure 4.11) showed well-defined crystal faces. The typical particle size was 20–40 nm in agreement with the data of powder manufacturer. The investigation of morphology of HEBM powders showed particles of irregular shapes which resulted from particle grinding (Figure 4.2B). The typical particle size was below 20 nm, and the

powders contained many particles with sizes below 10 nm. It was hypothesized that particle size reduction can be beneficial for obtaining electrodes with higher capacitance. However, it should be noted that other investigations of different materials did not show correlation between electrochemical capacitance and BET surface area [31,32,33].

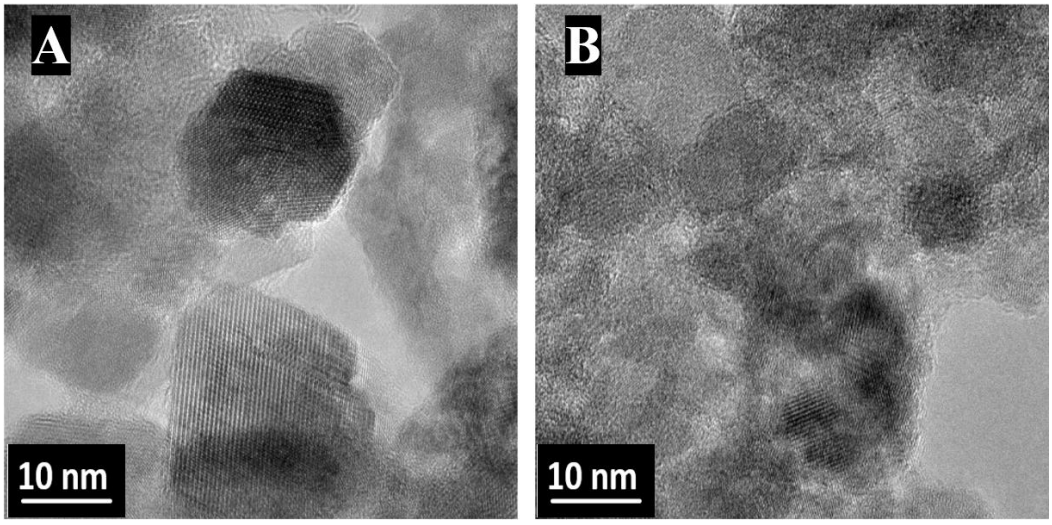

Figure 4.2 TEM images of (A) as-received and (B) HEBM NFO.

Figure 4.3 and Figures and 4.12–4.14 (supplementary) compare electrochemical testing results for as-received NFO and HEBM NFO prepared with and without GCD. The CV data for as-received NFO (Figure 4.3A(a)) showed a reduction in current with increasing potential from −0.8 to 0 V, which indicated decreasing differential capacitance at higher potentials. The use of GCD as a dispersant for the NFO particles led to significant changes in CV shape (Figure 4.3A(b)) for RD = 0.02. The NFO electrodes prepared with GCD showed a significant increase in current in the potential range of −0.6–0 V, and redox peaks were observed at about −0.2 V. It was found that the increase in RD from 0.02 to 0.1 did not result in significant changes in CV shape (Figure 4.2). The changes in CV shape can be attributed to the effect of adsorbed GCD. It is suggested that for RD = 0.02, only part of GCD adsorbed on NFO and non-adsorbed GCD was removed during

washing. Further addition of GCD ($0.02 < RD \leq 0.1$) did not result in higher capacitance. The NFO electrodes, prepared without and with GCD (RD = 0.02) showed capacitances of 0.55 and 0.91 F cm^{-2}, respectively, at 2 mV s^{-1}. HEBM NFO showed significantly higher currents, especially for potentials above −0.6 V (Figure 4.3B(a)).

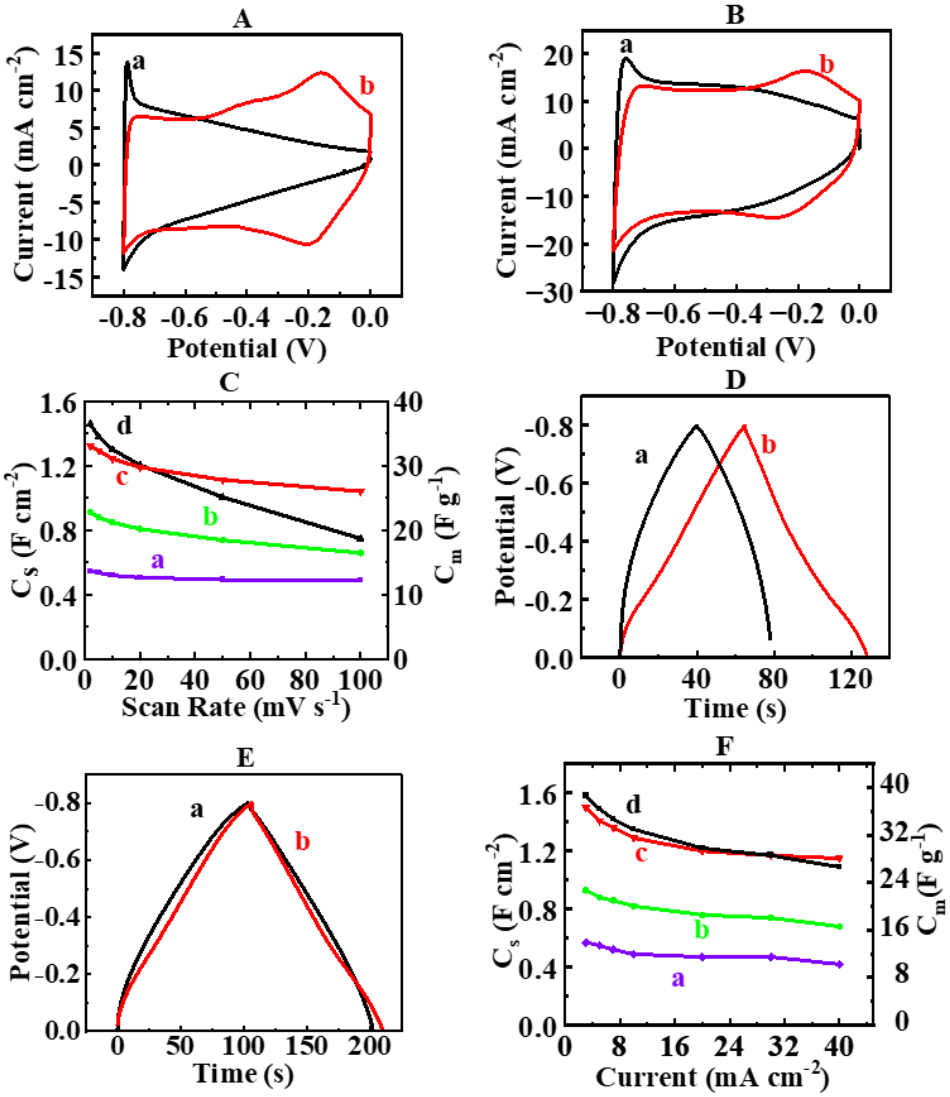

Figure 4.3 (A,B) CVs at 10 mV s^{-1}; (C) capacitance calculated from CV data versus sweep rate; (D,E) CP data at 10 mA cm^{-2}; (F) capacitance calculated from CP data versus current density for electrodes prepared using (A(a)), (C(a)), (D(a)), (F(a)) as-received NFO; (A(b)), (C(b)), (D(b)), (F(b)) as-received NFO with GCD for RD = 0.02; (B(a)), (C(c)), (E(a)), (F(c)) HEBM NFO; and (B(b)), (C(d)), (E(b)), (F(d)) HEBM NFO with GCD for RD = 0.02.

The use of GCD (RD = 0.02) resulted in a further increase in currents for potentials above −0.4 V. Redox peaks were also observed for the electrode prepared with GCD dispersant (Figure 4.3B(b)). The HEBM NFO electrodes prepared without and with GCD showed capacitances of 1.32 and 1.46 F cm^{-2}, respectively, at 2 mV s^{-1}. The analysis of dependences of capacitance versus sweep rate (Figure 4.3C) showed that the use of GCD and HEBM resulted in improved capacitive properties in the range of 2–100 mV s^{-1}. The use of GCD for HEBM NFO resulted in improved capacitive properties at low sweep rates below 20 mV s^{-1}. However, at higher sweep rates the use of GCD for HEBM resulted in reduced capacitance. CP testing results showed that the use of GCD for as-prepared NFO and HEBM resulted in longer charge–discharge times (Figure 4.3D,E), which led to higher capacitances at different current densities (Figure 4.3F). However, the use of GCD for HEBM samples did not result in enhanced capacitance (Figure 4.3E,F).

GCD (Figure 4.4A) belongs to catechol family of molecules, which exhibit strong adsorption on inorganic particles by complexation of surface metal atoms. The adsorption mechanism of catecholate molecules is similar to that of mussel protein bonding to different surfaces by the catechol groups of the individual monomers. GCD can be adsorbed on NFO particles by complexation of Ni or Fe atoms (Figure 4.4B). GCD is a polyaromatic molecule (Figure 4.4A). Polyaromatic molecules show adsorption on CNT by π-π interactions. The positive charge of GCD is beneficial for application of this molecule as a dispersant for electrostatic stabilization of particles in suspensions. It is known that charged polyaromatic catecholates can be used as dispersants for inorganic particles and CNT. Therefore, it was hypothesized that GCD adsorbed on NFO and CNT, acting as a co-dispersant for both materials. Therefore, enhanced capacitance of electrodes prepared using GCD can result from better mixing of NFO with conducting CNT

additives. It is also known that catechol molecules can facilitate charge transfer. For example, Tiron and other anionic catechol molecules facilitated anodic electro-polymerization of polypyrrole on non-noble substrates acting as charge transfer mediators, which reduce electropolymerization potential [34,35]. The use of dopamine as a charge transfer mediator facilitated the fabrication of photovoltaic devices with enhanced efficiency [36]. GCD was used as a charge transfer mediator for advanced electrochemical sensors [37].

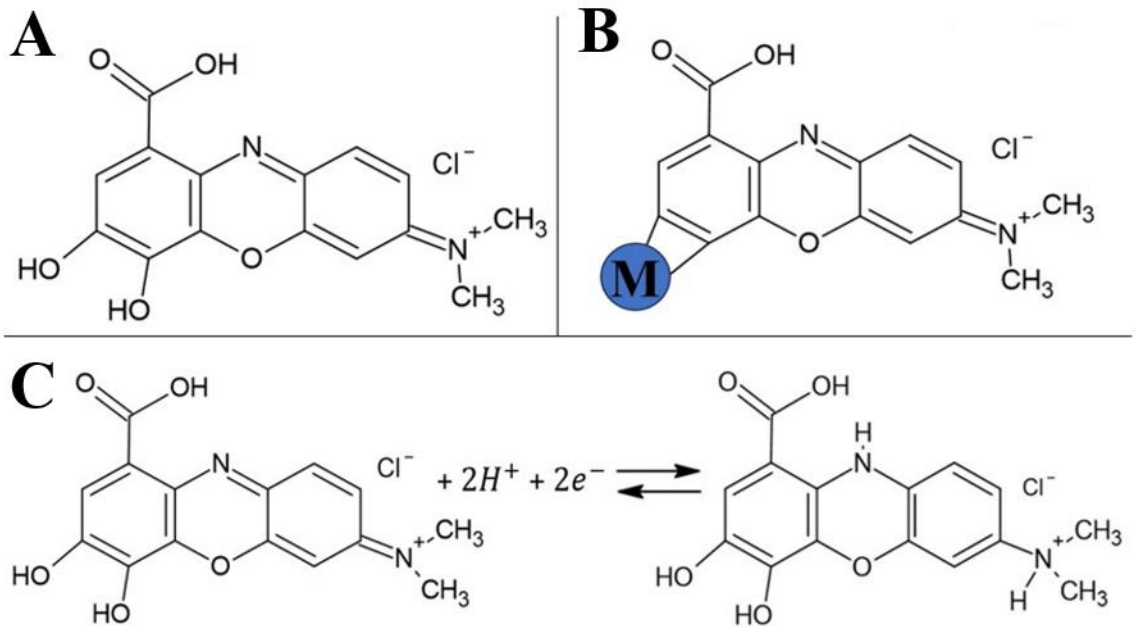

Figure 4.4 (A) Chemical structure of GCD; (B) adsorption of GCD on NFO involving catecholate-type bonding to surface atoms (M = Ni, Fe); (C) redox reaction of GCD.

It is suggested that GCD can potentially facilitate charge storage reactions of NFO. It is in this regard that GCD is a redox active molecule (Figure 4.4C). The mass normalized capacitance of GCD is low due to the large molecular mass of this molecule. Therefore, due to the low gravimetric capacitance and low amount of GCD adsorbed, the direct contribution of GCD to the

electrode capacitance is negligible. However, GCD can act as charge transfer mediator for NFO. The charge storage mechanism of NFO in the negative potential range can be described by the following equation:

$$Ni^{2+}Fe_2^{3+}O_4 + \delta e^- + \delta Na^+ \leftrightarrow (\delta Na^+)Ni^{2+}Fe_2^{(3-\delta/2)} + O_4 \qquad \text{Eq. (4.5)}$$

EIS data were obtained at different electrode potentials, such as 0, −0.2, −0.4, −0.6 and −0.8 V, versus SCE. Figure 4.5 presents EIS data for NFO and HEBM NFO electrodes prepared without and with GCD. The Nyquists plots (Figure 4.5A) for as-received NFO prepared without GCD showed significant differences in components of complex impedance $Z^* = Z' + iZ''$ at different electrode potentials. The highest Z^* values were obtained for potentials of 0 V and −0.2 V versus SCE, which indicated low capacitance and high electrical resistance. The NFO electrodes prepared using GCD (Figure 4.3.5B) showed reduced values of Z' and Z'' at −0.4 V. HEBM resulted in a reduced imaginary component of Z^*, which indicated an increase in differential capacitance (Figure 4.5C). However, the HEBM NFO electrodes showed higher resistance $R = Z'$ at all the electrode potentials. The HEBM NFO electrodes (Figure 4.5D) prepared using GCD showed the lowest values of $R = Z'$ and highest slopes of the Nyquist plots, which indicated improved capacitive behavior.

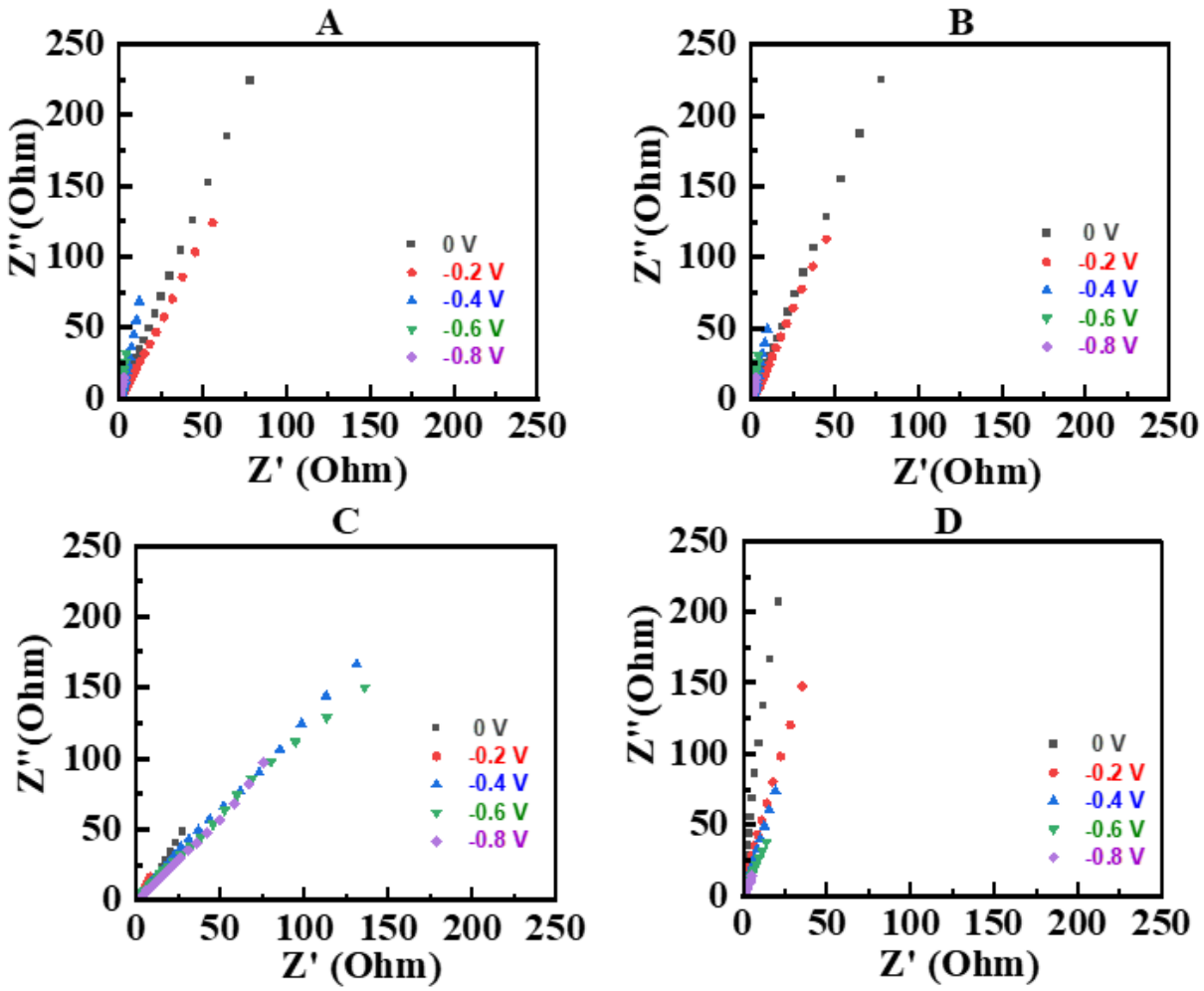

Figure 4.5 Nyquist plots of EIS data at different potentials for electrodes prepared using (A), as-received NFO, (B) as-received NFO with GCD for RD = 0.02, (C) HEBM NFO, and (D) HEBM NFO with GCD for RD = 0.02.

The HEBM NFO prepared using GCD was used for the fabrication of composites with PPy, which allowed for further improvement in properties. Figure 4.6 shows electrochemical testing results for PPy electrodes, containing 20% CNT. CV data (Figure 4.6A) showed higher currents and a wider CV area for potentials of −0.4–0 V vs. SCE, compared to the potential range of −0.8–−0.4 V vs. SCE. This is in contrast to the data for NFO electrodes, which showed higher currents in the low potential range. Therefore, the combination of PPy and NFO is promising for

overcoming disadvantages of both materials in different potential ranges. The capacitance of PPy electrodes (Figure 4.6B) was found to be 6.64 F cm^{-2} at 2 mV s^{-1}. However, it sharply reduced to the level of 4.4 F cm^{-2} at 10 mV s^{-1}. The electrodes showed a capacitance of 2.6 F cm^{-2} at 100 mV s^{-1}.

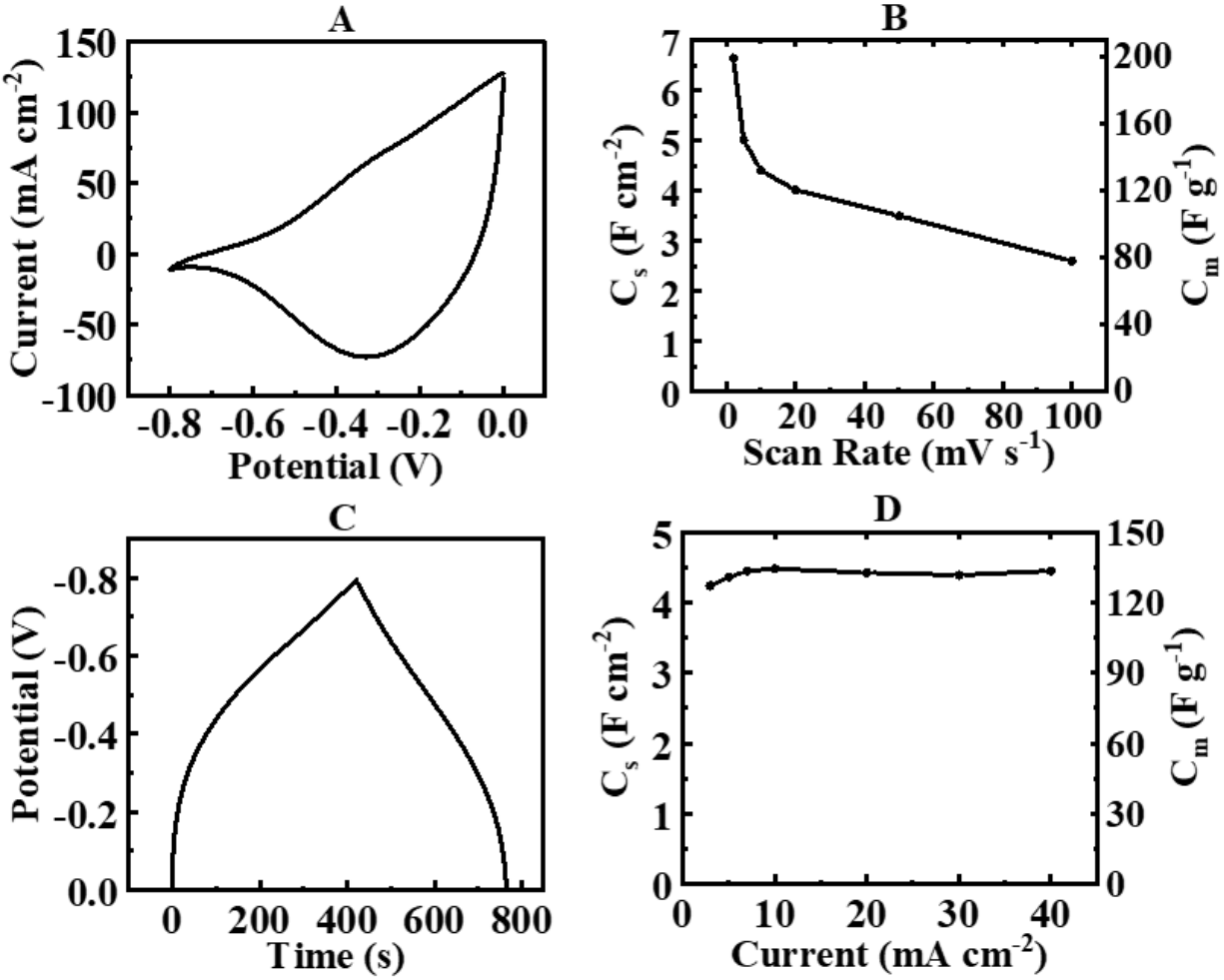

Figure 4.6 (A) CV at 10 mV s^{-1}, (B) capacitance derived from CVs versus sweep rate, (C) CP data at 10 mA cm^{-2}, (D) capacitance derived from CP data versus current density for PPy electrode.

The pseudocapacitive charge storage mechanism of PPy, doped with anions is given by the following equation [38,39]:

$$PPy + nA^{2-} \leftrightarrow PPy^{2n}+nA^{2-} + 2ne^{-} \qquad \text{Eq. (4.6)}$$

where A^{2-} is $Tiron^{2-}$ or SO_4^{2-}.

The CP data (Figure 4.6C) showed a deviation from linear charge–discharge potential–time dependences at constant current densities. The capacitance of 4.2 F cm^{-2} was obtained at 3 mA cm^{-2}, and relatively small variations in capacitance were observed in the range of 3–40 mA cm^{-2} (Figure 4.6D).

HEBM NFO prepared using GCD (RD = 0.02) and PPy were used for the fabrication of composites, combining ferrimagnetic and capacitive properties. The formation of composites was confirmed by X-ray diffraction studies (Figure 4.15). Figure 4.7 and Figures 4.16 and 4.17 show electrochemical testing results for Composite 1, containing NFO and PPy in a mass ratio of 1:1. The CV deviated from an ideal rectangular shape. However, reduced variations in current (Figure 4.7A) were observed in the potential range −0.8–0 V, compared to the PPy electrode (Figure 4.6A). The Composite 1 electrodes exhibited capacitances of 3.86 and 1.39 F cm^{-2} at sweep rates of 2 and 100 mV s^{-1}, respectively (Figure 4.7B). Figure 4.7 C, D shows CP data. The capacitance calculated from the CP data was found to be 4.22 and 3.58 F cm^{-2} for current densities of 3 and 40 mA cm^{-2}, respectively.

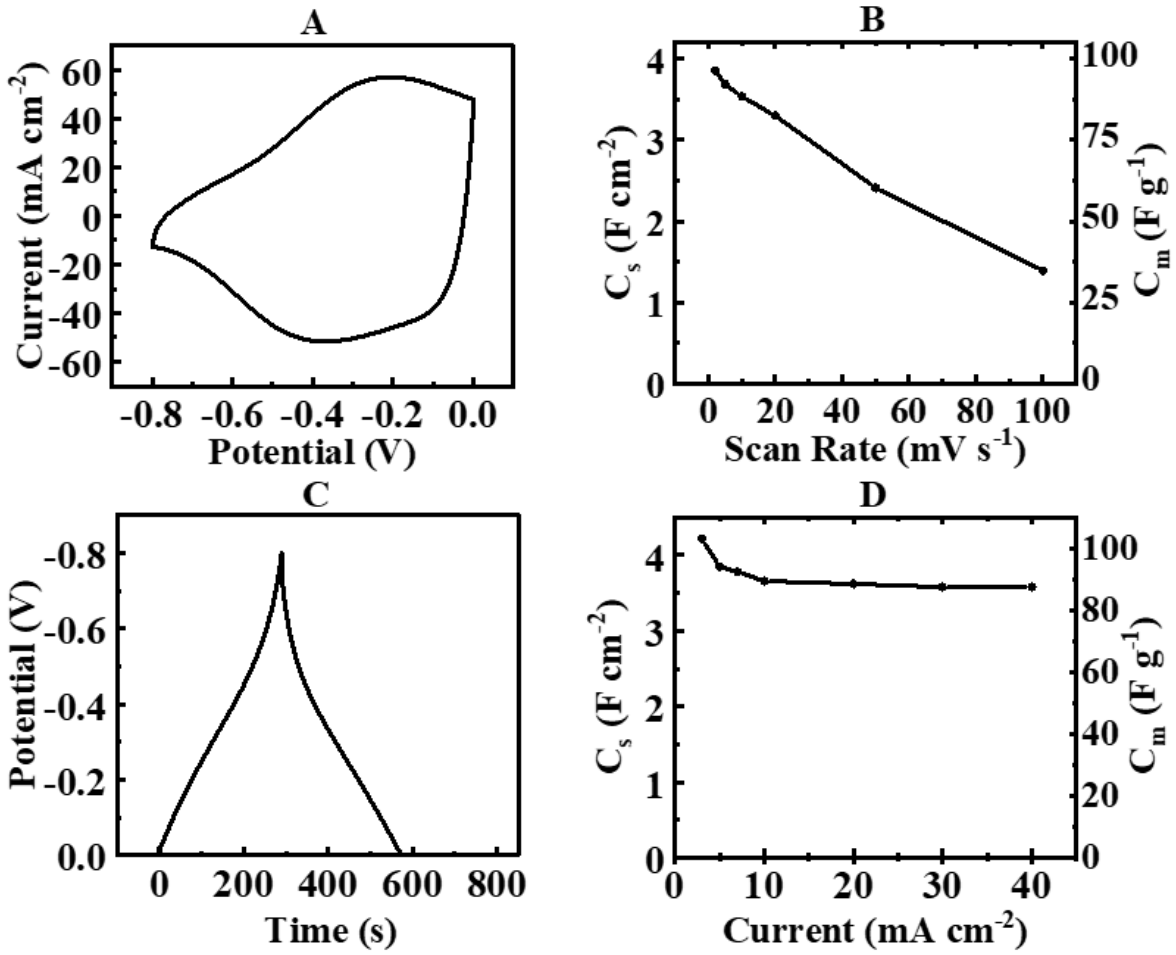

Figure 4.7 (A) CV at 10 mV s^{-1}, (B) capacitance derived from CVs versus sweep rate, (C) CP data at 10 mA cm^{-2}, (D) capacitance derived from CP data versus current density for Composite 1 electrode.

The capacitance for the Composite 1 electrode, calculated from the CP data, was comparable with the capacitance of PPy electrodes, despite the 50% lower PPy content and lower capacitance of NFO compared to PPy. This indicated a synergy of contributions of the individual components. The capacitance of the composite materials involves the contributions of the individual components. The corresponding charging mechanisms are described by Equations (5) and (6). It is known [26] that mass normalized capacitance usually decreases with increasing electrode mass

due to limited electronic and ionic conductivities. As a result, high gravimetric capacitance is usually observed only in thin films with mass below 0.1–1.0 mg cm^{-2}. The mass loading increase to the level of 10–50 mg cm^{-2} often results in reduction of the gravimetric capacitance by 2–3 orders of magnitude [26]. Therefore, it is challenging to utilize the capacitive properties of materials at high active mass loadings and achieve high areal capacitance. Special techniques are currently under development for the fabrication of electrodes with high active mass loadings, such as the use of coated particles, agglomerate-free processing using advanced dispersants, and liquid–liquid extraction techniques [26]. The combination of PPy and NFO is promising for the fabrication of advanced electrodes with high active mass loading. Conductive PPy improves the electronic conductivity of the composite materials and allows for better utilization of the capacitive properties of NFO. The use of ferrimagnetic NFO can facilitate electrolyte transfer via the magnetohydrodynamic effect [40], which is governed by the Lorentz force acting on the ions in the local magnetic field of the ferrimagnetic NFO particles. The magnetohydrodynamic effect can result in better utilization of capacitive properties of PPy in the bulk electrodes. This can explain the synergy of contribution of PPy and NFO.

Figure 4.8 presents testing results for Composite 2 with an NFO–PPy mass ratio of 3:1. The analysis of CV and CP data showed lower capacitances compared to the corresponding data for Composite 2. The capacitance calculated from the CV data decreased from 2.53 to 1.69 F cm^{-2} with an increasing sweep rate from 2 to 100 mV s^{-1}. CP data showed capacitances of 2.54 and 2.00 F cm^{-2} for current densities of 3 and 40 mA cm^{-2}, respectively. It should be noted that Composite 2 had a higher content of ferrimagnetic NFO compared to Composite 2. Therefore, the capacitive and magnetic properties of NFO-PPy composites can be varied.

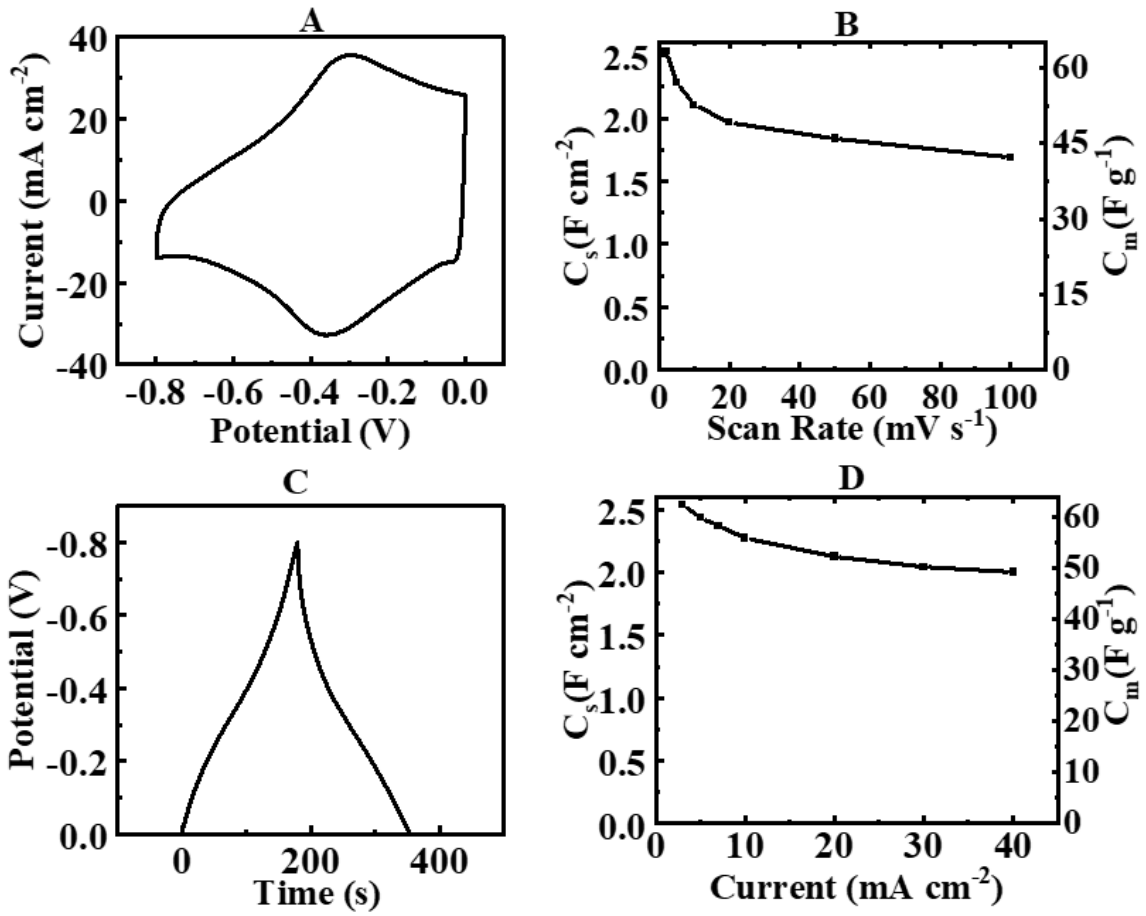

Figure 4.8 (A) CV at 10 mV s−1, (B) capacitance derived from CVs versus sweep rate, (C) CP data at 10 mA cm−2, (D) capacitance derived from CP data versus current density for Composite 2 electrode.

The EIS data for PPy, Composite 1 and Composite 2 electrodes are summarized in Figure 4.9. PPy electrodes showed significant differences in impedance at different electrode potentials. Relatively high values of real and imaginary parts of the complex impedance at −0.8 V indicated low differential capacitance in agreement with CV data and high resistance. However, low impedance was observed at higher potentials. Composite 1 showed significant reduction of impedance at −0.8 V. The reduction of the imaginary part indicated an increase in the differential capacitance. The decrease in the real part is attributed to the reduction in resistance. However, the

electrodes showed increased resistance at −0.6 V. The EIS data were analyzed using an equivalent circuit developed for high active mass composite electrodes [41]. It included an R–C (Q) transmission line with double-layer capacitance, pseudocapacitance, Warburg impedance, solution resistance and charge transfer resistance (Figure 4.8). High-energy ball-milling resulted in increasing Warburg impedance. It is suggested that particle size reduction resulted in better packing of the particles, reduced porosity, and an increase in the bulk density of the electrodes. This can result in diffusion limitations and larger Warburg impedance. PPy electrodes showed significant Warburg impedance at an electrode potential of −0.8 V. The addition of NFO resulted in reduced Warburg impedance of Composites 1 and 2. The larger NFO content in the Composite 2 compared to the Composite 1 allowed for lower Warburg impedance. This can result from the magnetohydrodynamic effect of the ferrimagnetic particles. As pointed out above, such an effect facilitates electrolyte diffusion [40].

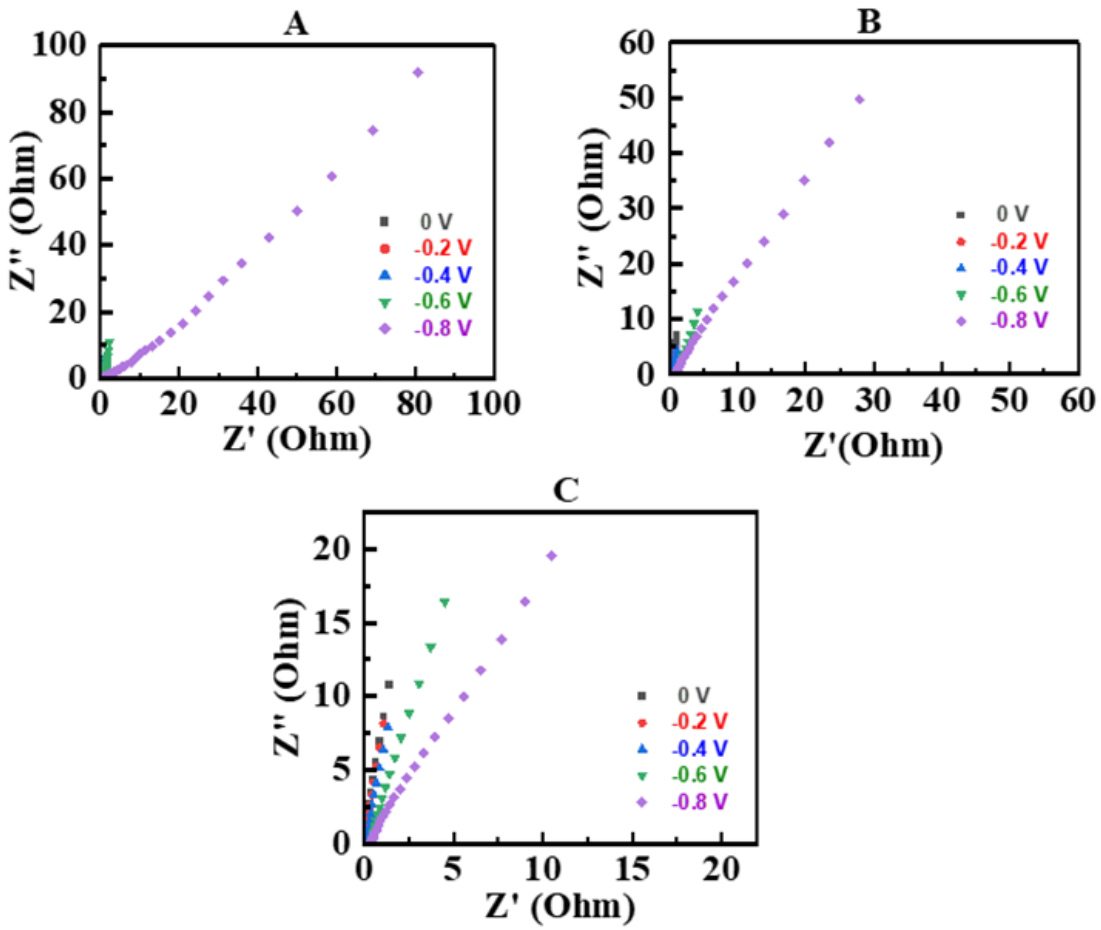

Figure 4.9 EIS data presented in Nyquist plots at different electrode potentials for (A) PPy, (B) Composite 1 and (C) Composite 2 electrodes.

Composite 2 showed a significant reduction in impedance at −0.8 V, compared to PPy and Composite 1. Increased impedance was observed at −0.6 and −0.4 V. It should be noted that Composites 1 and 2 showed significantly lower impedance values at potentials of −0.2 and 0 V, compared to NFO. In general, Composites 1 and 2 showed reduced variations in impedance in the potential range of −0.8–0 V, which illustrates the benefits of the composite materials compared to the individual components.

Figure 4.10 shows the capacitance retention of Composite 1, which exhibited higher capacitance compared to Composite 2. The initial increase in capacitance during the first 100 cycles can be attributed to different factors, such as changes in the microstructure of the bulk of the electrode or improved wetting of the electrode by the electrolyte. The capacitance retention after 1000 cycles was found to be 93.5%. It should be noted that HEBM NFO electrodes showed a slight reduction in capacitance during the first 50 cycles, and then capacitance increased. The capacitance retention after 1000 cycles was found to be 103.5% (Figure 4.19).

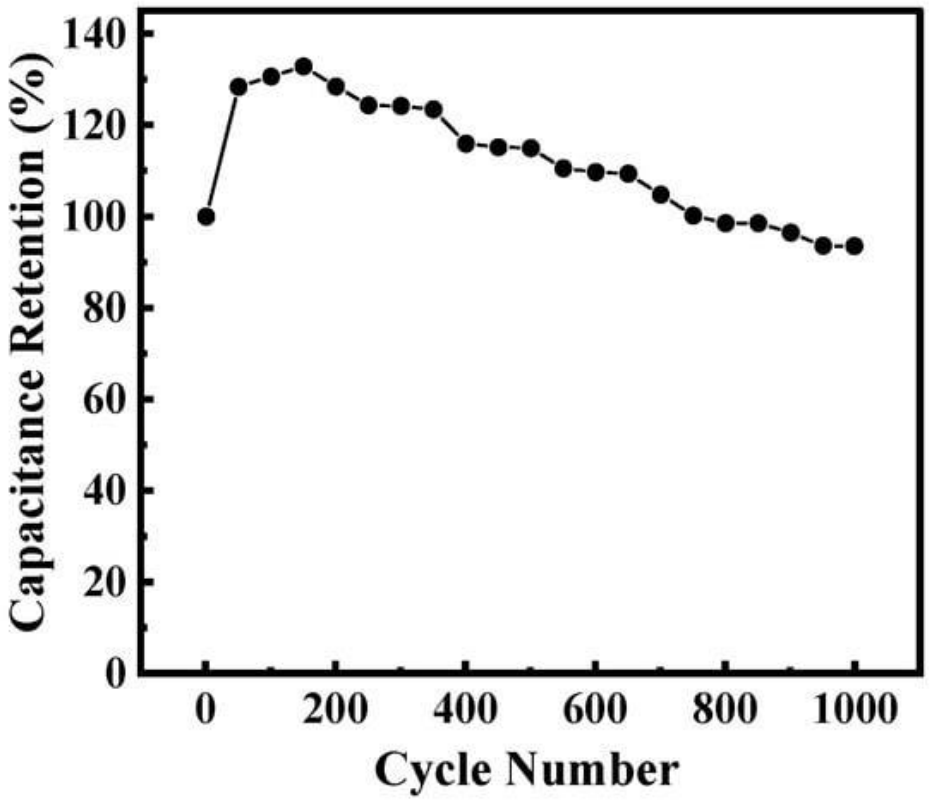

Figure 4.10 Capacitance retention of the Composite 1 electrode.

Composites 1 and 2 combine capacitive and ferrimagnetic properties, which are promising for novel applications based on magnetocapacitive phenomena. Such phenomena are currently

under intensive investigation in various magnetically ordered pseudocapacitive materials [40]. Composites 1 and 2 are promising for energy storage in supercapacitors and magnetic capacitive water deionization devices.

4.4 Conclusions

NFO nanoparticles showed magnetization of 30 emu g^{-1} and capacitive properties in 0.5 M Na_2SO_4 electrolyte in a negative potential range. The capacitive properties of NFO can be increased significantly using HEBM and GCD, which acted as a dispersant and charge transfer mediator. The NFO electrodes with high active mass loading of 40 mg cm^{-2} showed a capacitance of 1.46 F cm^{-2}. The ability to achieve high capacitance of NFO was beneficial for the fabrication of PPy–NFO composites, which showed a capacitance of 6.64 F cm^{-2}. The analysis of CV, CP and EIS data at different electrode potentials showed a synergy of the contributions of the individual components to the capacitance of PPy–NFO composites. The capacitive properties, impedance, and magnetization of the composites can be varied by variation of PPy and NFO content. The high capacitance in the negative potential range in Na_2SO_4 electrolyte overcomes the problem of the lower capacitance of materials for negative electrodes compared to the capacitance of positive electrodes, such as MnO_2. Therefore, the composite material prepared in this investigation is promising for the fabrication of asymmetric capacitors with an enlarged voltage window. The combination of capacitive and magnetic material in the composite opens an avenue for the preparation of advanced magnetically enhanced devices for energy storage and capacitive deionization of water.

4.5 Supplementary Information

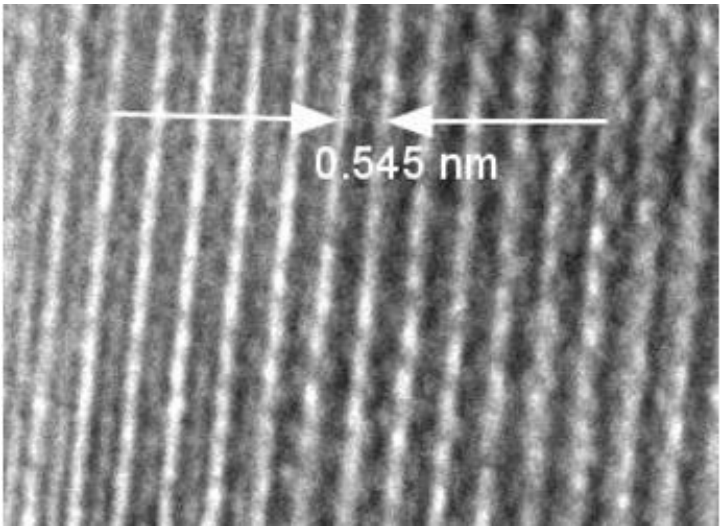

Figure 4.11 High resolution TEM image of NFO showing (111) planes.

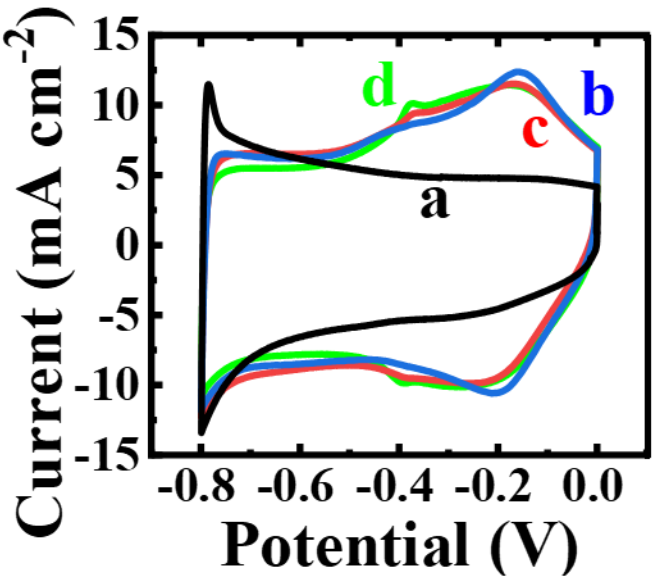

Figure 4.12 CVs at 10 mV s^{-1} for NFO electrodes, prepared using as-received NFO: (a) without GCD and (b-d) with GCD for (b) RD=0.02, (c) RD=0.05 and (d) RD=0.1.

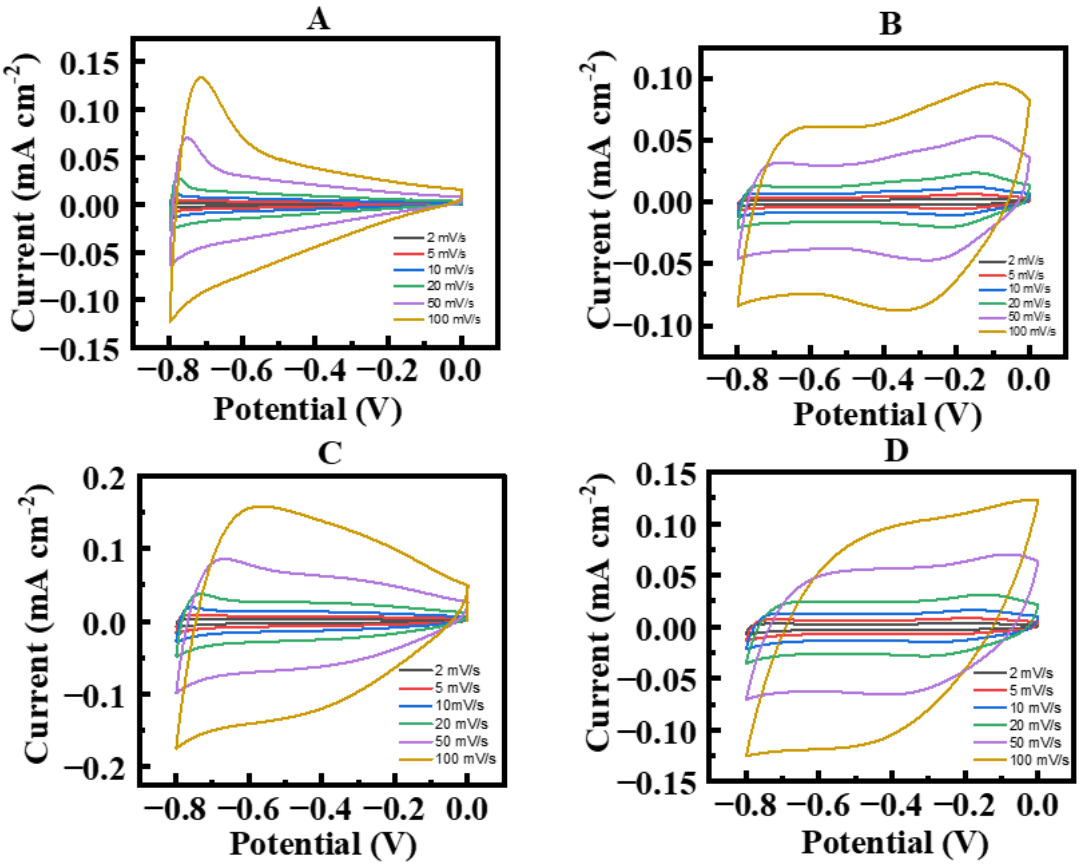

Figure 4.13 CVs at different sweep rates for (A) as-received NFO, (B) as-received NFO with GCD at different scan rates, (C) HEBM NFO and (D) HEBM NFO with GCD.

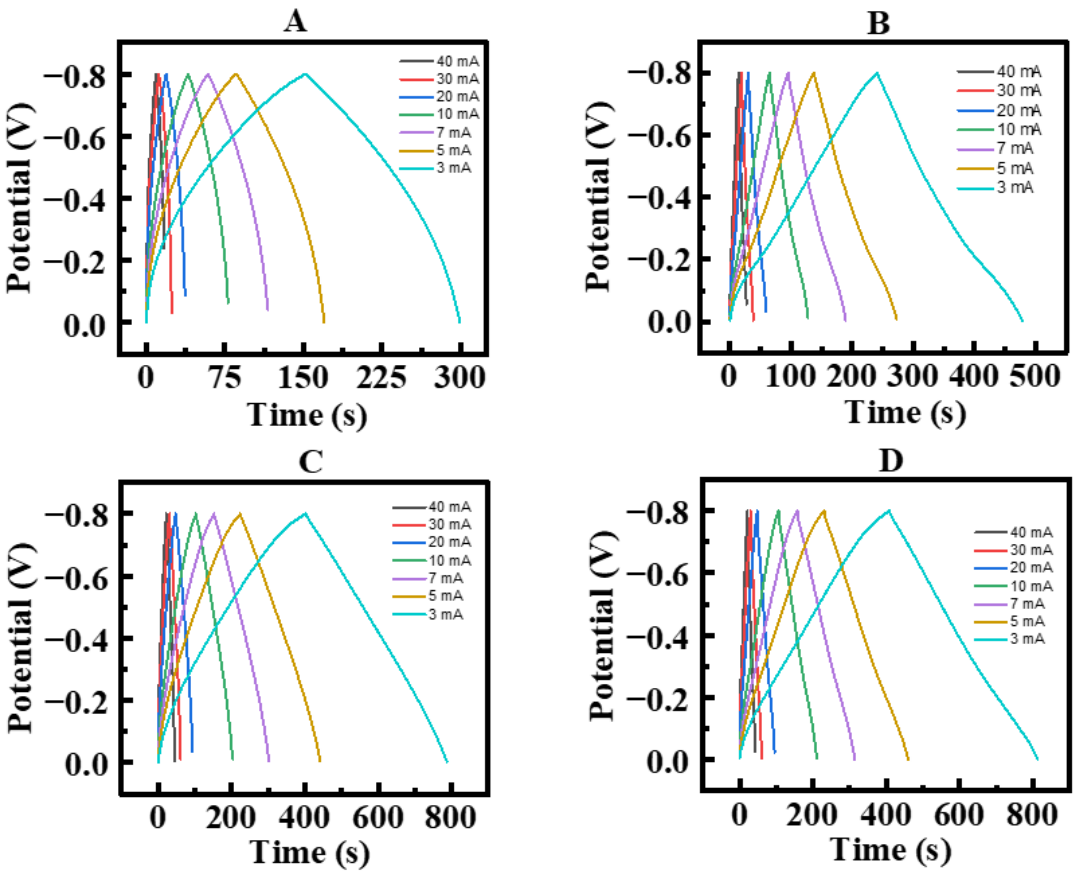

Figure 4.14 CP data at different current densities for (A) as-received NFO, (B) as-received NFO with GCD at different scan rates, (C) HEBM NFO and (D) HEBM NFO with GCD.

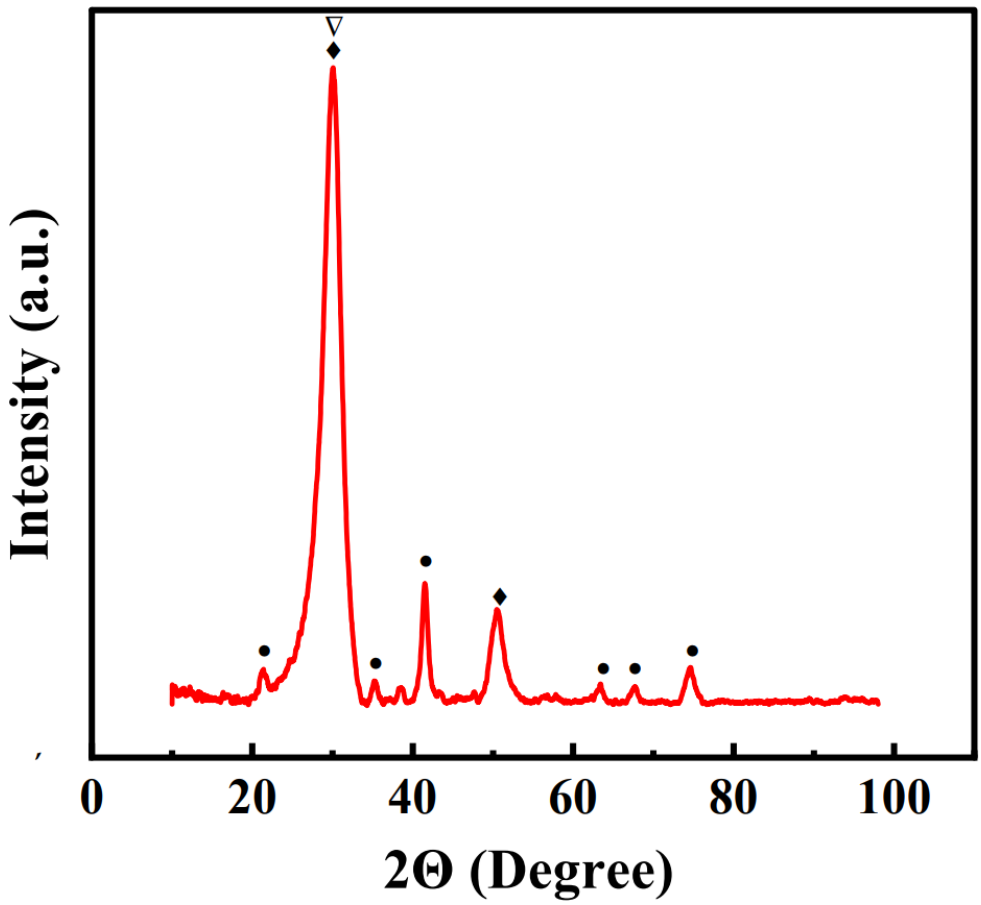

Figure 4.15 X-ray diffraction pattern of Composite 1. (♦- MWCNT, JCPDS file 00-058-1638, ∇-PPy[1, 2], ● -NFO, JCPDS file 00-044-1485).

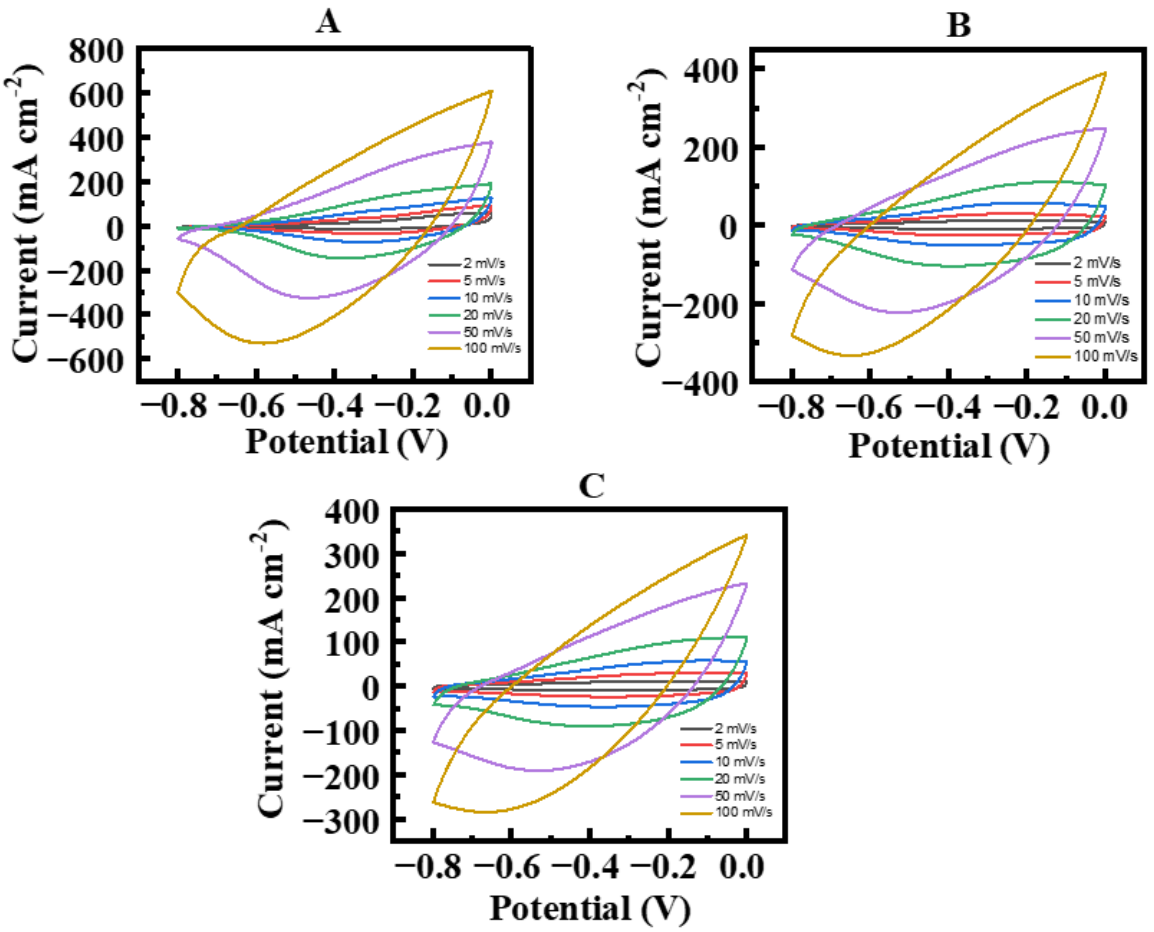

Figure 4.16 CVs at different sweep rates for (A) PPy, (B) Composite 1 and (C) Composite 2

electrodes.

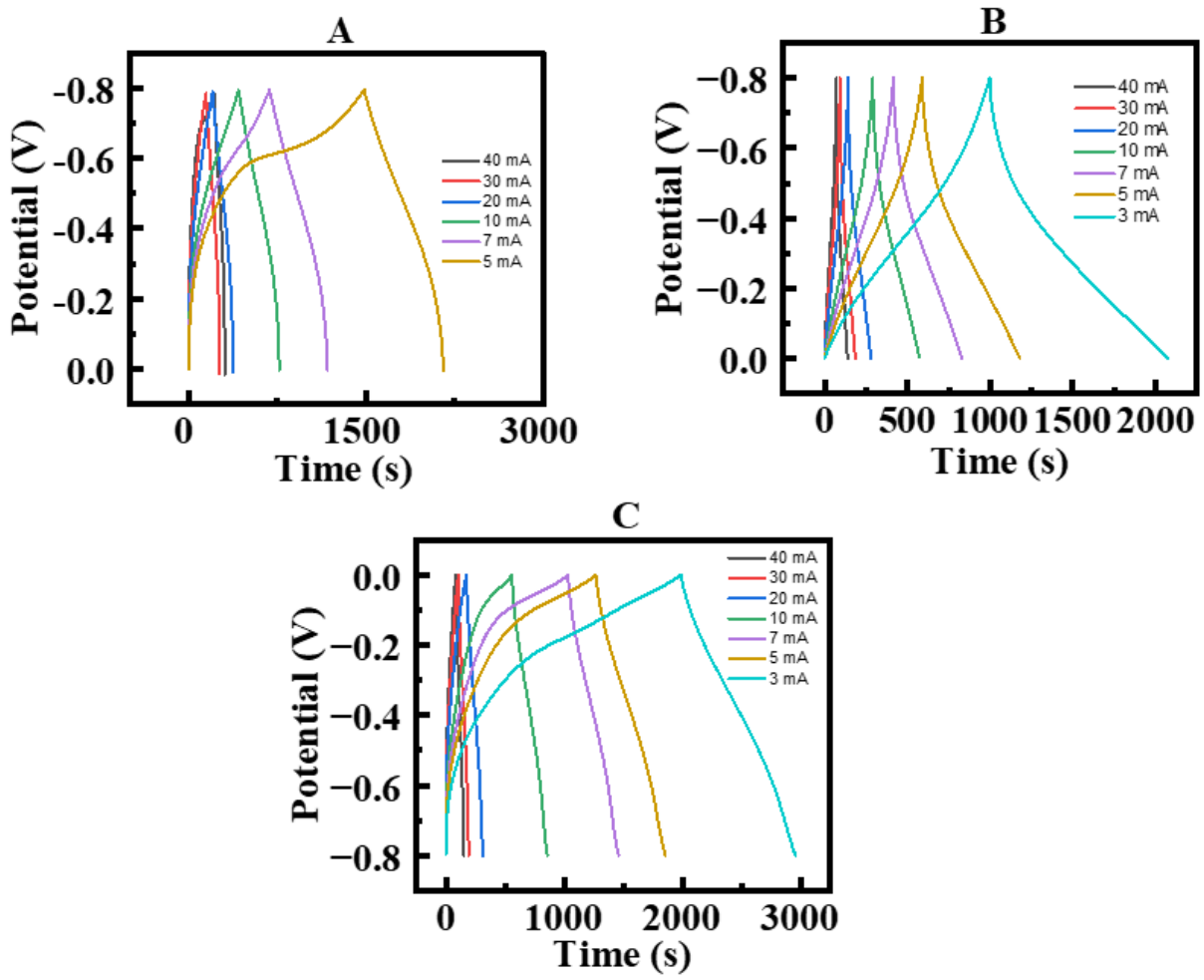

Figure 4.17 CP data at different current densities for (A) PPy, (B) Composite 1 and (C) Composite 2 electrodes.

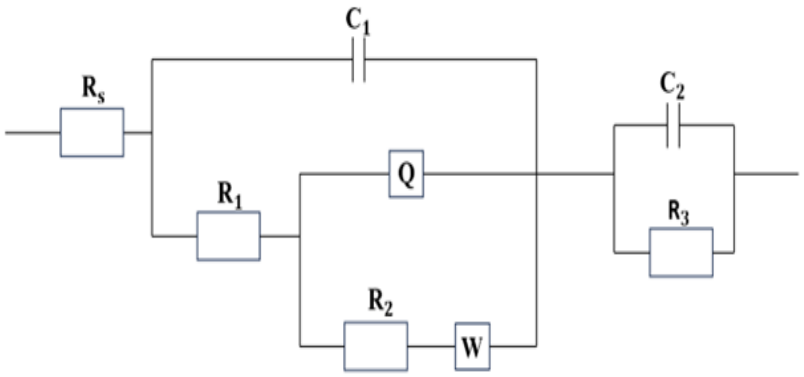

Figure 4.18 Shows the magnified impedance spectroscopy data for as received NFO (A) vs as received NFO with 2 mg gallocyanine (B), HEBM NFO (C), and HEBM NFO with 2 mg of GC.

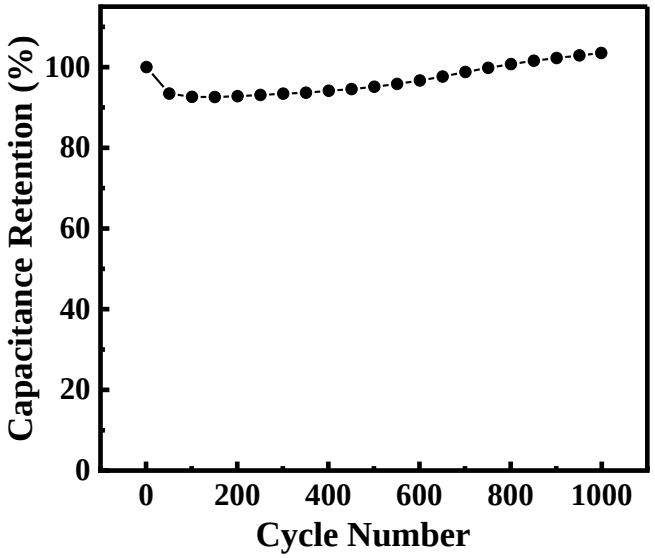

Figure 4.19 Capacitance retention of HEBM NFO with GCD for RD=0.02.

4.6 References

1. Romero, M.; Faccio, R.; Montenegro, B.; Tumelero, M.A.; Cid, C.C.P.; Pasa, A.A.; Mombrú, A.W. Role of conducting polyaniline interphase on the low field

magnetoresistance for LSMO-PANI nanocomposites. J. Magn. Magn. Mater. 2018, 466, 446–451.
2. Romero, M.; Faccio, R.; Pardo, H.; Tumelero, M.A.; Cid, C.C.P.; Pasa, A.A.; Mombrú, Á.W. Microstructure, interparticle interactions and magnetotransport of manganite-polyaniline nanocomposites. Mater. Chem. Phys. 2016, 171, 178–184.
3. Pana, O.; Soran, M.; Leostean, C.; Macavei, S.; Gautron, E.; Teodorescu, C.; Gheorghe, N.; Chauvet, O. Interface charge transfer in polypyrrole coated perovskite manganite magnetic nanoparticles. J. Appl. Phys. 2012, 111, 044309.
4. Gupta, K.; Jana, P.; Meikap, A.; Nath, T. Synthesis of La0.67Sr0.33MnO3 and polyaniline nanocomposite with its electrical and magneto-transport properties. J. Appl. Phys. 2010, 107, 073704.
5. Patil, P.H.; Kulkarni, V.V.; Dongale, T.D.; Jadhav, S.A. α-Manganese Dioxide (α-MnO2) Coated with Polyaniline (PANI) and Reduced Graphene Oxide (rGO)-Based Nanocomposite for Supercapacitor Application. J. Compos. Sci. 2023, 7, 167.
6. Patil, P.H.; Kulkarni, V.V.; Jadhav, S.A. An Overview of Recent Advancements in Conducting Polymer–Metal Oxide Nanocomposites for Supercapacitor Application. J. Compos. Sci. 2022, 6, 363.
7. Kausar, A.; Ahmad, I.; Zhao, T.; Aldaghri, O.; Ibnaouf, K.H.; Eisa, M.H. Cutting-Edge Graphene Nanocomposites with Polythiophene–Design, Features and Forefront Potential. J. Compos. Sci. 2023, 7, 319.
8. Kausar, A.; Ahmad, I. Electrospinning Processing of Polymer/Nanocarbon Nanocomposite Nanofibers—Design, Features, and Technical Compliances. J. Compos. Sci. 2023, 7, 290.
9. Wang, Y.; Wang, Y.; Wang, C.; Wang, Y. A Hierarchical Architecture of Functionalized Polyaniline/Manganese Dioxide Composite with Stable-Enhanced Electrochemical Performance. J. Compos. Sci. 2021, 5, 129.
10. Amarnath, C.A.; Ghamouss, F.; Schmaltz, B.; Autret-Lambert, C.; Roger, S.; Gervais, F.; Tran-Van, F. Polypyrrole/lanthanum strontium manganite oxide nanocomposites: Elaboration and characterization. Synth. Met. 2013, 167, 18–24.
11. Al-Rubaye, S.; Rajagopalan, R.; Subramaniyam, C.; Tai, Z.; Xian, J.; Wang, X.; Dou, S.X.; Cheng, Z. NiFe(2)O(4) nanoparticles coated on 3D graphene capsule as electrode for advanced energy storage applications. Dalton Trans. 2018, 47, 14052–14059.
12. Arun, T.; Kavinkumar, T.; Udayabhaskar, R.; Kiruthiga, R.; Morel, M.J.; Aepuru, R.; Dineshbabu, N.; Ravichandran, K.; Akbari-Fakhrabadi, A.; Mangalaraja, R.V. NiFe2O4 nanospheres with size-tunable magnetic and electrochemical properties for superior supercapacitor electrode performance. Electrochim. Acta 2021, 399, 139346.
13. Askari, M.B.; Salarizadeh, P. Binary nickel ferrite oxide (NiFe2O4) nanoparticles coated on reduced graphene oxide as stable and high-performance asymmetric supercapacitor electrode material. Int. J. Hydrog. Energy 2020, 45, 27482–27491.
14. Baig, M.M.; Pervaiz, E.; Azad, M.; Jahan, Z.; Khan Niazi, M.B.; Baig, S.M. NiFe2O4/SiO2 nanostructures as a potential electrode material for high rated supercapacitors. Ceram. Int. 2021, 47, 12557–12566.
15. Bandgar, S.B.; Vadiyar, M.M.; Ling, Y.-C.; Chang, J.-Y.; Han, S.-H.; Ghule, A.V.; Kolekar, S.S. Metal Precursor Dependent Synthesis of NiFe2O4 Thin Films for High-Performance Flexible Symmetric Supercapacitor. ACS Appl. Energy Mater. 2018, 1, 638–648.

16. Deyab, M.A.; Awadallah, A.E.; Ahmed, H.A.; Mohsen, Q. Progress study on nickel ferrite alloy-graphene nanosheets nanocomposites as supercapacitor electrodes. J. Energy Storage 2022, 46, 103926.
17. Gao, X.; Bi, J.; Wang, W.; Liu, H.; Chen, Y.; Hao, X.; Sun, X.; Liu, R. Morphology-controllable synthesis of NiFe2O4 growing on graphene nanosheets as advanced electrode material for high performance supercapacitors. J. Alloys Compd. 2020, 826, 154088.
18. Gao, X.; Wang, W.; Bi, J.; Chen, Y.; Hao, X.; Sun, X.; Zhang, J. Morphology-controllable preparation of NiFe2O4 as high performance electrode material for supercapacitor. Electrochim. Acta 2019, 296, 181–189.
19. Hua, M.; Xu, L.; Cui, F.; Lian, J.; Huang, Y.; Bao, J.; Qiu, J.; Xu, Y.; Xu, H.; Zhao, Y.; et al. Hexamethylenetetramine-assisted hydrothermal synthesis of octahedral nickel ferrite oxide nanocrystallines with excellent supercapacitive performance. J. Mater. Sci. 2018, 53, 7621–7636.
20. Huang, T.; Cui, W.; Qiu, Z.; Hu, Z.; Zhang, Z. 2D porous layered NiFe2O4 by a facile hydrothermal method for asymmetric supercapacitor. Ionics 2021, 27, 1347–1355.
21. Zhang, X.; Zhu, M.; Ouyang, T.; Chen, Y.; Yan, J.; Zhu, K.; Ye, K.; Wang, G.; Cheng, K.; Cao, D. NiFe2O4 nanocubes anchored on reduced graphene oxide cryogel to achieve a 1.8 V flexible solid-state symmetric supercapacitor. Chem. Eng. J. 2019, 360, 171–179.
22. Javed, M.S.; Zhang, C.; Chen, L.; Xi, Y.; Hu, C. Hierarchical mesoporous NiFe2O4 nanocone forest directly growing on carbon textile for high performance flexible supercapacitors. J. Mater. Chem. A 2016, 4, 8851–8859.
23. Hareesh, K.; Shateesh, B.; Joshi, R.P.; Dahiwale, S.S.; Bhoraskar, V.N.; Haram, S.K.; Dhole, S.D. PEDOT:PSS wrapped NiFe2O4/rGO tertiary nanocomposite for the super-capacitor applications. Electrochim. Acta 2016, 201, 106–116.
24. Chang, Z.; Li, T.; Li, G.; Wang, K. One-pot in-situ synthesis of Ni(OH)2–NiFe2O4 nanosheet arrays on nickel foam as binder-free electrodes for supercapacitors. J. Mater. Sci. Mater. Electron. 2018, 30, 600–608.
25. Scindia, S.S.; Kamble, R.B.; Kher, J.A. Nickel ferrite/polypyrrole core-shell composite as an efficient electrode material for high-performance supercapacitor. AIP Adv. 2019, 9, 055218.
26. Chen, R.; Yu, M.; Sahu, R.P.; Puri, I.K.; Zhitomirsky, I. The development of pseudocapacitor electrodes and devices with high active mass loading. Adv. Energy Mater. 2020, 10, 1903848.
27. Kinemuchi, Y.; Ishizaka, K.; Suematsu, H.; Jiang, W.; Yatsui, K. Magnetic properties of nanosize NiFe2O4 particles synthesized by pulsed wire discharge. Thin Solid Film. 2002, 407, 109–113.
28. Tien, N.A.; Mittova, V.; Sladkopevtsev, B.; Mai, V.Q.; Mittova, I.Y.; Vuong, B.X. Structural, optical and magnetic properties of Y-doped NiFe2O4 nanoparticles prepared by simple co-precipitation method. Solid State Sci. 2023, 138, 107149.
29. Bashir, A.; Matinise, N.; Sackey, J.; Kaviyarasu, K.; Madiba, I.; Kodseti, L.; Ezema, F.; Maaza, M. Investigation of electrochemical performance, optical and magnetic properties of NiFe2O4 nanoparticles prepared by a green chemistry method. Phys. E Low-Dimens. Syst. Nanostructures 2020, 119, 114002.
30. Dippong, T.; Cadar, O.; Levei, E.A. Effect of Transition Metal Doping on the Structural, Morphological, and Magnetic Properties of NiFe2O4. Materials 2022, 15, 2996.

31. Reddy, R.N.; Reddy, R.G. Sol–gel MnO2 as an electrode material for electrochemical capacitors. J. Power Sources 2003, 124, 330–337.
32. Jeong, Y.; Manthiram, A. Nanocrystalline manganese oxides for electrochemical capacitors with neutral electrolytes. J. Electrochem. Soc. 2002, 149, A1419.
33. Dong, W.; Sakamoto, J.S.; Dunn, B. Electrochemical properties of vanadium oxide aerogels. Sci. Technol. Adv. Mater. 2003, 4, 3–11.
34. Tallman, D.; Vang, C.; Wallace, G.; Bierwagen, G. Direct electrodeposition of polypyrrole on aluminum and aluminum alloy by electron transfer mediation. J. Electrochem. Soc. 2002, 149, C173.
35. Chen, S.; Zhitomirsky, I. Influence of dopants and carbon nanotubes on polypyrrole electropolymerization and capacitive behavior. Mater. Lett. 2013, 98, 67–70.
36. Wang, G.-L.; Xu, J.-J.; Chen, H.-Y. Dopamine sensitized nanoporous TiO2 film on electrodes: Photoelectrochemical sensing of NADH under visible irradiation. Biosens. Bioelectron. 2009, 24, 2494–2498.
37. Seung-Hoon, S.; Young-Je, Y. Characteristics of mediated enzymatic nitrate reduction by gallocyanine-bound nanoporous electrode. J. Microbiol. Biotechnol. 2006, 16, 505–510.
38. Snook, G.A.; Kao, P.; Best, A.S. Conducting-polymer-based supercapacitor devices and electrodes. J. Power Sources 2011, 196, 1–12.
39. Raudsepp, T.; Marandi, M.; Tamm, T.; Sammelselg, V.; Tamm, J. Influence of ion-exchange on the electrochemical properties of polypyrrole films. Electrochim. Acta 2014, 122, 79–86.
40. Sikkema, R.; Zhitomirsky, I. Magnetic supercapacitors: Charge storage mechanisms, magnetocapacitance, and magnetoelectric phenomena. Appl. Phys. Rev. 2023, 10, 021307.
41. Wang, Y.; Liu, Y.; Zhitomirsky, I. Surface modification of MnO2 and carbon nanotubes using organic dyes for nanotechnology of electrochemical supercapacitors. J. Mater. Chem. A 2013, 1, 12519–12526.
42. Shrikrushna, S.; Kher, J.A.; Kulkarni, M.V. Influence of dodecylbenzene sulfonic acid doping on structural, morphological, electrical and optical properties on polypyrrole/3C-SiC nanocomposites. J. Nanomed. Nanotechnol. 2015, 6, 1.
43. Hu, J.; Li, Y.; Gao, G.; Xia, S. A mediated BOD biosensor based on immobilized B. subtilis on three-dimensional porous graphene-polypyrrole composite. Sensors 2017, 17, 2594.

5. Pseudocapacitive and Magnetic Properties of $SrFe_{12}O_{19}$-Polypyrrole Composites

The information contained in this chapter has been submitted to the journal of composites sciences and is currently under peer review:

M. MacDonald and I. Zhitomirsky, "Pseudocapacitive and Magnetic Properties of $SrFe_{12}O_{19}$-Polypyrrole Composites," *Journal of Composites Science*, vol. 8, no. x, 2024, doi: 10.3390/xxxxx.

Abstract

This study is motivated by interest in advanced composites, combining spontaneous magnetization with electrical charge storage properties. It is focused on investigation of magnetically hard $SrFe_{12}O_{19}$ (SFO) material and its composites with conductive polypyrrole (PPy) polymer. For the first time, high-energy ball milling (HEBM) and organic dispersant-charge transfer mediators were used for the fabrication of SFO and composite electrodes with high active mass loading. An important finding was the ability to achieve high capacitance of SFO and composites in a negative potential range in a neutral Na_2SO_4 electrolyte. The benefits of the Na_2SO_4 electrolyte and charge storage mechanism are discussed. Another important finding was the synergy of properties of SFO and PPy, which facilitated the fabrication of composites with high capacitance and low impedance. The effects of HEBM and SFO content in the composites on capacitive properties were studied. Magnetic measurements revealed the effect of HEBM on magnetic properties and demonstrated good magnetic properties of the composites, which exhibited advanced capacitive properties. The composites were used for the fabrication of an asymmetric device, which showed good capacitive properties in a voltage window of 1.5 V.

Keywords: strontium ferrite; polypyrrole; composite; supercapacitor; magnetization; device

5.1 Introduction

Multifunctional materials and composites, combining advanced magnetic and electrical properties, are currently under investigation for applications based on magnetoelectric interactions[2-4]. $SrFe_{12}O_{19}$ (SFO) combines ferrimagnetic and ferroelectric properties and belongs to multiferroic materials[5, 6]. Moreover, SFO exhibits semiconducting and magnetooptical properties[7]. The magnetoplumbite-type crystal structure of SFO facilitates super-exchange interactions of Fe^{3+} ions, which result in antiparallel spin ordering with uncompensated magnetic moments of the individual sublattices and high net magnetization [7]. SFO exhibits high coercive field and belongs to the category of hard magnetic materials, which are beneficial for permanent magnets and memory applications. The magnetic properties of SFO are also characterized[8] by a relatively high Neel temperature of 450°C. Ferroelectric properties of SFO were reported in literature[8-11]. However, the observation of ferroelectric hysteresis loops presents difficulties due to relatively high conductivity of SFO. Moreover, relatively high electric fields are required for the analysis of the hysteresis loops[9]. As a result of high conductivity, the hysteresis loops showed a "banana" shape[12], which was reported in several investigations[8, 10, 12-14]. However, annealing in oxygen[12] or in air[11] at high temperatures resulted in enhanced resistivity and classical hysteresis loops with ferroelectric saturation were observed for annealed SFO. In addition to improved ferroelectric loops, the classical peaks in current-voltage dependences and a maximum of dielectric permittivity at the Curie point were observed[12]. The annealed SFO showed significant changes in capacitance under the influence of a magnetic field[12]. Other investigations revealed a 9% change in SFO magnetization under the influence of an electric field[8]. The difficulties related to the applications of ferroelectric properties of this material were addressed by the development of composites of SFO with advanced ferroelectrics, such as $BaTiO_3$[15, 16], $PbTiO_3$[17], $BiFeO_3$[18, 19] and polymers[20, 21].

A new wave of interest in SFO resulted from the development of magnetically ordered pseudocapacitive (MOPC) materials and composites. The electrical capacitance of MOPC is by 6-8 orders of magnitudes higher than the capacitance of advanced ferroelectrics[22]. Investigations of MOPC revealed interesting magnetoelectric and magnetocapacitive effects, such as influence of electric/magnetic field on magnetization/electric capacitance, shift of magnetic Curie point under the influence of electric field, enhancement of high frequency capacitance in a magnetic field, improved charge-discharge cycling stability and other effects[22]. The capacitance of MOPC is based on various electrochemical charge storage mechanisms[22]. Spinel ferrites, such as Fe_3O_4, γ-Fe_2O_3, $NiFe_2O_4$ and $CuFe_2O_4$ showed high capacitance related to reduction of Fe^{3+} to Fe^{2+} ions at applied negative potentials[22]. Therefore, $SrFe_{12}O_{19}$ is a promising electrochemical charge storage material due to the large Fe content in this material.

The electrochemical charge storage properties of SFO were reported in several investigations. The investigations[23-25] in KOH electrolyte showed significant deviation from ideal pseudocapacitive response. Cyclic voltammetry revealed redox peaks and galvanostatic charge-discharge curves were essentially nonlinear[23, 24]. The electrodes showed a relatively high resistance[25], which is detrimental for electrochemical charge storage. The charge storage mechanism in the positive potential range[23, 25] is not well understood. Difficulties in the fabrication of SFO composites with conductive additives and other materials are related to strong magnetic interactions of SFO particles, which result in their agglomeration and poor mixing with other materials. Previous investigations focused on SFO composites with low mass. A significantly higher active mass is necessary for practical applications of SFO, which facilitates the fabrication of composites with high active material to current collector mass ratio.

This investigation is motivated by interesting magnetic and capacitive properties of SFO and potential of this material for the development of multifunctional materials. It was suggested that SFO is promising for the development of MOPC materials. Another driving factor for this research is the possibility to combine SFO with polypyrrole (PPy) in a composite material. PPy is a conductive polymer, which exhibits excellent pseudocapacitive properties[26]. Of particular importance are recent studies of PPy-metal oxide composites, which showed interesting interface phenomena resulting in enhanced magnetization of magnetic oxides [27] and improved conductivity[28] due to electron and spin transfer from PPy.

The goal of this investigation was the fabrication of SFO-PPy composites and investigation of their magnetic and electrochemical capacitive properties. In contrast to the previous studies, we targeted the fabrication of composites with high active mass, which allowed for enlarged active material to current collector mass ratio and higher areal capacitance. The approach was based on the use of different strategies, such as high-energy ball milling (HEBM) and application of a co-dispersant, which acted as a charge transfer mediator. Unlike previous investigations, based on the use of KOH electrolyte, we tested individual materials and composites in a neutral Na_2SO_4 electrolyte. The careful selection of an electrolyte is critically important for composite performance.

PPy shows good performance in neutral electrolytes, such as Na_2SO_4 or acidic electrolytes, such as H_2SO_4. However, the use of alkaline electrolytes, such as KOH can result in degradation of PPy properties. The use of H_2SO_4 can lead to the dissolution of SFO. Therefore, Na_2SO_4 was selected as an electrolyte for the composite electrodes. It is important that in comparison with acid or alkali, the use of Na_2SO_4 offers environmental benefits. In contrast to the previous investigations performed in the positive potential range[23, 25], we tested SFO and composites in a negative

potential range, where contributions of redox Fe^{3+}/Fe^{2+} reactions to the capacitive response were expected. We proposed a charging mechanism of SFO in the negative potential range. An important finding was good capacitance retention at high charge-discharge rates, which was linked to magnetohydrodynamic effect of SFO particles.

Following the work objective, we tested individual SFO electrodes and revealed a strong effect of HEBM and a dispersant-charge transfer mediator on electrode performance. We achieved a high capacitance of 1.29 F cm^{-2}. We analyzed capacitances of SFO-PPy composites with different PPy content and achieved a capacitance of 3.61 F cm^{-2} at a low impedance. We analyzed the effect of HEBM of SFO on capacitive and magnetic properties of the composites and demonstrated that composites combine advanced magnetic and capacitive properties. The composites were used for the fabrication of asymmetric supercapacitor devices, which showed good performance in a voltage window of 1.5 V.

5.2 Materials and Methods

$SrFe_{12}O_{19}$ (SFO), gallocyanine dye (GD), Na_2SO_4, ammonium persulfate (APS), pyrrole (Py), 4,5-dihydroxy-1,3-benzenedisulfonic acid disodium salt monohydrate (Tiron), ethanol, and poly(vinyl butyral) (PVB, 200–300 kDa) were purchased from MilliporeSigma, Burlington, ON, Canada). Carbon nanotubes (CNT, multiwalled, 13 nm diameter, 1–2 μm length, Bayer, Leverkusen, Germany) and commercial Ni foam current collectors (95% porosity, 1.6 mm thickness, Vale, Mississauga, ON, Canada) were used. Polypyrrole (PPy) polymerization was performed using aqueous 0.1 M pyrrole solutions containing 0.01 M Tiron; this was achieved by adding 0.1 M APS at 0 °C.

High-energy ball-milling (HEBM) of SFO was conducted using a Mixer Mill MM 500 Nano (Retsch GmbH, Haan, Germany). HEBM consisted of milling steps at a frequency of 15 Hz during 5 min with 90 s intervals between the steps. The milling duration was 2 h. After HEBM, the SFO material was washed with ethanol and dried.

SFO and CNT were co-dispersed in ethanol using GD as a dispersant. The mass ratio of SFO:CNT was 4:1. The mass ratio of GD dispersant to the total mass of SFO and CNT was 0.02. The mixtures underwent ultrasonication, washing, and drying and re-dispersion in ethanol containing dissolved PVB binder. PPy–SFO–CNT composite powders were also dispersed in PVB solution in ethanol. The mass ratio of SFO-PPy was 7:1 (Composite 1), 6:2 (Composite 2), 5:3 (Composite 3), 1:1 (Composite 4). Composites 1-4 contained as-received SFO (ARSFO) or high energy ball milled SFO (HEBMSFO). The mass ratio of (SFO+PPy):CNT in the composites was 4:1. The obtained slurries were then utilized for electrode fabrication by impregnating Ni foam current collectors. In each electrode, the mass ratio of PVB to the total mass of SFO, PPy and CNT was 0.03. The final mass of the impregnated material, after drying, was 40 mg cm^{-2}. The impregnated Ni foams were pressed to 25% of their initial thickness.

After electrochemical testing, Composite 2, containing HEBMSFO was selected for the fabrication of anodes for an asymmetric device. The procedure for the preparation of MnO_2 cathodes was described in a previous investigation[29].

A SQUID magnetometer (Quantum Design, San Diego, CA, USA) was used for investigation of magnetic properties. XRD testing was conducted with a diffractometer Bruker D8 Advance with Cu-Kα radiation (Bruker, USA). The microstructure investigations involved the use of transmission electron microscopy (TEM, Talos 200 microscope, Thermo Fisher Scientific, Waltham, MA, USA). Electrochemical characterization was carried out in aqueous 0.5 M

Na_2SO_4 electrolyte using a Biologic potentiostat (VMP 300, BioLogic, Seyssinet-Pariset, France). Individual electrodes were tested with a three-electrode system, using a saturated calomel reference electrode (SCE), an SFO-based working electrode, and a Pt mesh counter electrode. Cyclic voltammetry (CV), electrochemical impedance spectroscopy (EIS), and chronopotentiometry (CP) methods were used for electrode characterization. The capacitance was calculated from the CV, EIS and CP data as described in Ref.[30].

Areal (C_S) and gravimetric (C_m) capacitances were derived from the CV data using the following equation:

$$C = \frac{\Delta Q}{\Delta U} = \frac{|\int_0^{t(U_{max})} I dt| + |\int_{t(U_{max})}^0 I dt|}{2U_{\max}} \qquad \text{Eq. (5.1)}$$

where DQ is charge, I is current, t is time, DU is potential range, and from the CP data:

$$C = \frac{I\Delta t}{\Delta U} \qquad \text{Eq. (5.2)}$$

The complex capacitance $C^*(\omega) = C'(\omega) - iC''(\omega)$ was derived at different frequencies (ω) from the complex impedance $Z^*(\omega) = Z'(\omega) + iZ''(\omega)$:

$$C'(\omega) = \frac{-Z''(\omega)}{\omega|Z(\omega)|^2} \qquad \text{Eq. (5.3)}$$

$$C''(\omega) = \frac{Z'(\omega)}{\omega|Z(\omega)|^2} \qquad \text{Eq. (5.4)}$$

5.3 Results

Figure 5.1 shows X-ray diffraction pattern of as-received SFO (ARSFO). The diffraction peaks correspond to JCPDS file 04-016-5959 of the magnetoplumbite structure.

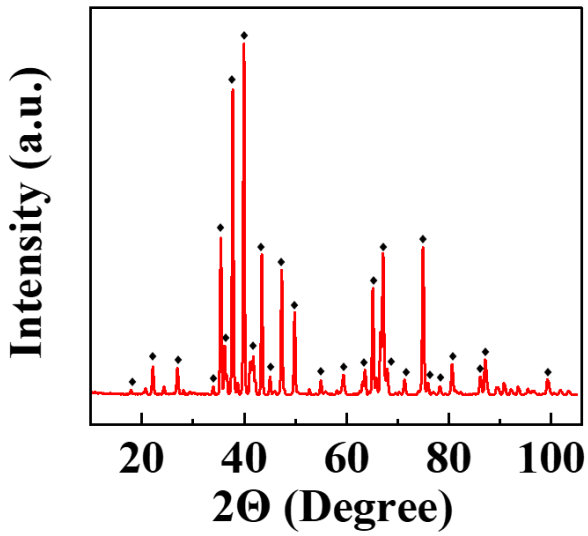

Figure 5.1 X-ray diffraction pattern of ARSFO. ♦ - peaks corresponding to JCPDS file 04-016-5959.

TEM studies showed that particle size of ARSFO was about 200-400 nm (Figure 5.2A). High energy ball milled SFO (HEBMSFO) showed a significantly smaller particle size, which was below 100 nm (Figure 5.2B). However, the TEM image showed (Figure 5.2B) many agglomerated particles with a size below 10 nm. The observed agglomeration of ARSFO and HEBMSFO resulted from Van der Waals and magnetic attraction forces.

Figure 5.3A shows CVs for ARSFO electrodes prepared without and with GD. The CV for ARSFO prepared without GD deviated significantly from the ideal rectangular shape. A relatively low current was observed at potentials above -0.4 V. The electrodes showed a capacitance of 0.054 F cm^{-2} at a scan rate of 2 mV s^{-1}. The use of GD resulted in increasing current, especially in the

range -0.4 - 0 V. The CVs showed redox peaks at -0.3 - - 0.4 V. The electrodes prepared using GD showed a capacitance of 0.099 F cm^{-2} at a scan rate of 2 mV s^{-1}. HEBM resulted in a significant increase of CV currents (Figure 5.3B). HEBMSFO electrodes prepared without and with GD showed capacitances of 0.79 and 1.12 F cm^{-2}, respectively, at 2 mV s^{-1}. CP data showed longer charge/discharge times for electrodes prepared using GD and HEBM (Figures 5.3.3C, D), which indicated higher capacitances. The capacitances of ARSFO electrodes prepared without and with GD were found to be 0.067 and 0.10 F cm^{-2}, respectively, at a current density of 3 mA cm^{-2}. The HEBMSFO electrodes prepared without and with GD showed capacitances of 0.91 and 1.29 F cm^{-2}, respectively at the same current density. Figure 5.3 E, F and Supplementary Information Figure 5.10 compare capacitances for the electrodes, measured at different scan rates and different current densities. Such data provide additional evidence of the beneficial effect of HEBM and GD.

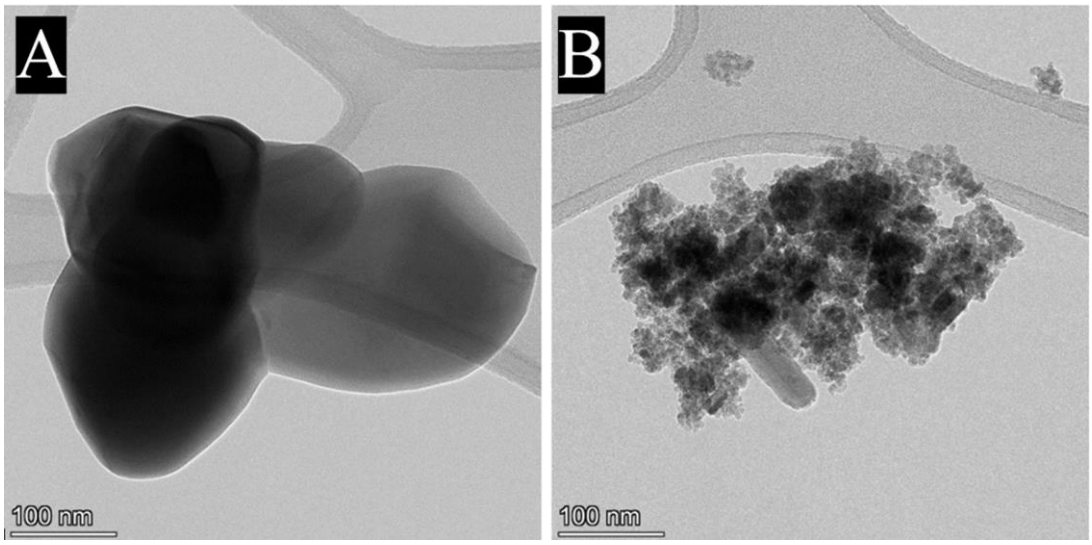

Figure 5.2 TEM images of (A) ARSFO and (B) HEBMSFO.

The mechanism of charge storage of SFO can be described by the equation:

$$SrFe^{3+}_{12}O_{19} + \delta e^- + \delta Na^+ \leftrightarrow SrFe^{3+}_{12-\delta}Fe^{2+}_{\delta}O_{19}Na_{\delta} \qquad \text{Eq. (5.5)}$$

Turning again to the TEM data, it is observed that HEBM resulted in significant reduction of particle size. The smaller particle size is beneficial for improved electrolyte access to the particle surface, which facilitates redox charge-storage reactions. However, it is important to note that investigations of pseudocapacitor materials [31-33] did not show correlation between BET surface area and capacitance. In some cases, materials with lower surface area showed higher capacitances, compared to the capacitances of the materials with higher surface area [31-33]. The influence of GD on the capacitance of the ARSFO and HEBMSFO is not well understood. Figure 5.11A shows the chemical structure of GD. The catechol group of this molecule facilitates its chemical bonding (Figure 5.11B) to surface metal atoms on SFO particles and facilitates adsorption on the particles. The polyaromatic structure of GD facilitated its adsorption on CNT due to π-π interactions.

The adsorbed charged GD molecules can improve co-dispersion of SFO and CNT and facilitate their mixing. It was hypothesized that improved mixing of SFO with conductive CNT additives can potentially result in enhanced capacitance. It should be noted that due to the very small amount of GD used, the analysis of adsorption by FTIR and other absorption methods presented difficulties. Other difficulties were related to the SEM observations of bulk microstructure of impregnated Ni foam current collectors. However, CV data provide evidence of the GD adsorption on the active material. The observed peaks in CVs of ARSFO and HEBMSFO are related to the redox reactions (Figure 5.11C) of the adsorbed GD. Such peaks were not observed for electrodes prepared without GD. It should be noted that the amount of GD used for electrode

preparation was only 2% of the total mass of the active material. Non-adsorbed GD was removed during washing.

The electrode preparation using 5 or 10 % of GD did not show improvement in capacitance. Therefore, the direct contribution of GD redox reaction to the electrode capacitance is negligibly small due to the small amount of GD used and a large mass of the GD molecule. However, GD can act as a charge transfer mediator, which facilitates redox reactions of SFO. It is in this regard that adsorbed charge transfer mediator molecules facilitated electrochemical reactions in electrochemical sensors[34, 35], photovoltaic devices[36, 37], and electropolymerization[38, 39] processes. GD adsorbed on TiO_2 particles was used as a charge transfer mediator for enzymatic nitrate reduction[40]. The HEBMSFO showed relatively good capacitance retention at high charge-discharge rates, which can be attributed to the magnetohydrodynamic effect[22] of magnetically hard SFO.

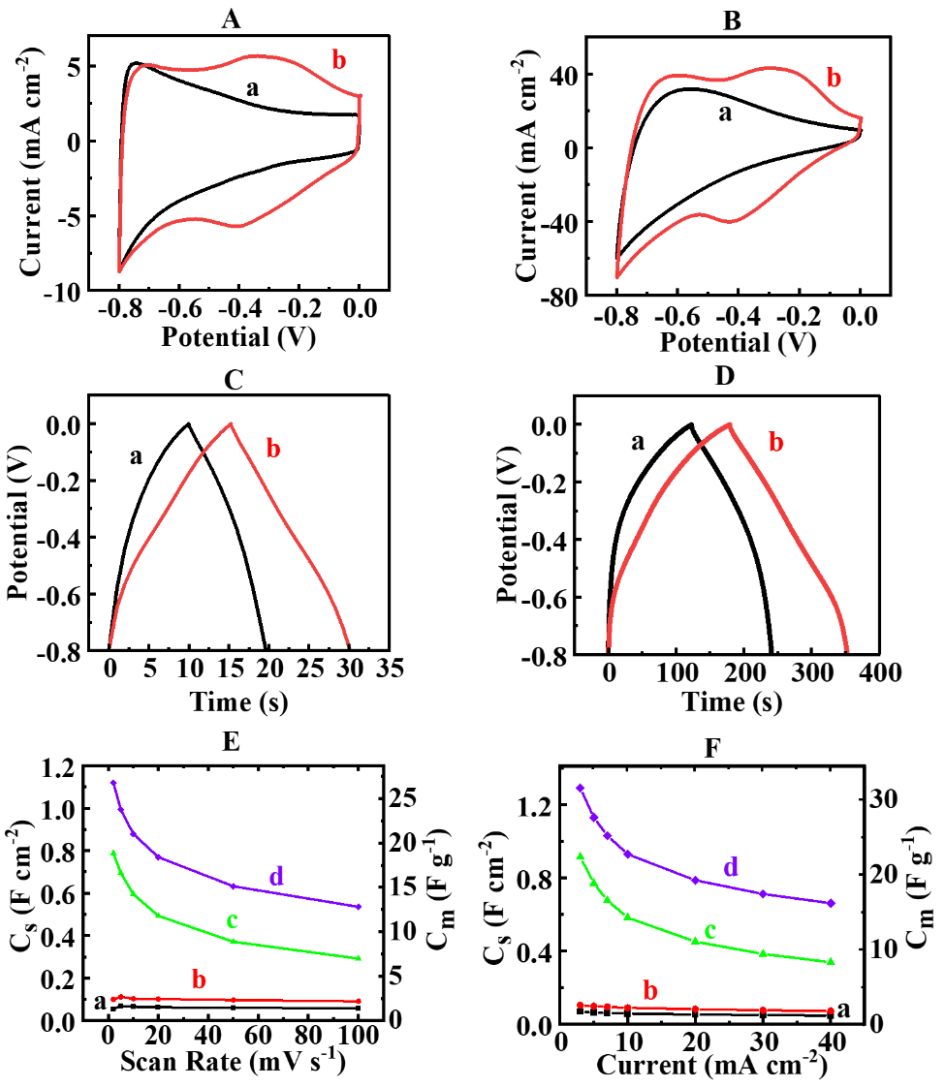

Figure 5.3. (A,B) CVs at a scan rate of 50 mV s^{-1} for (A) ARSFO and (B) HEBMSFO, prepared (a) without GD and (b) using GD; (C,D) CP data at a current density of 5 mA cm^{-2} for (C) ARSFO and (D) HEBMSFO, prepared (a) without GD and (b) using GD; (E,F) capacitance derived from (E) CV data at different scan rates and (F) CP data at different current densities for (a,b) ARSFO, (c,d) HEBMSFO for electrodes prepared (a,c) without GD and (b,d) with GD.

The results obtained for ARSFO and HEBMSFO provided a platform for the development of composites, containing SFO and PPy. Figure 5.4A shows CVs for Composite 1 prepared using ARSFO and HEBMSFO. Composite 1 prepared using ARSFO showed enhanced current at potentials above -0.5 V (Figure 5.4A(a)). This can be attributed to capacitive contribution of PPy.

It should be noted that ARSFO showed current decrease with increasing potential above -0.5 V (Figure 5.3A(a)). HEBM resulted in enhanced contribution of SFO and the CV of the Composite 1, prepared using HEBMSFO, exhibited improved shape, which approached to the desired ideal rectangular shape of CV for pseudocapacitive materials (Figure 5.4A(b)). The Composite 2 electrode showed a similar CV shape and enhanced current (Figure 5.4B(a)). The improved CV shape indicated a synergy of contributions of SFO and PPy in different parts of the CV window. The CV for Composite 3 deviated from the rectangular shape (Figure 5.4B(b)). The Composite 4 with larger PPy content showed a similar CV (Figure 5.14). The analysis of capacitances of Composite 1, prepared using ARSFO and HEBM SFO provided additional evidence of beneficial effect of HEBM, which resulted in higher capacitances at different scan rates (Figures 5.4C and 5.13). The capacitance of the Composite 1 prepared using HEBMSFO was 1.77 F cm^{-2} at 2 mV s^{-1}. Composites 2 and 3 showed capacitances of 2.68 and 3.61 F cm^{-2}, respectively at 2 mV s^{-1}. However, composite 2 showed better capacitance retention and higher capacitance at high scan rates (Figure 5.4D). Composite 4 with larger PPy content did not show improvement in capacitance, compared to Composite 3 (Figures S3 and S5).

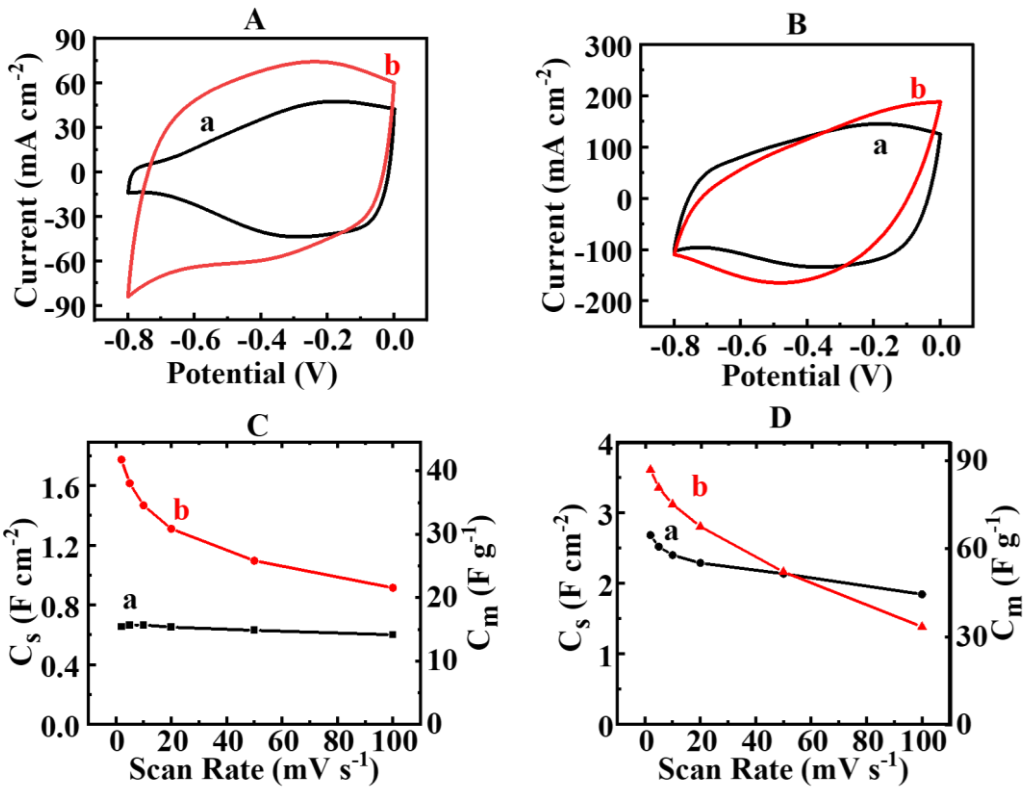

Figure 5.4. (A, B) CVs at a scan rate of 50 mV s^{-1} for (A) Composite 1, prepared using (a) ARSFO and (b) HEBMSFO, (B) (a) Composite 2 and (b) Composite 3 prepared using HEBMSFO; (C,D) capacitances at different scan rates for (C) Composite 1, prepared using (a) ARSFO and (b) HEBMSFO and (D) (a) Composite 2 and (b) Composite 3 prepared using HEBM SFO.

Figures 5.5 and 5.12 show CP data for Composites 1-4. The CP data showed significantly longer charge/discharge time for Composite 1 prepared using HEBMSFO, compared to that for prepared using ARSFO at a current density of 3 mA cm^{-2} and at higher current densities in the range of 3-40 mA cm^{-2}. The longer charge/discharge time indicated higher capacitance. Composite 3 showed slightly longer charge/discharge time, compared to Composite 2 at a current density of 3 mA cm^{-2}. However, the difference decreased with increasing current density. The capacitances calculated from the CP data were found to be 0.75 and 1.94 F cm^{-2} at 3 mA cm^{-2}, 0.62 and 1.27 F

cm^{-2} at 40 mA cm^{-2} for Composite 1 electrodes prepared using ARSFO and HEBMSFO, respectively. Composites 2 and 3 prepared using HEBMSFO showed capacitances of 2.57 and 3.14 F cm^{-2} at 3 mA cm^{-2}, 1.94 and 2.09 F cm^{-2} at 40 mA cm^{-2}, respectively. The Composite 4 with a larger PPy content did not show essential improvement in capacitance, compared to Composite 3.

The impedance spectroscopy data are summarized in Figures 5.6 and 5.12E. The use of HEBM resulted in the reduced resistance R = Z´ of SFO and composite electrodes. The analysis of data for electrodes prepared using ARSFO and HEBMSFO showed beneficial effect of GD, which also resulted in lower resistances. The investigation of composite electrodes showed that adding conductive PPy polymer led to significantly lower resistances.

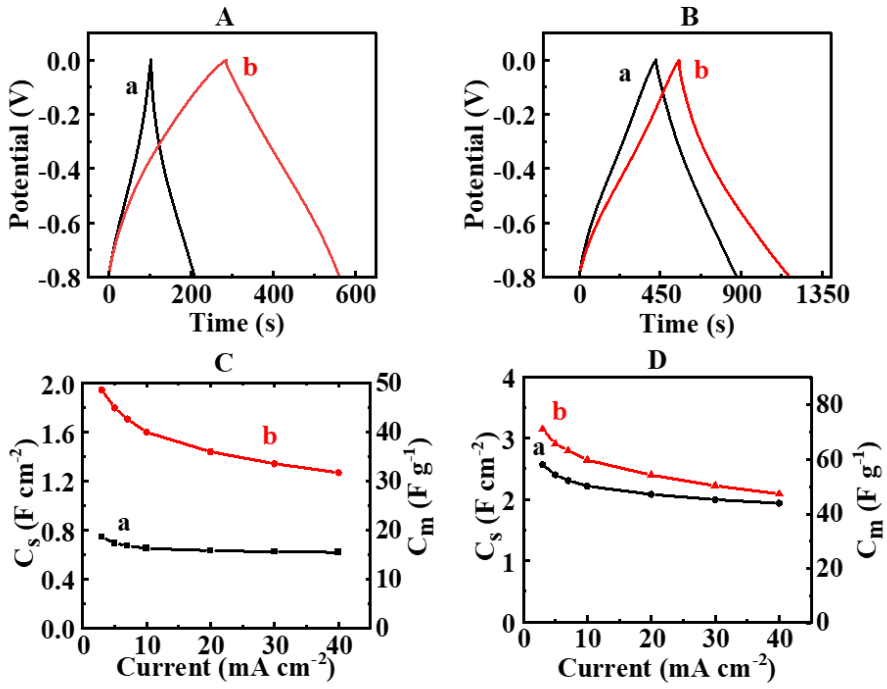

Figure 5.5. (A,B) CP data at a current density of 5 mA cm^{-1} for (A) Composite 1, prepared using (a) ARSFO and (b) HEBMSFO, (B) (a) Composite 2 and (b) Composite 3 prepared using HEBMSFO; (C,D) capacitances at different current densities for (C) Composite 1, prepared

using (a) ARSFO and (b) HEBMSFO and (D) (a) Composite 2 and (b) Composite 3 prepared using HEBMSFO.

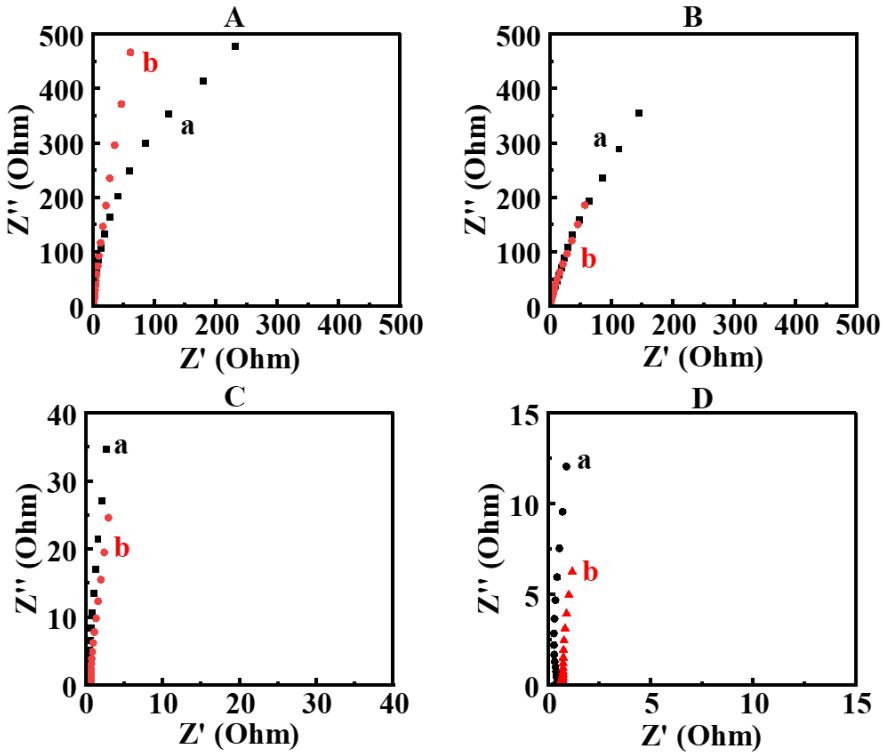

Figure 5.6 EIS data for (A) ARSFO prepared (a) without GD and (b) with GD; (B) HEBMSFO prepared (a) without GD and (b) with GD; (C) Composite 1 prepared using (a) ARSFO and (b) HEBMSFO; (D) (a) Composite 2 and (b) Composite 3.

Testing results revealed good capacitive properties of Composite 2, which showed higher capacitance, compared to Composite 1, improved CV shape and better capacitance retention and higher capacitance at high scan rates, compared to Composites 3 and 4. Moreover, Composite 2 showed better cycling stability, compared to Composite 3. Figure 5.7 shows cycling behavior of Composites 2 and 3. The capacitance retention of Composite 2 was 89.5% after 1000 cycles, whereas the capacitance retention of Composite 3 was only 69.8% for the same number of cycles.

Therefore, Composite 2 was selected for further investigation of magnetic properties and fabrication of a supercapacitor device.

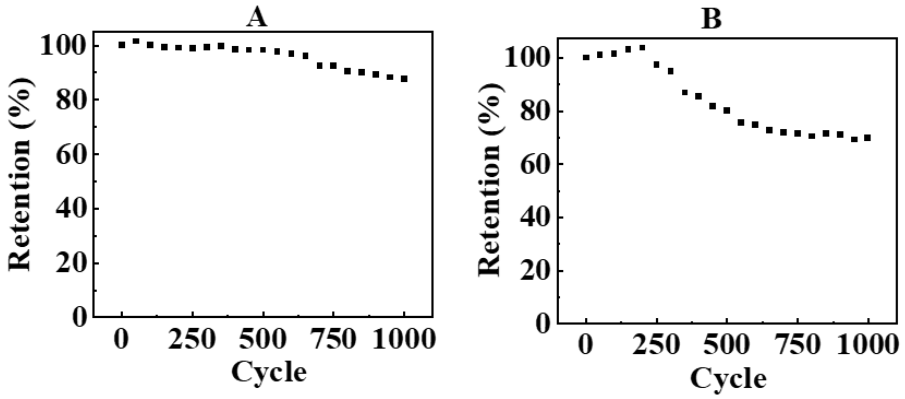

Figure 5.7 Cyclic behavior of (A) Composite 2 and (B) Composite 3.

In addition to high capacitance, the Composite 2 showed magnetic properties. Figure 5.8 showed magnetic measurement results. ARSFO exhibited typical magnetic hysteresis curves with a spontaneous magnetization of about 50 emu g^{-1}.

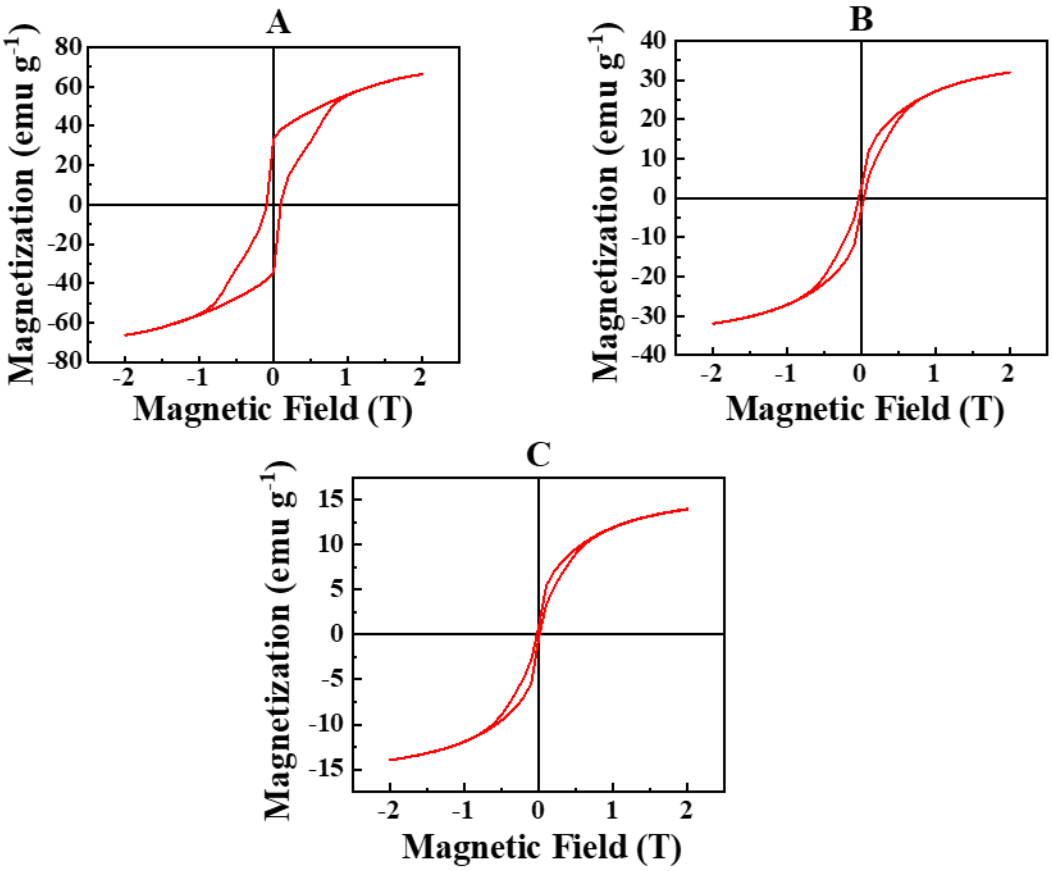

Figure 5.8 Magnetization versus magnetic field for (A) ARSFO, (B) HEBMSFO and (C) Composite 2.

HEBM resulted in reduction of spontaneous magnetization and coercive field. The spontaneous magnetization of SFO after HEBM was about 27 emu g^{-1}. The reduction of spontaneous magnetization and coercive field of magnetic materials with reduction of particle size was reported in literature [41-44]. It was linked to different factors, such as formation of the magnetically "dead" layer on the particle surface with a partially disordered crystalline structure, increase in blocking temperature and transition to a superparamagnetic state. Composite 2 showed

a typical ferrimagnetic hysteresis loop with a spontaneous magnetization of about 12 emu g^{-1}. Therefore, Composite 2 combines high electrochemical capacitance with ferrimagnetic properties.

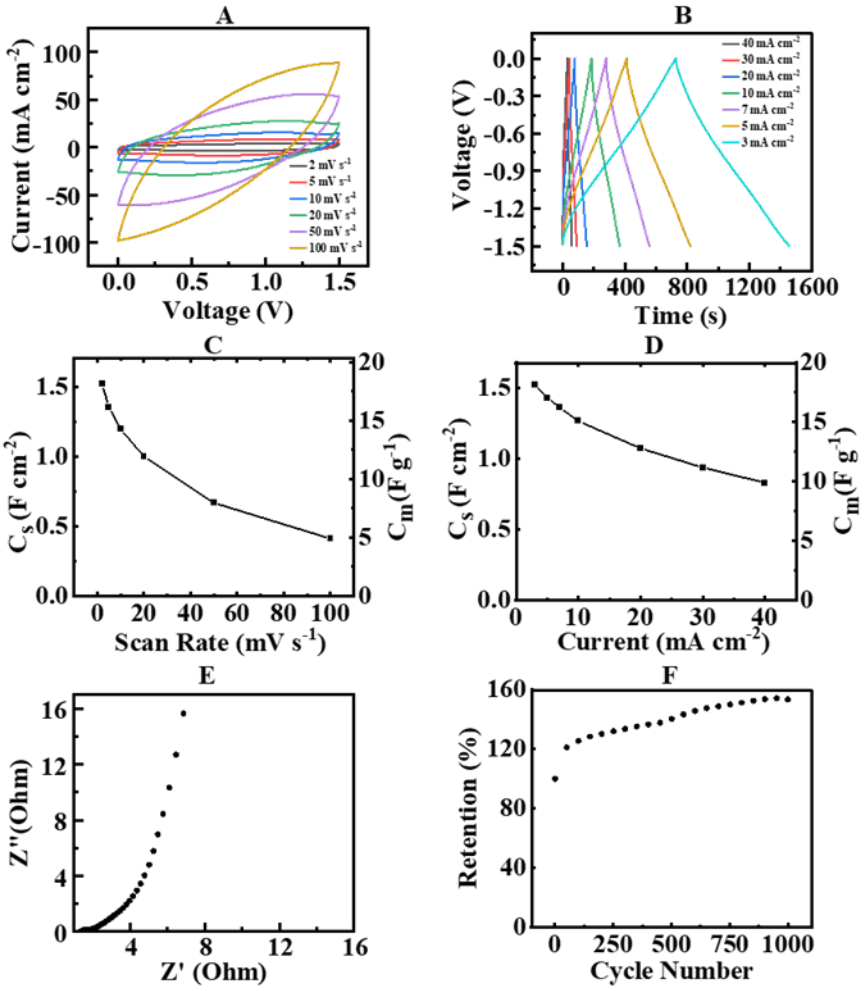

Figure 5.9 (A) CVs at different scan rates, (B) CP data at different current densities, (C) capacitance calculated from CV data versus scan rate, (D) capacitance calculated from CP data versus current density, (E) Nyquist plot of EIS data, (F) cyclic stability for a device containing Composite 2 anode and MnO_2 cathode.

Composite 2 was used for the fabrication of an anode of a supercapacitor device. MnO_2 was selected for the fabrication of a cathode. It is known that MnO_2 exhibits high capacitance in the positive potential range in Na_2SO_4 electrolyte[45-47]. Therefore, MnO_2 is an important cathode material for the fabrication of asymmetric supercapacitor devices[48-50]. The mass loadings of the individual electrodes were 40 mg cm^{-2}. CVs of the device did not show redox peaks in the voltage range of 1.5 V (Figure 5.9A). At low scan rates the CVs were of nearly ideal rectangular shape. The CP measurements showed nearly triangular dependencies (Figure 5.9B). The devices showed capacitances of 1.52 F cm^{-2} at a scan rate of 2 mV s^{-1} and at a current density of 3 mA cm^{-2} (Figure 5.9 C, D). The electrolyte diffusion limitations resulted in reduction in capacitance with reducing charge-discharge time. The total device impedance (Figure 5.9E) contained contributions of cathode, anode and electrolyte in the separator membrane. The capacitance of the device showed an increase during the first 700 cycles. The capacitance increase was observed in other asymmetric devices, containing MnO_2 cathodes and was attributed to partial oxidation of non-stoichiometric MnO_2 phase[51]. It is in this regard that the precipitation method [29] used for the fabrication of MnO_2 powders for cathodes resulted in the fabrication of a birnessite phase [52, 53], containing not only Mn^{4+}, but also Mn^{3+} ions.

5.4 Conclusions

The application of HEBM and GD allowed the fabrication of SFO electrodes with high areal capacitance of 1.29 F cm^{-2}, which is on par with capacitances of advanced MOPC materials. In contrast to previous investigations, good capacitive behavior was achieved in a negative potential range. The ability of achieving high capacitance in Na_2SO_4 electrolyte offers environmental benefits and opens an avenue for the fabrication of advanced asymmetric devices. The use of HEBM and GD allowed good electrochemical performance of SFO material at a high active mass loading of 40 mg cm^{-2}. HEBM resulted in significant reduction of particle size, which facilitated electrolyte access to the particle surface. GD acted as a co-dispersant and charge transfer mediator, which facilitated charge storage reactions. The charging mechanism of SFO was proposed, which was based on the reduction Fe^{3+}/Fe^{2+} reactions in the negative potential range. HEBM of SFO allowed the fabrication of SFO-PPy electrodes with enhanced capacitance. Composites 1-4 showed enhanced capacitive properties and reduced impedance due to synergy of contributions of SFO and PPy. The best capacitive performance was achieved using Composite 2. Magnetic measurements showed reduction of magnetization with decreasing particle size of SFO. Composite 2 combines advanced capacitive properties and relatively high magnetization, which makes it a promising MOPC material. An asymmetric supercapacitor device with a Composite 2 anode and MnO_2 cathode showed high capacitance of 1.52 F cm^{-2} in a voltage window of 1.5 V.

5.5 Chapter 5 SFO Supplementary Information

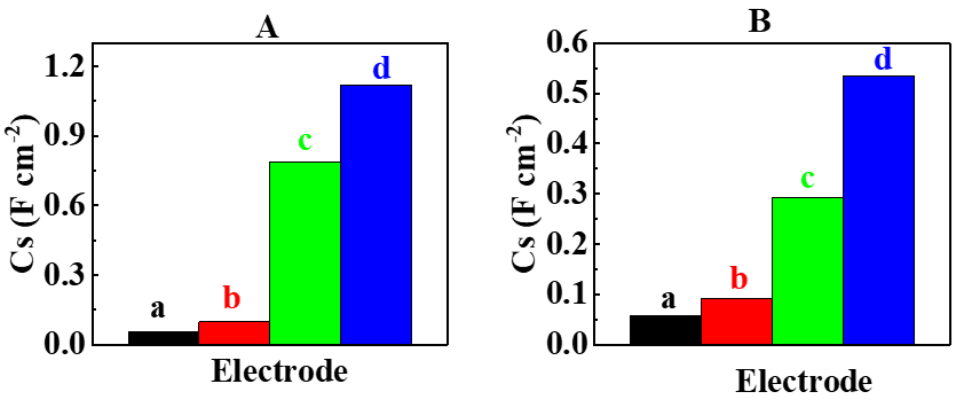

Figure 5.10 Areal capacitances at (A) 2 and (B) 100 mV s^{-1} for different electrodes: (a) ARSFO prepared without GD, (b) ARSFO prepared using GD, (c) HEBMSFO prepared without GD and (d) HEBMSFO prepared using GD.

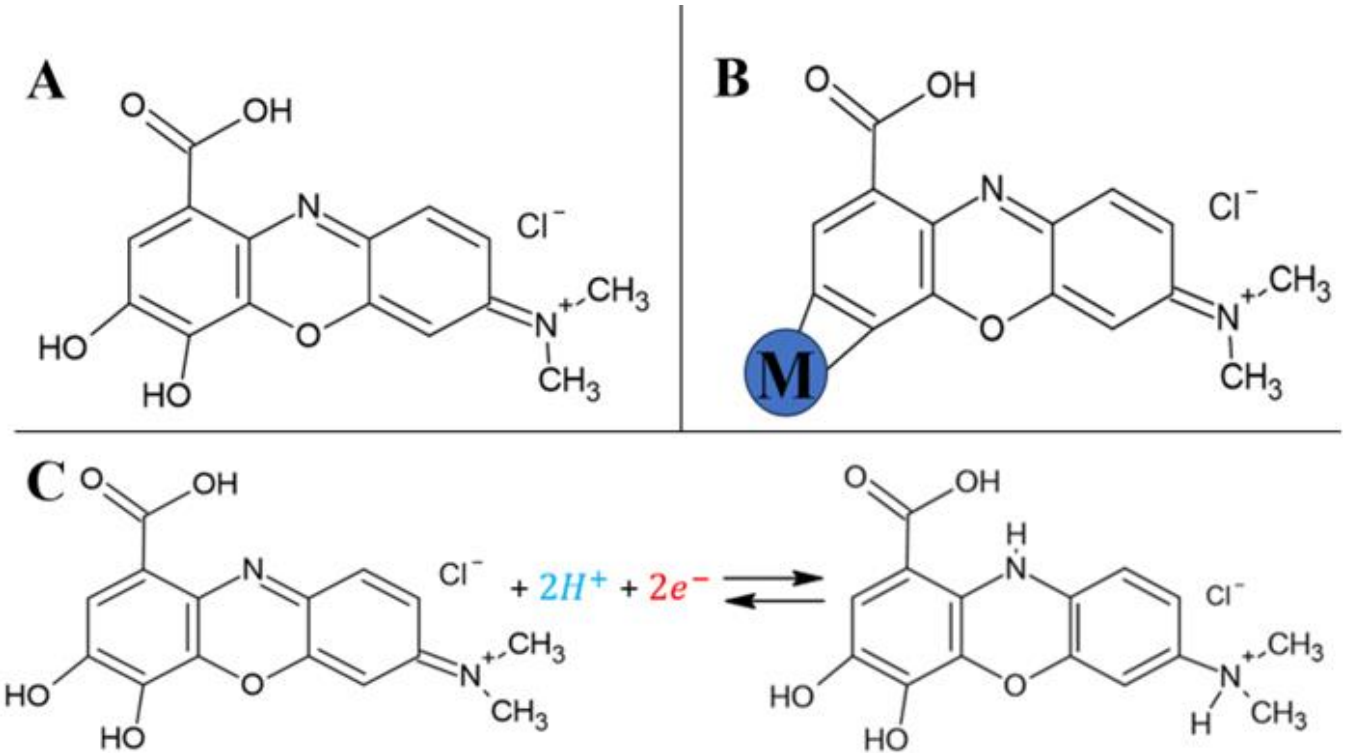

Figure 5.11 (A) Chemical structure of GD, (B) adsorption of GD on SFO involving chemical bonding to metal atoms (M=Fe, Sr) on the particle surface, (C) redox reaction of SFO.

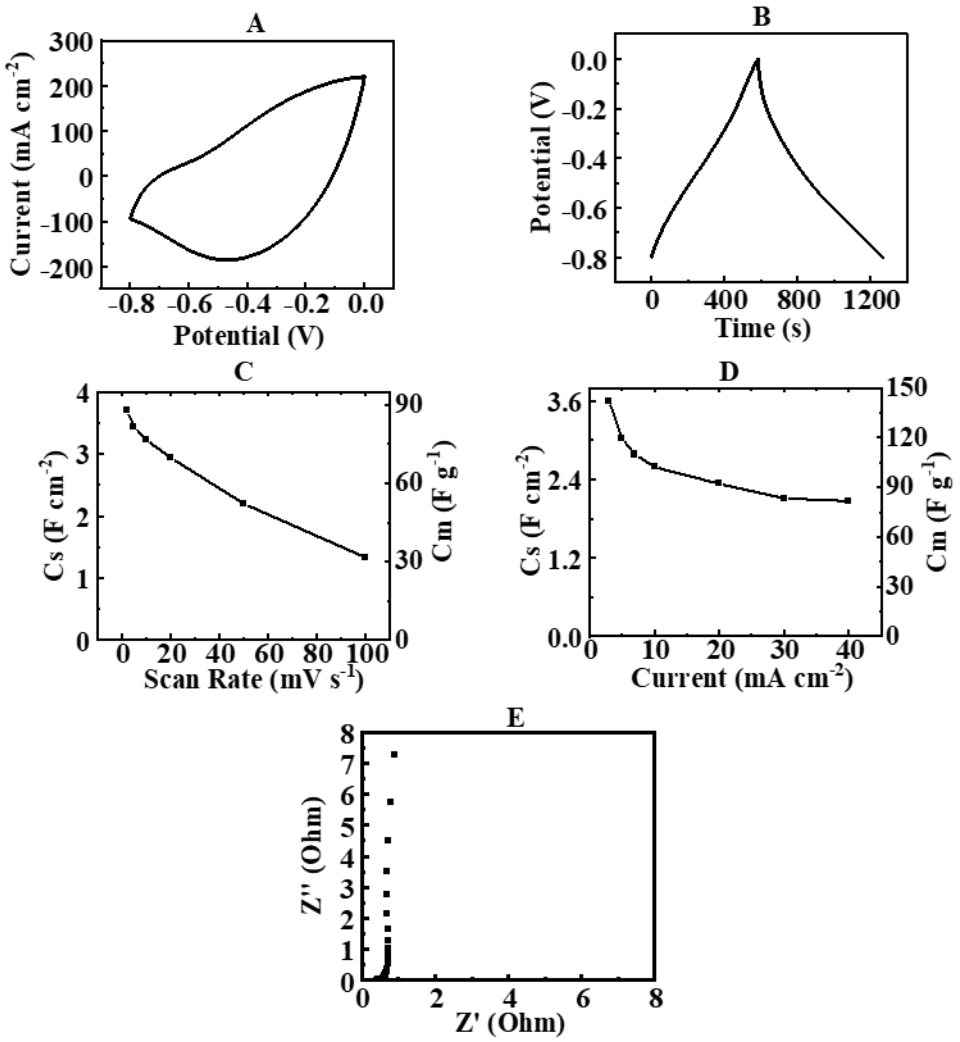

Figure 5.12 (A) CV at a scan rate of 50 mV s^{-1}, (B) CP at a current density of 3 mA cm^{-2}, (C) capacitance obtained from CV data at different scan rates, (D) capacitance obtained for CP data at different current densities, (E) Nyquist plot of complex impedance for Composite 4.

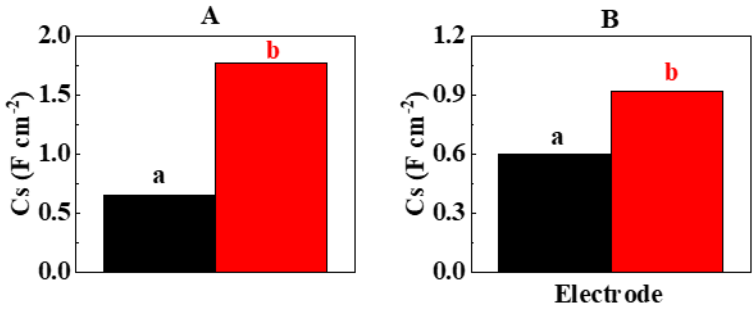

Figure 5.13 Areal capacitances at (A) 2 and (B) 100 mV s^{-1} for Composite 1: prepared using (a) ARSFO and (b) HEBMSFO.

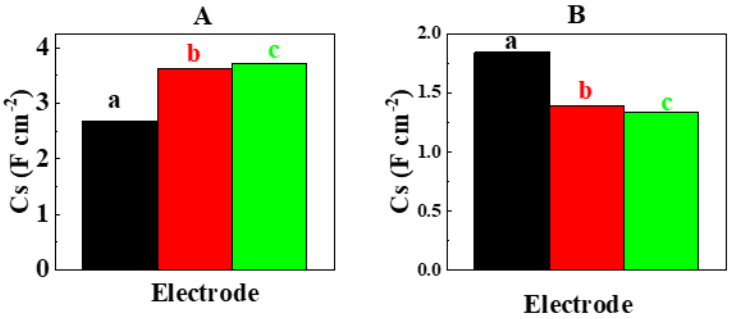

Figure 5.14 Areal capacitances at (A) 2 and (B) 100 mV s^{-1} for (a) Composite 2, (b) Composite 3, (c) Composite 4, prepared using HEBMSFO.

5.6 References

[1] M. MacDonald, I. Zhitomirsky, Capacitive Properties of Ferrimagnetic NiFe2O4-Conductive Polypyrrole Nanocomposites, Journal of Composites Science 8(2) (2024).
[2] G. Srinivasan, Magnetoelectric composites, Annual Review of Materials Research 40 (2010) 153-178.
[3] W. Eerenstein, N. Mathur, J.F. Scott, Multiferroic and magnetoelectric materials, nature 442(7104) (2006) 759-765.
[4] C.-W. Nan, M. Bichurin, S. Dong, D. Viehland, G. Srinivasan, Multiferroic magnetoelectric composites: Historical perspective, status, and future directions, Journal of applied physics 103(3) (2008).
[5] Y.N. Venevtsev, V.V. Gagulin, I.D. Zhitomirsky, Material science aspects of seignette-magnetism problem, Ferroelectrics 73(1) (1987) 221-248.
[6] H. Schmid, Multi-ferroic magnetoelectrics, Ferroelectrics 162(1) (1994) 317-338.
[7] C. Fang, F. Kools, R. Metselaar, R. De Groot, Magnetic and electronic properties of strontium hexaferrite SrFe12O19 from first-principles calculations, Journal of Physics: Condensed Matter 15(36) (2003) 6229.

[8] V. Kostishyn, L. Panina, A. Timofeev, L. Kozhitov, A. Kovalev, A. Zyuzin, Dual ferroic properties of hexagonal ferrite ceramics BaFe12O19 and SrFe12O19, Journal of Magnetism and Magnetic Materials 400 (2016) 327-332.
[9] J. Lee, S.Y. Cho, I. Kim, C.M. Rouleau, K. Kang, S. Ryu, Y. Heo, J.K. Keum, D.M. Pajerowski, Y. Kim, Multiferroism in strained strontium hexaferrite epitaxial thin films, Physical Review Materials 8(2) (2024) 024401.
[10] G. Tan, X. Chen, Synthesis, structures, and multiferroic properties of strontium hexaferrite ceramics, Journal of electronic materials 42 (2013) 906-911.
[11] F. Santos-López, S. Díaz-Castañón, Magnetic Properties and Electric Hysteresis in SrFe12O19 Hexaferrites at Low Sintered Temperatures, Journal of Superconductivity and Novel Magnetism (2024) 1-8.
[12] G. Tan, Y. Huang, H. Sheng, Magnetoelectric response in multiferroic SrFe12O19 ceramics, PLoS One 11(12) (2016) e0167084.
[13] V. Kostishyn, L. Panina, L. Kozhitov, A. Timofeev, A. Kovalev, Synthesis and multiferroic properties of M-type SrFe12O19 hexaferrite ceramics, Journal of Alloys and Compounds 645 (2015) 297-300.
[14] G. Qiang, Y. Jin, X. Lu, X. Cui, D. Deng, B. Kang, W. Yang, S. Cao, J. Zhang, Temperature effect on the magnetic property and ferroelectricity in hexaferrite SrFe 12 O 19, Applied Physics A 122 (2016) 1-6.
[15] S. Katlakunta, P. Raju, S.S. Meena, S. Srinath, R. Sandhya, P. Kuruva, S.R. Murthy, Multiferroic properties of microwave sintered BaTiO3–SrFe12O19 composites, Physica B: Condensed Matter 448 (2014) 323-326.
[16] M. Stingaciu, P. Reuvekamp, C.-W. Tai, R. Kremer, M. Johnsson, The magnetodielectric effect in BaTiO 3–SrFe 12 O 19 nanocomposites, Journal of Materials Chemistry C 2(2) (2014) 325-330.
[17] A. Singh, S. Suri, P. Kumar, B. Kaur, A.K. Thakur, V. Singh, Effect of temperature and frequency on electrical properties of composite multiferroic of lead titanate and strontium hexaferrite (PbTiO3–SrFe12O19), Journal of Alloys and Compounds 764 (2018) 599-615.
[18] J. Martínez-Pérez, A. Bolarín-Miró, F. Pedro-García, C. Cortés-Escobedo, A. Barba-Pingarrón, F. Sánchez-De Jesús, Magnetic and dielectric characterization of xBiFeO3:(1-x) SrFe12O19 multiferroic composites, Journal of Alloys and Compounds 808 (2019) 151700.
[19] A. Das, S. Chatterjee, S. Bandyopadhyay, D. Das, Enhanced magnetoelectric properties of BiFeO3 on formation of BiFeO3/SrFe12O19 nanocomposites, Journal of Applied Physics 119(23) (2016).
[20] X. Yao, J.-P. Zhou, X.-L. Zhang, R.-Y. Lei, Investigation on the electrical and magnetic properties of PVDF/SrFe12O19 composite membranes, Journal of Magnetism and Magnetic Materials 572 (2023) 170601.
[21] S. Prathipkumar, J. Hemalatha, Magnetoelectric behavior and magnetic field-tuned energy storage capacity of SrFe12O19 nanofiber reinforced P (VDF-HFP) composite films, Journal of Magnetism and Magnetic Materials 555 (2022) 169378.
[22] R. Sikkema, I. Zhitomirsky, Magnetic supercapacitors: Charge storage mechanisms, magnetocapacitance, and magnetoelectric phenomena, Applied Physics Reviews 10(2) (2023) 021307.
[23] E. Elanthamilan, S.-F. Wang, Surfactant assisted synthesis of strontium hexaferrite microspheres for the fabrication of high-performance asymmetric supercapacitors, New Journal of Chemistry 47(19) (2023) 9174-9185.
[24] E. Rezaie, A. Rezanezhad, L.S. Ghadimi, A. Hajalilou, N. Arsalani, Effect of calcination on structural and supercapacitance properties of hydrothermally synthesized plate-like SrFe12O19 hexaferrite nanoparticles, Ceramics International 44(16) (2018) 20285-20290.
[25] M. Fu, W. Chen, X. Zhu, B. Yang, Q. Liu, Crab shell derived multi-hierarchical carbon materials as a typical recycling of waste for high performance supercapacitors, Carbon 141 (2019) 748-757.
[26] G.A. Snook, P. Kao, A.S. Best, Conducting-polymer-based supercapacitor devices and electrodes, Journal of power sources 196(1) (2011) 1-12.
[27] O. Pana, M. Soran, C. Leostean, S. Macavei, E. Gautron, C. Teodorescu, N. Gheorghe, O. Chauvet, Interface charge transfer in polypyrrole coated perovskite manganite magnetic nanoparticles, Journal of Applied Physics 111(4) (2012).

[28] J. Xu, D. Wang, Y. Yuan, W. Wei, S. Gu, R. Liu, X. Wang, L. Liu, W. Xu, Polypyrrole-coated cotton fabrics for flexible supercapacitor electrodes prepared using CuO nanoparticles as template, Cellulose 22 (2015) 1355-1363.
[29] Y. Wang, Y. Liu, I. Zhitomirsky, Surface modification of MnO 2 and carbon nanotubes using organic dyes for nanotechnology of electrochemical supercapacitors, Journal of Materials Chemistry A 1(40) (2013) 12519-12526.
[30] R. Chen, M. Yu, R.P. Sahu, I.K. Puri, I. Zhitomirsky, The development of pseudocapacitor electrodes and devices with high active mass loading, Advanced Energy Materials 10(20) (2020) 1903848.
[31] R.N. Reddy, R.G. Reddy, Sol–gel MnO2 as an electrode material for electrochemical capacitors, Journal of Power Sources 124(1) (2003) 330-337.
[32] Y. Jeong, A. Manthiram, Nanocrystalline manganese oxides for electrochemical capacitors with neutral electrolytes, Journal of the Electrochemical Society 149(11) (2002) A1419.
[33] W. Dong, J.S. Sakamoto, B. Dunn, Electrochemical properties of vanadium oxide aerogels, Science and Technology of Advanced Materials 4(1) (2003) 3-11.
[34] E. Kim, Y. Liu, X.W. Shi, X. Yang, W.E. Bentley, G.F. Payne, Biomimetic approach to confer redox activity to thin chitosan films, Advanced Functional Materials 20(16) (2010) 2683-2694.
[35] E. Kim, Y. Liu, W.E. Bentley, G.F. Payne, Redox capacitor to establish bio-device redox-connectivity, Advanced Functional Materials 22(7) (2012) 1409-1416.
[36] G.-L. Wang, J.-J. Xu, H.-Y. Chen, Dopamine sensitized nanoporous TiO2 film on electrodes: photoelectrochemical sensing of NADH under visible irradiation, Biosensors and Bioelectronics 24(8) (2009) 2494-2498.
[37] E.J. Radich, N.R. Peeples, P.K. Santra, P.V. Kamat, Charge transfer mediation through Cu x S. The hole story of CdSe in polysulfide, The Journal of Physical Chemistry C 118(30) (2014) 16463-16471.
[38] D. Tallman, C. Vang, G. Wallace, G. Bierwagen, Direct electrodeposition of polypyrrole on aluminum and aluminum alloy by electron transfer mediation, Journal of the Electrochemical Society 149(3) (2002) C173.
[39] D. Ariyanayagamkumarappa, I. Zhitomirsky, Electropolymerization of polypyrrole films on stainless steel substrates for electrodes of electrochemical supercapacitors, Synthetic Metals 162(9-10) (2012) 868-872.
[40] S. Seung-Hoon, Y. Young-Je, Characteristics of mediated enzymatic nitrate reduction by gallocyanine-bound nanoporous electrode, Journal of microbiology and biotechnology 16(4) (2006) 505-510.
[41] A. Berkowitz, W. Schuele, P. Flanders, Permanent magnets and fine particles, J. Appl. Phys 39 (1968) 1261.
[42] M. Morales, M. Andres-Verges, S. Veintemillas-Verdaguer, M. Montero, C. Serna, Structural effects on the magnetic properties of γ-Fe2O3 nanoparticles, Journal of Magnetism and Magnetic Materials 203(1-3) (1999) 146-148.
[43] S. Liu, J. Zhou, L. Zhang, Effects of crystalline phase and particle size on the properties of plate-like Fe2O3 nanoparticles during γ-to α-phase transformation, The Journal of Physical Chemistry C 115(9) (2011) 3602-3611.
[44] J.R. Jeong, S.J. Lee, J.D. Kim, S.C. Shin, Magnetic properties of γ-Fe2O3 nanoparticles made by coprecipitation method, physica status solidi (b) 241(7) (2004) 1593-1596.
[45] X. Zhang, P. Yu, H. Zhang, D. Zhang, X. Sun, Y. Ma, Rapid hydrothermal synthesis of hierarchical nanostructures assembled from ultrathin birnessite-type MnO2 nanosheets for supercapacitor applications, Electrochimica Acta 89 (2013) 523-529.
[46] M. Jayachandran, A. Rose, T. Maiyalagan, N. Poongodi, T. Vijayakumar, Effect of various aqueous electrolytes on the electrochemical performance of α-MnO2 nanorods as electrode materials for supercapacitor application, Electrochimica acta 366 (2021) 137412.
[47] S. Srither, A. Karthik, S. Arunmetha, D. Murugesan, V. Rajendran, Electrochemical supercapacitor studies of porous MnO2 nanoparticles in neutral electrolytes, Materials Chemistry and Physics 183 (2016) 375-382.

[48] J. Cao, Y. Wang, Y. Zhou, J.-H. Ouyang, D. Jia, L. Guo, High voltage asymmetric supercapacitor based on MnO2 and graphene electrodes, Journal of Electroanalytical Chemistry 689 (2013) 201-206.
[49] T.-M. Ou, C.-T. Hsu, C.-C. Hu, Synthesis and characterization of sodium-doped MnO2 for the aqueous asymmetric supercapacitor application, Journal of The Electrochemical Society 162(5) (2015) A5124.
[50] G. Zhang, L. Ren, D. Hu, H. Gu, S. Zhang, Sulfuric acid etching for fabrication of porous MnO2 for high-performance supercapacitor, Journal of colloid and interface science 518 (2018) 84-91.
[51] L. Demarconnay, E. Raymundo-Piñero, F. Béguin, Adjustment of electrodes potential window in an asymmetric carbon/MnO2 supercapacitor, Journal of Power Sources 196(1) (2011) 580-586.
[52] L. Athouël, F. Moser, R. Dugas, O. Crosnier, D. Bélanger, T. Brousse, Variation of the MnO2 Birnessite Structure upon Charge/Discharge in an Electrochemical Supercapacitor Electrode in Aqueous Na2SO4 Electrolyte, The Journal of Physical Chemistry C 112(18) (2008) 7270-7277.
[53] B. Ming, J. Li, F. Kang, G. Pang, Y. Zhang, L. Chen, J. Xu, X. Wang, Microwave–hydrothermal synthesis of birnessite-type MnO2 nanospheres as supercapacitor electrode materials, Journal of Power Sources 198 (2012) 428-431.

6. Future Work

There are many components of this project that can be investigated further for future research purposes:

6.1 Active Materials Selection

The ferrimagnetic materials researched in this thesis are only two of many in the class of magnetically ordered pseudocapacitive materials as mentioned in section 2.10 of the literature review. There exists many other magnetically ordered materials such as Fe_3O_4, γ-Fe_2O_3, $CuFe_2O_4$, $CoFe_2O_4$, $MnFe_2O_4$ spinels, hexagonal ferrites ($BaFe_{12}O_{19}$), different magneto-plumbites, garnets, and perovskites that the principles of this investigation can be applied to, in order to improve the capacitive properties of these materials as well. Each material in the class of MOPC possesses their own unique capacitive and magnetic properties, therefore the extent of magneto-capacitive

coupling differs between individual materials. Various experiments can be conducted on individual materials to study their unique capacitive properties, especially the effect of an externally applied magnetic field on the capacitance of soft ferrimagnetic spinels. Studying as many different MOPC materials as possible is of utmost importance, because more data collected on these novel materials translates to a better understanding of their capacitive behaviour, which can lead to a standardization of synthesis, improvement and manufacturing procedure. Additionally, when a class of materials is better understood the possibility of discovering novel applications becomes greater as well as identifying materials with similar characteristics opening up the field of MOPC to wider variety of practical applications.

6.2 Conducting Polymers and Dopants:

Polypyrrole doped with the anionic Tiron molecule was investigated in these projects, however, there exists many different conducting polymers such as polyaniline, polythiophene and poly(3,4-ethylenedioxythiophene) with varying conductivities ranging from 5-500 S cm^{-1}. The great conductivity of these pseudocapacitive conducting polymers makes them great candidates for the fabrication of composite electrodes with MOPC to enhance their capacitive performance as they are greatly hindered by low conductivity attributes. Each conducting polymer can be p-doped or n-doped at varying dopant:polymer ratios with various dopants to achieve pseudocapacitive properties. For polypyrrole alone, there are many dopants such as HCl, $FeCl_3$, p-TSA, CSA, Tiron, PSSA and Ponceau S to name a few that can be explored for the development of composite electrodes. It is a necessity to explore the many possibilities for producing novel MOPC composite electrode chemistries in order to further push the boundary of knowledge in this field and produce the best performing electrochemical capacitor devices for practical applications.

6.3 Dispersing Agents:

The gallocyanine dye dispersing agent was investigated among many others such as 3,4DHB, Lauryl gallate, Basic Fuchsin and calcon-carboxylic acid for the sake of this project with the performance of gallocyanine dye being the best of the ones tested. Although the optimization of gallocyanine mass ratio was performed for NFO and SFO, it may not be the best dispersing agents for other ferrimagnetic materials, therefore this variable is subject to change among MOPC materials, and the plethora of other catechol dispersing agents can be investigated and optimized as well.

6.4 Multiwalled Carbon Nanotubes:

The mass ratio of multi-walled carbon nanotubes was held constant throughout the duration of the experiments conducted, aside from a few, where the mass ratio was increased from 20%-30%. This drastically lowered the overall impedance of the electrode while also slightly lowering the capacitance. Low impedance is a very desirable quality, but the increasing ratio of carbon nanotubes lowers electrochemical activity as it replaces a portion of active material. This suggests room for optimization at varying carbon nanotubes mass ratios to achieve the best performance, additionally with increasing carbon nanotube content it is suggested that the dispersing agent may need to be increased proportionally to complement the change.

6.5 Hydrothermal Synthesis:

Hydrothermal synthesis is a great nanomaterials production technique to optimize the shape and size of nanoparticles for electrochemical capacitor applications. Many variables

involved in this procedure can be varied to achieve an optimal result, such as the alkalizing agent, dispersing or chelating agents, precursor materials, pH, temperature and time. The project currently in progress employs this technique and will be discussed in more detail in the next section.

6.6 Graphene based composites:

TiO_2 nanoparticles possess great chemical stability, tunable shape and size, low cost, low toxicity and great stability in water, making them viable materials to add and potentially benefit EC systems. The project in progress is currently investigating various hydrothermal synthesis routes to obtain TiO_2 nanoparticles with optimum shape and size to add to graphene based EDLCs. The conductivity of graphene along with its high active surface area and stability in aqueous media make it a great material for EDLC applications. The performance of EDLCs is heavily dependent on the practical active surface area of the electrode, the goal of the current project is to add TiO_2 nanoparticles to act as "spacers" in between the thin graphene sheets and form multilayer sandwich structures to increase the practical active surface area. This work can involve the use of organic alkalizers for synthesis of TiO_2 nanoparticles.

7. Final Conclusions

Magnetically ordered pseudo-capacitive materials such as $NiFe_2O_4$ and $SrFe_{12}O_{19}$ possess interesting magnetic and charge storage properties. The capacitive performance of ferrimagnetic SFO and NFO - based high active mass loaded electrodes was investigated throughout the projects described in this thesis. The main objective was to increase the capacitance SFO and NFO based electrodes through elucidating the effects of various materials preparation techniques on capacitance such as high energy ball milling, optimizing mass ratio of the gallocyanine dispersing

agent, and forming composite electrodes with varying mass ratios of polypyrrole doped with Tiron. Each electrode was fabricated with a mass loading of 40 mg cm^{-2} and tested in a three-electrode cell in a potential window of 0- -0.8 V against a saturated calomel reference electrode and a platinum counter electrode in a 0.5 M Na_2SO_4 in DI water electrolyte. Throughout these experiments the capacitance of NFO based electrodes was increased from 0.1 F cm^{-2} to 4.01 F cm^{-2} at a scan rate of 2 mV s^{-1} for a HEBMNFO-PPy composite electrode with mass ratios of 4 HEBM NFO:4 PPy: 2 mg MWCNT. Although the highest capacitance at low scan rates was observed for the HEBMNFO-PPy (4:4:2) composite electrode, the best performance at high scan rates was displayed by the HEBMNFO-PPy composite electrode with a mass ratio of 6:2:2 for HEBMNFO: PPy: MWCNT, displaying high capacitance retention of 90% over 1000 cycles. The capacitance of $SrFe_{12}O_{19}$ was increased from 0.05 F cm^{-2} to 3.7 F cm^{-2} at 2 mV s^{-1} for a HEBMSFO-PPy composite electrode with mass ratios of 4:4:2 for HEBM SFO: PPy: MWCNT. However, the best performance at high scan rates and over long cycles for $SrFe_{12}0_{19}$ was the HEBMSFO-PPy composite electrode with mass ratios of 6:2:2 for HEBMSFO: PPy: MWCNT resulting in a capacitance of 2.7 F cm^{-2} and enhanced capacitance retention at high scan rates over the 4:4:2 electrode. Furthermore, this electrode was successfully utilized as an anode in a 2-electrode aqueous asymmetric cell with MnO_2 acting as the cathode displaying a capacitance of 1.52 F cm^{-2} in a 1.5 V window with a mass loading of 40 mg cm^{-2}. The overall improvement in capacitance displayed by these MOPC based electrodes along with their great capacitance retention over 1000 cycles is demonstrative of their potential for practical applications in high active mass loaded EC systems. The implications of such results are that MOPC materials not only possess novel magneto-capacitive and magneto-electric properties, allowing for application in various multifunctional devices, but also possess the ability to achieve high capacitance values at practical

high active mass loading levels. Further improvements in energy and power density of these MOPC materials at high active mass loading levels can lead to applications in necessary-mainstream technologies such as: grid level energy storage, capacitive water deionization, computer memory back up, various mobile electronics, electric public transportation systems and even personal electric vehicles.